CIVIL ENGINEERING STUDIES
STRUCTURAL RESEARCH SERIES NO. 361

FINAL REPORT

LOW CYCLE FATIGUE OF BUTT WELDMENTS OF HY-100(T) AND HY-130(T) STEEL

By

J. B. Radziminski
F. V. Lawrence
T. W. Wells
R. Mah
and
W. H. Munse

A REPORT OF AN INVESTIGATION CONDUCTED
by
THE CIVIL ENGINEERING DEPARTMENT
UNIVERSITY OF ILLINOIS, URBANA
in cooperation with
The Naval Ship Systems Command, U.S. Navy
Contract NOOO24-69-C-5297
Project Serial No. SF51-541-002; Task 729

UNIVERSITY OF ILLINOIS
URBANA, ILLINOIS

JULY 1970

Final Report

LOW CYCLE FATIGUE OF BUTT WELDMENTS OF HY-100(T) AND HY-130(T) STEEL

by

J. B. Radziminski
F. V. Lawrence
T. W. Wells
R. Mah
and
W. H. Munse

A Report of an Investigation Conducted

by

THE CIVIL ENGINEERING DEPARTMENT
UNIVERSITY OF ILLINOIS, URBANA

in cooperation with

The Naval Ship Systems Command, U.S. Navy
Contract N00024-69-C-5297
Project Serial No. SF51-541-002; Task 729

University of Illinois
Urbana, Illinois
July 1970

ABSTRACT

An evaluation of the axial fatigue behavior of plain plates and full penetration butt-welded joints in HY-130(T) steel is presented. The weldments were fabricated using GMA and SMA welding processes. Fatigue tests were conducted with sound weldments and weldments containing internal defects including slag, porosity, and lack of fusion. Radiographic and ultrasonic inspection techniques were used to study the initiation and propagation of fatigue cracks originating at internal weld flaws. Acoustic emission measurements were taken for smooth and notched HY-130(T) specimens tested in static tension and in fatigue. The results of preliminary tests of plain plates and butt weldments of HY-100(T) [HY-110] steel are presented.

Comparison of the fatigue results for the HY-130(T) specimens with equivalent data for HY-80 and HY-100 steel has indicated that, within the range of lives from approximately 10^4 to 10^6 cycles, the fatigue behavior of as-rolled (mill-scale intact) plain plates of the three materials may be described by a single S-N regression line. Surface treatments, including grit-blasting and polishing, were found to significantly increase the fatigue lives of the HY-130(T) plate specimens.

Wide variations in fatigue life were exhibited by the HY-130(T) and HY-100(T) butt-welded specimens in which cracking initiated at internal weld discontinuities. The scatter in lives could not be explained on the basis of the type of weld defect initiating failure, nor could it be attributed to differences in the weld metal composition or the welding process. However, through application of the concepts of fracture mechanics, it was found that the fraction of the total fatigue life spent in macroscopic crack propagation could be

estimated with reasonable reliability if the through-thickness dimension of the crack-initiating defect, its position relative to the specimen surface, and the nominal cyclic stress are known.

Results obtained from the monitoring of the acoustic emission from specimens subjected to both static and cyclic loading have indicated that this technique is potentially an effective tool for in-service nondestructive testing of structural components.

TABLE OF CONTENTS

TABLE OF CONTENTS (CON'T)

LIST OF TABLES

LIST OF TABLES (CON'T)

LIST OF FIGURES

LIST OF FIGURES (CON'T)

LIST OF FIGURES (CON'T)

LIST OF FIGURES (CON'T)

I. INTRODUCTION

1.1 Object of Study

The development of high-yield-strength steels intended for use in naval construction has precipitated numerous investigations of the behavior of these materials under various environments and service loading histories. This report presents a summary of the latest results in a continuing investigation (1-8) of the resistance, under repeated axial loadings, of plain plates and weldments fabricated from several grades of the high-strength, HY-series steels. The purpose of the current project has been to continue an investigation of the influence of various types of internal defects on the fatigue behavior of butt welds of HY-130(T) steel, and to initiate studies of the fatigue response of plain plates and butt welds of HY-100(T) steel.

As part of the evaluation of the effect of weld defects, including porosity, slag, and lack of fusion, on the fatigue resistance of the HY-130(T) butt welds, the initiation and propagation characteristics of cracks originating at the various internal defect sites have been examined; radiographic and ultrasonic inspection techniques have been used to identify the weld flaws and to monitor the progression of internal fatigue cracking. In addition, recently developed acoustic emission techniques have been used in an attempt to determine the onset of internal cracking.

1.2 Scope of Investigation

A total of twenty-one HY-130(T) butt-welded specimens, most of which contained intentionally deposited weld defects, were tested with the weld

reinforcement removed; the tests were conducted using a stress cycle of zero-to-tension. Both gas metal-arc (GMA) and shielded metal-arc (SMA) processes were used in the preparation of the test weldments.

The results of the fatigue tests of the HY-130(T) specimens failing at internal defects have been compared on the basis of the type and size of defect at the crack initiation site. The fatigue lives of these specimens have been compared also to the fatigue behavior of butt welds in which failure initiated at the toe of the weld reinforcement and to the behavior of the HY-130(T) plain plate material. For the weldments in which fatigue crack initiation and propagation were studied, fracture mechanics concepts were used to relate the propagation life to the size and position of the crack-initiating defect for each of the stress levels studied.

Both plain plate specimens and butt weldments were examined using the HY-100(T) material; as with the HY-130 (T) specimens, all tests were performed using a zero-to-tension stress cycle. The fatigue test results of the plain plates, having grit-blasted surfaces, have been compared with data from earlier tests of HY-100 plates in which the mill-scale surfaces remained intact. The HY-100(T) butt-welded specimens were fabricated using MIL-12018 electrodes and the SMA welding process. The results of the fatigue tests for both as-welded specimens and those in which the weld reinforcement was removed have been compared to tests of similar weldments fabricated using the older HY-100 plate material. Due to late arrival of the HY-100(T) plate from the fabricator, only limited data have been obtained for the weldments.

1.3 Acknowledgments

The tests reported in this study are from an investigation conducted

in the Civil Engineering Department of the University of Illinois, Urbana, Illinois. The program was supported by funds provided by the Naval Ship Systems Command, U. S. Navy, under Contract N00024-69-C-5297, Project Serial No. SF51-541-002; Task 729.

This investigation constitutes a part of the structural research program of the Department of Civil Engineering, of which Dr. N. M. Newmark is the Head. The program is under the supervision of W. H. Munse, Professor of Civil Engineering; the fatigue tests and associated research studies were conducted by T. W. Wells, G. J. Patterson, and P. N. Panjwani, Research Assistants in Civil Engineering, under the direction of Dr. J. B. Radziminski, Assistant Professor of Civil Engineering. Metallurgical studies and associated data analyses have been performed by R. Mah, Research Assistant in Metallurgical Engineering, under the direction of Dr. F. V. Lawrence, Jr., who holds a joint appointment as Assistant Professor in Civil Engineering and Metallurgical Engineering.

The authors wish to express their appreciation for the conscientious work of the Civil Engineering Department's laboratory technicians, especially J. R. Williams, who was responsible for welding of the fatigue test specimens, and to the many other members of the Department staff who have assisted in various phases of the investigation.

II. DESCRIPTION OF TEST PROGRAM

2.1 Materials

Both the HY-130(T) and the HY-100(T) specimens were fabricated from 1 in. thick plate stock obtained from the U. S. Steel Corporation in accordance with contract provisions. The chemical composition and mechanical properties of the HY-130(T) material used in the current investigation are presented in Tables 2.1 and 2.2, respectively. Fatigue specimen numbers designated by the prefix ND were fabricated with plates from heat number 5P2456; those identified by the prefix NE were from heat number 5P2004. Plates from both heats were received descaled and painted (one coat).

The chemical compositions of the GMA bare electrode welding wire, supplied by Linde Division of Union Carbide Corporation, and of the covered electrodes, supplied by the McKay Company, are given in Table 2.3. Both of these electrodes are "second-generation" electrodes which had been found acceptable for the welding of HY-130(T) steel.

The chemical composition and the mechanical properties of the HY-100(T) plain plate material, supplied by the U. S. Steel Corporation, are presented in Tables 2.4 and 2.5, respectively. The plates were received with the surfaces grit-blasted; all specimens fabricated from this stock are designated by the prefix LA. The chemical composition of the MIL-12018 covered electrodes used in the preparation of the HY-100(T) butt-welded specimens is given in Table 2.6.

2.2 Fabrication of Specimens

The details of the welded test specimens are presented in Fig. 2.1. The fabrication technique for all specimens was similar except for differences

in the base metal and welding processes. Specimen blanks, 9 in. by 48 in., were first flame cut from the 72 in. by 96 in. steel plate stock (1 in. thick). For the transverse butt-welded specimens, the blanks were sawed in half (9 in. x 24 in.) and the cut edges were machined to provide a double "V" groove for the weld deposit. The included angle of the groove was 60° for all procedures examined. All welding was performed in the flat position with the specimens loosely clamped in a jig which could be rotated about a horizontal axis (the longitudinal axis of the weld). The welding procedures used in the preparation of the specimens are presented in Sections III and IV for the HY-130(T) and HY-100(T) weldments, respectively.

After the welding operation was completed, holes were drilled in the ends of the specimens, Fig. 2.1, as required for insertion of the member in the fatigue testing machines. The specimens were then milled to shape so that a 5 in. long straight section remained at mid-length to form a test section which included the butt weld. No material in the region of the test section was removed by flame cutting. The net width at the test section was governed by the test load range and the capacity of the fatigue testing machine, the width being made as large as possible within the capacity of the machine.

In the final stage of fabrication, the edges of the specimens in the region of the test section were ground smooth and any sharp burrs filed off. For those butt joints tested with the reinforcement removed, the specimen faces were first milled, and then polished in the direction of subsequent loading (longitudinal) with a belt sander.

2.3 Non-Destructive Testing Equipment and Procedures

Prior to fatigue testing all welded specimens were subjected to

radiographic examination using a sensitivity level of two percent. The specimens were rated in accordance with the requirements for weld quality established by the U. S. Steel Corporation (9) and NAVSHIPS Specification No. 0900-006-9010. (10) The results of the defect examinations and weld ratings are reported in the tables containing the fatigue results for each specimen.

For the specimens examined radiographically during the course of fatigue cycling (initiation and propagation studies), the X-ray equipment was mounted on a portable platform and positioned so that the exposures could be made with the test specimen mounted in the fatigue machine. The radiographic apparatus, less a protective lead enclosure, is pictured in position in Fig. 2.2. With this arrangement, radiographs were taken periodically during the fatigue tests. The initial cyclic interval between radiographs was approximately 10 percent of the expected total life of the test specimen. After crack initiation, radiographs were taken at shorter cyclic intervals to obtain a measure of internal crack growth. This procedure was continued until the fatigue crack was visible on both surfaces of the specimen, thus indicating crack progression through the entire thickness of the plate.

Several specimens were ultrasonically inspected to obtain another indication of initial weld defect density and in an attempt to detect internal fatigue crack initiation for comparison with the radiographic information. The ultrasonic testing apparatus, together with the auxiliary equipment, is shown in Fig. 2.3. A 5 MHz, 70° shear-wave miniature transducer was used in the inspections. The transducer is mounted in a ball bushing and spring loaded against the test specimen to ensure reproducibility of response from one scan

to another. This device is mounted on a movable platen which can be traversed across the test surface while the specimen is in the fatigue machine.

The position of the transducer on the surface of the specimen is sensed by two linear resistors, connected to the platen, and recorded on an X-Y plotter. In this manner, the position of an individual response is projected and plotted on a plane parallel to the surface of the test specimen. The apparent depth of this signal into the specimen is scaled from the oscilloscope screen.

The ultrasonic tests were performed with the welded specimen in the fatigue machine and set at the maximum tensile load used for the particular fatigue test under study. The specimen faces were polished, as described earlier, to improve contact between the probe and the test surface, and to minimize wear on the face of the probe. Light machine oil was used as an acoustic couplant. As illustrated in Fig. 2.4, the weld area of a specimen was scanned by traversing horizontally across the specimen face below the weld and in 1/8 in. vertical increments until the weld area and adjacent heat affected zones had been searched. The detector test range and trace position were adjusted so that the echo from a flaw lying between the transducer-plate contact surface and the rear surface of the test plate was observed (see Fig. 2.4).

2.4 Fatigue Testing Equipment and Procedure

The fatigue tests were conducted using the University of Illinois' 250,000 lb. and 200,000 lb. lever-type fatigue machines. The operating speeds of the machines are approximately 100 and 140 cycles per minute, respectively.

The essential features of the fatigue machines are shown schematically in Fig. 2.5. The lever system provides a force multiplication ratio of

approximately 15 to 1. The load range is adjusted through the throw of the eccentric, while the maximum load is controlled by the adjustable turnbuckle mounted just below the dynamometer.

The testing procedure was similar for all specimens. After the load had been set and the machine started, a microswitch was set so that the machine would automatically shut off when a crack had propagated partially through the specimen. The load was maintained within limits of about ±0.5 ksi by periodic checks, with adjustments made when necessary. Fatigue failure was taken, as reported herein, as the number of cycles at which the microswitch shut off the testing machine. Cycling was then continued until complete fracture occurred so that the fracture surfaces could be examined and photographed. In each case, less than a 1 percent increase in fatigue life existed from the time of the microswitch cutoff to the point of complete separation.

2.5 Method of Data Analysis

For materials subjected to constant amplitude, controlled stress cycling, a linear log-log relationship generally may be established empirically between applied stress and fatigue response for failures occurring over several orders of magnitude of life. In the present study, regression analyses of the fatigue data obtained from tests of the plain plates and of the butt weldments exhibiting toe-initiated failures were performed by applying the method of least squares (11) to the linear logarithmic expression between fatigue life, N, and applied (nominal) stress, S:

$$\log N = C + m \log S$$

or

$$N = k S^{m}$$

where $k = \log^{-1} C$. Both k amd m are considered empirical constants which are dependent upon the material and the type of specimen being tested, as well as upon the nature of the loading spectrum.

S-N curves were generated with the above relationship using data from specimens tested at cyclic stresses equal to or below the nominal material yield strength as the upper limit, and for stresses equal to or above those producing lives on the order of 10^6 cycles as the lower limit.

III. STUDIES OF HY-130(T) PLAIN PLATES AND BUTT WELDS

3.1 Comparison with Previous Studies

3.1.1 Fatigue of Plain Plates

During the earlier stages of the testing program on the fatigue behavior of plates and weldments using HY-130(T) steel, the plate stock used for the test specimens was received with the surface mill-scale intact. Using the regression analysis described in Section 2.5, S-N curves were generated from the results of fatigue tests of plain plate specimens containing this mill-scale surface; (8) the data are presented in Table 3.1, and the S-N curve is plotted with the data in Fig. 3.1.* Also shown on the figure, as dashed lines, are two standard deviation limits for the S-N curve.

To compare the behavior of the HY-130(T) plate material with the fatigue response of the lower strength HY-series steels, the HY-130(T) data of Fig. 3.1 are compared in Fig. 3.2 to the test results of similar plain plate specimens of HY-80 and HY-100 steel which were studied during earlier investigations. (2, 4-8) As seen in Fig. 3.2, the fatigue lives at the several stress levels examined are quite similar for the three steels. Since analysis of the data sets for each of the steels individually resulted in essentially coincident regression lines, a single S-N curve was generated to represent the combined data for all of the as-rolled plates.

It should be noted that the single curve of Fig. 3.2 is representative

---

* Specimen NC-35 (see Table 3.3), an as-welded butt weldment, has been included in Fig. 3.1; this specimen failed on the base metal surface well removed from the region of the weld.

Numbers adjacent to the data points indicate the failure of two or more specimens at approximately the same life.

of the combined data specifically for the surface condition (mill-scale intact) considered. Schwab and Gross, (12) and Haak, *et al.*, (13) found that, for polished rotating beam specimens tested in air, the fatigue strength increased with increasing tensile strength for lives beyond approximately 10^4 cycles to failure. This suggests, then, that surface condition influences considerably the fatigue response of these materials, especially with regard to the number of cycles to fatigue crack initiation.

To obtain a measure of the effect of surface finish on fatigue, several HY-130(T) specimens were tested with the plate surfaces either polished or descaled (grit-blasted) and painted; the fatigue data for these tests are given in Table 3.1. The tests conducted at a stress cycle of 0 to +80 ksi resulted in an average fatigue life of 255,000 cycles for both treatments, or a four-fold increase in life over the average exhibited by the specimens tested with the mill-scale intact, as seen in Table 3.2. Similar variations in fatigue resistance between as-rolled and polished plates have been reported for other high-yield-strength steels as well. (14)

Examination of the fracture surfaces after testing generally revealed single crack initiation sites for the polished and for the descaled and painted specimens, usually occurring at or near a corner of the test section. The as-rolled HY-130(T) plates, however, contained a loose mill-scale surface underlain by a coarse oxidized layer (see Ref. 6), the surface of which served as the site for the formation of multiple fatigue cracks dispersed over the entire specimen test section. Following the coalescence of several such cracks into a single, continuous line, propagation then progressed through the cross-section

of the specimen. Since the rate of crack propagation has been found to be very nearly the same for the HY-80 and HY-130(T) steels, (15, 16) the similarity in fatigue response of the as-rolled plates of the three materials may be attributable to a like number of cycles being required to initiate cracking (on a macro-scale), such initiation, in turn, being governed by the plate surface conditions. Also, with the HY-130(T) specimens, the plate surface treatments were apparently responsible for delaying the initiation of fatigue cracking, thereby providing the increased fatigue life reported in Table 3.1.

From the above, it is evident that the fatigue behavior of these high-strength steels, to be fully described, must be expressed not only in terms of the applied stresses, but by the type and condition of the test specimen (and testing environment) as well.

3.1.2 Fatigue of Butt Welds - Failure at Toe of Weld

A summary of the results of fatigue tests of as-welded HY-130(T) butt-welded specimens fabricated using second generation welding wires, and which exhibited fatigue crack initiation at the toe of the weld reinforcement, is presented in Table 3.3. A photograph of a fracture surface typical of specimens failing at the toe of the weld is shown in Fig. 3.3. The NDT ratings in Table 3.3 are based on the results of radiographic inspection; specimens failing the radiographic standards were tested without repair (except NC-41) to provide some indication of the applicability of the standards in designing for fatigue.

The data for the HY-130(T) butt welds which failed at the toe of the weld are plotted in Fig. 3.4. No S-N curve has been fitted to this data because only one specimen exhibited a fatigue life over 150,000 cycles and

extrapolation of an S-N curve into the low stress, long life region was not considered justified. (The dashed line shown in the figure is from Fig. 3.5.) The data have been compared with the results of earlier fatigue tests of both HY-80 and HY-100 butt-welded specimens which likewise exhibited fatigue crack initiation at the toe of the weld; (1,2,3,7,8) these comparisons are shown in Fig. 3.5.* As with the plain plates, the data for the three steels have been combined to generate a single S-N curve. It is evident that, at cyclic maximum stresses of 60 ksi and above, the fatigue results for the three steels are essentially the same. Additional test data for the HY-130(T) weldments at stresses below 60 ksi are needed to determine whether the fatigue lives of the HY-130(T) specimens would be similar to those of the HY-80 and HY-100 weldments in the long life fatigue region.

In Fig. 3.5 it is seen that the range of fatigue lives obtained at each of the stress levels studied is within the normal scatter expected of specimens having a common joint geometry and similar weld reinforcement contour. Comparison of the behavior of the weldments exhibiting toe initiated failures with the S-N curve data for the plain plates in Table 3.4 (combined data for all steels, Figs. 3.2 and 3.5) shows a marked reduction in fatigue strength for the as-welded specimens at the longer lives and corresponding to nominal stresses which are well within the elastic range of each of the three steels. At 500,000 cycles, for example, a fatigue strength of 27.5 ksi is indicated by the S-N curve for the as-welded specimens, a value just slightly more than

---

* The HY-130(T) data points in Fig. 3.5 which are not included in Fig. 3.4 represent weldments fabricated using first generation welding wires.(7)

Data points marked with an arrow in Fig. 3.5 represent as-welded specimens in which failure initiated away from the toe of the weld (e.g., at an internal defect, or in the test specimen pull-head) but which had lives at least equivalent to those of the specimens actually exhibiting toe failures.

one-half of the 50 ksi fatigue strength found for the base material. This significant difference in behavior between the as-welded and the plain plate specimens is attributable in part to the earlier activation of fatigue cracking in the weldments, resulting from the concentration of stress introduced by the geometry at the toe of the weld.

The difference between the fatigue resistance of the butt weldments exhibiting failure at the toe of the weld and the base metal specimens diminishes at the shorter lives corresponding to the higher stress amplitudes. In this low cycle region, the number of cycles to crack initiation was observed to occupy a proportionately smaller percentage of the total life of a specimen than at the lower stress levels. With the major portion of life thus spent in crack propagation at the high stress amplitudes, the similarity in behavior of the plain plates and the weldments is to be expected. Moreover, if only the crack propagation phase of the total fatigue lives were considered, the two specimen types should exhibit essentially the same behavior.

3.2 Fatigue of Butt Welds - Failure at Internal Defects

3.2.1 Results of Fatigue Tests

The welding procedures used in the fabrication of the butt-welded specimens for the current series of tests are shown in Fig. 3.6 (Linde bare electrode wire) and Fig. 3.7 (McKay covered electrode). Both of the procedures, using 1-in. thick base material, were successfully qualified in accordance with procedures recommended by the U. S. Steel Corporation (9) and those required by the U. S. Navy for fabrication of HY-80 submarine hulls. (10) The qualification tests included reduced section tension tests, side bend tests, macro-etch specimens, and radiographic inspection; the quantitative results of

these tests are reported in Reference 8.

The welding procedures described above were used also in the preparation of test specimens containing intentional defects, except that specific measures were taken (stripping of electrode coating, wetting of bare wire, weaving back over a deposit to entrap slag, etc.) to deposit specific types and quantities of flaws in the weldments. A list of the specimens prepared for the current study, including the type and size of the detected defects, is presented in Table 3.5. The defect types were identified by radiographic examination and rated in accordance with the specifications noted in Section 2.3. The comparators of Reference 17 were used as interpretive guides to aid in the identification of the internal defects shown on the radiographs. It should be noted that it was not always possible to hold the defect sizes within the tolerances desired. Thus several test specimens contained flaw sizes exceeding the radiographic standards while others were found to be "radiographically sound" even when measures were used which were intended to introduce a specific type of defect in the weld deposit.

The welded specimens were tested with the reinforcement removed to insure the initiation of fatigue cracking at internal defect sites, thus permitting a direct comparison of the relative severity of the various defect types on the fatigue response of the weldments. The results of the fatigue tests, conducted at a stress cycle of zero-to-tension, are presented in Table 3.5. Also included are descriptions of the defects present at the locations of crack initiation. (It can be seen that the radiographs taken prior to testing did not always reveal the type of defect that was present at the eventual location of fatigue crack initiation.) Specimens reported in Table 3.5 and in subsequent tables as having failed "in weld metal" are those in

which no physical internal flaw was discernible, with the unaided eye, on the fracture surfaces. Subsequent metallographic inspection of the fracture surfaces and of transverse sections taken from these specimens indicated, in most instances, that cracking initiated either at microporosity, or in the nugget papilla or region of deep weld bead penetration common to GMA weldments fabricated using the argon-oxygen gas mixture. Other investigators (18) have found microcracking in the heat-affected zone adjacent to the nugget papilla in such weldments. Therefore, in the absence of obvious macroflaws, such as slag or lack of fusion, in specimens having the weld reinforcement removed, it appears that the region of lower toughness and ductility associated with the nugget papilla can be a preferential site for the activation of fatigue cracking.

In addition to the data of Table 3.5 from the current study, the defect descriptions and fatigue test results for previously tested HY-130(T) butt weldments (7,8) which also failed at internal weld defects are presented in Tables 3.6 and 3.7. Table 3.6 contains data for specimens prepared using both first and second generation welding wires and tested with the weld reinforcement removed; Table 3.7 contains the test results for similar specimens tested in the as-welded condition. The analyses of the test data, presented in the following paragraphs, include data for specimens prepared using both the first and second generation welding wires because it was felt that the nature of the internal weld defect at the fatigue crack initiation site, and not the type of wire, *per se*, was the most significant parameter governing the fatigue response of those weldments.

3.2.2 Analysis of Data

The fatigue test results for all of the specimens listed in Tables

3.5, 3.6 and 3.7 which were rated acceptable in accordance with the radiographic standards (9,10) are shown in Fig. 3.8. (The data are plotted on semi-logarithmic axes simply for clarity of presentation.) The S-N curves for plain plates (from Fig. 3.2) and for butt welds exhibiting toe failures (from Fig. 3.5) are also presented. The most significant aspect of the data presented in Fig. 3.8 is the very large scatter in fatigue lives at the several stress levels investigated, encompassing some two orders of magnitude of life at stress cycles of 0 to +50 ksi and 0 to +80 ksi. Such wide variations in life are not unexpected in view of the many different types (and sizes) of internal weld discontinuities present at the crack initiation sites. To ascertain if a particular type of defect was associated primarily with failures occurring at either extreme of the range of lives observed for tests conducted at one stress level, the fatigue data have been grouped by defect type and compared, in Figs. 3.9 and 3.10, for maximum cyclic stresses of 50 ksi and 80 ksi, respectively. The defect types specified in the figures are those actually observed at the internal crack initiation sites regardless of the radiographic descriptions of the welds. These defects were not always the ones which appeared to be most severe on inspection prior to cycling. Consequently, when the fatigue data for specimens failing the NDT standards are included in the comparisons of Figs. 3.9 and 3.10, they are seen often to have exhibited lives equal to or exceeding the lives of specimens rated as acceptable by the standards.

Inspection of Figs. 3.9 and 3.10 shows that the scatter in fatigue lives of specimens with internal cracking is only slightly diminished when the results are separated on the basis of the individual defect types. By examination of Tables 3.5, 3.6 and 3.7, it can be seen also that there were no differences in fatigue behavior which could be related to one or another of

the several electrodes used in the preparation of the HY-130(T) weldments, when failure initiated at comparable defects. The principal conclusion concerning flaw severity afforded by the comparisons in Figs. 3.9 and 3.10 is the broad generalization that planar discontinuities can be somewhat more deleterious to the fatigue strength of a welded joint than the spheroidal defect configurations associated with porosity.

It would be reasonable to assume that the total fatigue life of a weld containing internal discontinuities is dictated by a variety of interacting factors, including the dimensions of the defects, the proximity of one defect to another and to the surface of the test specimen, and, for certain states of applied stress, the nature of the residual stress field. For the weldments tested in this program, an attempt was made to correlate, for an individual type of defect, defect size with fatigue life at a specific stress level. In Figs. 3.11 and 3.12, for tests conducted at 0 to +50 ksi and 0 to +80 ksi, respectively, the fatigue lives of specimens initiating fatigue cracking at isolated pores or clustered porosity are compared on the basis of a simple two-dimensional representation of the defect (i.e., the total area of all pores in the cluster observed on the weld fracture surface reported as a percentage of the specimen cross-sectional area). Although a general trend toward a reduction in fatigue life with increasing defect area may be noted, the trend is far from consistent. An even less consistent correlation was encountered when the specimens were compared on the basis of defect area measured from radiographs obtained by X-raying at normal incidence to the surface of the specimen. This was to be expected, for cracks initiating at one elevation in the weldment (on a plane through the weld and perpendicular to the faces of the specimen) would progress normal to the direction of loading and be relatively

unaffected by the presence of pores located at other elevations, unless additional cracks had initiated at those pores as well. It is evident, therefore, that a planar measure of defect density such as total area reduction, although adequately quantifying the degree of deviation of a weld from complete soundness and, presumably, offering a measure of the integrity of the weld under static load, cannot in itself be used to reliably predict the total performance of the weldment under cyclic loading.*

A similar comparison between defect size and fatigue life, for welds containing lack of fusion or lack of penetration, is presented in Figs. 3.13 (tests at 0 to +50 ksi) and 3.14 (0 to +80 ksi), and for welds containing slag, in Fig. 3.15 (0 to +80 ksi). In these figures the ordinate is the length of the discontinuity parallel to the weld axis, measured on the specimen fracture surface. As with porosity, it can be seen from Figs. 3.13 through 3.15 that this measurement was not a particularly reliable indicator of fatigue behavior, at least for the 1-in. thick specimens tested and for which failure is assumed to have occurred when a crack has progressed through the thickness of the plate.

If neither defect length nor area defined above are entirely satisfactory indicators of cyclic response for weldments exhibiting internal crack initiation, the question remains as to whether some one- or two-dimensional parametric quantities representative of an internal defect can be satisfactorily used to estimate fatigue behavior. In Section 3.3, it will be shown that the duration of crack propagation can be reasonably well described in terms of the

---

* This observation is limited to the conditions considered in this study, i.e., the behavior of weldments in which the area reductions for porosity are of the order of one percent or less. Other investigators have reported a reasonable correlation between fatigue life and defect area for area reductions between approximately one percent and fifteen percent. (19)

through-thickness dimension of the defect at the initiation site, the proximity of the defect to the surface of the specimen, and the ratio of defect (initial crack) width to specimen thickness. With the notch geometry at the tip of an advancing fatigue crack being the same, regardless of the configuration of the original defect at the initiation site, it can be expected that fracture mechanics concepts can be used to relate the rate of crack propagation with crack width and nominal applied stress - the total number of cycles of propagation available before failure then becoming a function of plate thickness and the distance from the flaw to the specimen surface. For specimens containing identical defect types (having similar boundary geometries which could be expected to foster crack initiation at the same number of cycles at a given nominal stress) the total fatigue lives would thus be expected to vary as an inverse function of the through-thickness dimension of the initial defect. Comparisons between the experimental data and the propagation lives predicted using expressions developed from the above assumptions are presented in detail in Section 3.3.

Although the crack propagation stage of the fatigue life of specimens exhibiting internal crack initiation can be reasonably well defined as indicated above, the number of cycles required to initiate active (macroscopic) cracking at a defect site is more difficult to ascertain. This arises in part from the difficulty encountered in quantifying those parameters critical to crack nucleation, especially the notch geometry at the defect boundary, which will, in turn, dictate the local cyclic strain history of the material immediately adjacent to the flaw. For example, in some of the specimens tested, crack initiation was encountered at a single pore well removed from a seemingly more

critical cluster of porosity; in other specimens cracking initiated along a short line of incomplete fusion encompassed by a porosity cluster and hidden from NDT detection by the cluster. Such problems should be alleviated in part as continued improvements are made in the use of the various available NDT techniques, thereby permitting more accurate definition of internal weld defects.

3.3 Studies of Fatigue Crack Initiation and Propagation

3.3.1 Introduction

The total fatigue life of a specimen can be divided into five phases: cyclic slip, crack nucleation, microcrack growth, macrocrack growth and failure. (20) For the purposes of the present study, the first three phases have been considered as the fraction of the fatigue life spent in crack initiation and the latter two phases as the fraction of the fatigue life spent in crack propagation.

In terms of welds containing internal defects, the total fatigue life can be divided into an initiation period in which the defect does not enlarge perceptibly, and a propagation period in which a crack originating at the flaw enlarges until fracture has occurred. In high-strength steel weldments tested at high stress levels, a significant portion of the fatigue life may be spent in fatigue crack propagation; consequently, there has been much recent interest in measuring the life spent in crack propagation and relating this life to that predicted using current theories of fracture mechanics. (19, 21 - 24)

The purpose of this phase of the present investigation was to determine the point at which active fatigue crack growth initiates at internal defects in HY-130(T) weldments; this was accomplished by periodically interrupting

testing and radiographing the specimen using the procedure outlined in Section 2.3. In this manner the fraction of the fatigue life spent in crack propagation could be determined and compared with that predicted using fracture mechanics analysis.

3.3.2 Test Results

Both radiographic and ultrasonic techniques were used to detect the nucleation of fatigue cracks at internal defects; radiography was further employed to examine the patterns of internal crack propagation beyond the stage of initiation. A description of the ultrasonic equipment, of the X-ray equipment, and of the procedures followed in the periodic examination of the fatigue test specimens is presented in Section 2.3.

Fourteen HY-130(T) butt-welded specimens, tested with the reinforcement removed, were subjected to radiographic inspection at periodic intervals during the course of cycling; these specimens are indicated in Table 3.5. Tracings of selected radiographs obtained during the progress of fatigue cycling are presented in Figs. 3.16 through 3.29 for each of the fourteen specimens. Also noted on the figures are the number of cycles at which the fatigue cracks had penetrated to the surfaces of the test specimens as observed visually.

Seven of the fourteen specimens used to study crack initiation and propagation were examined ultrasonically both before testing and at the time internal cracking was first indicated by radiography. For these inspections, the ultrasonic equipment was calibrated in accordance with the procedures and sensitivity standards established by NAVSHIPS 0900-006-3010 (25) for the inspection of full penetration butt welds. The scanning technique consisted

of traversing the probe across the face of the specimen in the transverse direction in 1/8 in. vertical increments until a response exceeding the disregard level (DRL) was detected. The probe position was then adjusted to maximize the signal amplitude from the internal defect or crack; this position was recorded on an X-Y plotter together with the depth beneath the surface of the test specimen from which the peak response originated and the pulse energy required to establish the response. Following this, the probe was traversed both vertically and horizontally from the point of peak response, with the four positions at which the signal amplitude fell below the DRL being recorded on the plotter. It should be emphasized that no attempt was made to further identify the type of detected defect, nor were the points used to identify the limits of a recordable indication intended to represent, necessarily, the physical extremities of the actual defect or crack. The technique was employed simply as a means of determining whether the initiation (or early stage of propagation) of a fatigue crack, as verified by radiographic inspection, could be detected by an increase in the amplitude of the ultrasonic response in the vicinity of the initial flaw, and/or by a lengthening of the distance over which the response remained above the DRL.

Sketches of the ultrasonic responses obtained before testing, and after the presence of fatigue cracking had been determined by radiography, are presented in Figs. 3.30 through 3.36 for the seven HY-130(T) butt welds examined in this study. Also shown on the figures are sketches and photographs of the specimen fracture surfaces; on the sketches of the fracture surfaces are indicated the position of the weld defects, and extent of fatigue crack growth at approximately the time of intersection of the progressing crack with the specimen surface. The ultrasonic plots represent the projection of

all detected responses above the DRL onto a cross-sectional plane through the weld perpendicular to the longitudinal axis of the fatigue specimen. The crosses represent the limits of the probe scan for which the echo amplitude remained above the DRL. The numbers corresponding to each response indicate a relative measure of the amplitudes of the peak signals; they are not a direct measure of the pulse energy required to establish the responses. The letter designation indicates the vertical position of the maximum or peak response in the direction of the longitudinal axis of the test specimen. It should be noted that many additional responses were established for most of the weldments, including areas in which no corresponding radiographic indications of defects were obtained. However, the peak amplitudes of these responses were generally below the DRL and are not shown in the figures.

The second ultrasonic trace shown in the sketches for the various welds generally indicates an increase in the relative height of the peak signal and/or an increase in the distance over which the signal remained above the DRL in the vicinity where fatigue cracking had been detected by radiography. However, at the time these traces were obtained, cracking was already clearly evident on the corresponding radiographs, so that the increase in signal amplitude does not correspond to the actual time of crack initiation. Due to the considerable amount of time involved in obtaining a complete ultrasonic trace using the manual traversing technique described earlier, no attempt was made to obtain such traces periodically during the course of fatigue crack propagation.

A summary of the results of the fatigue crack initiation and propagation studies, including data from an earlier investigation, (8) is presented

in Table 3.8. Also included in the table are the defect sizes and locations as measured on the specimen fracture surfaces after completion of testing. The defect length represents the dimension measured parallel to the axis of the weld, while the width is the dimension in the through-thickness direction.

The total and crack propagation segments of the fatigue lives of the weldments are plotted in Fig. 3.37. As can be seen in the figure, there was considerable variation in the total fatigue lives measured at the two stress levels used, 0 to +50 ksi and 0 to +80 ksi. At 0 to +80 ksi, the total fatigue lives ranged from 1,500 cycles to 170,000 cycles or over two orders of magnitude. The spread in the lives at 0 to +50 ksi is almost as great; the lives ranged from 27,500 to 651,900 cycles or well over one order of magnitude in life.

The measured propagation lives, on the other hand, exhibit much less variation. At 0 to +80 ksi the propagation lives ranged from 2,250 to 9,300 cycles, less than one order of magnitude.* At 0 to +50 ksi, the propagation lives ranged from 14,500 cycles to 44,000 cycles, again, less than one order of magnitude.

The difference between the total lives and the measured propagation lives of a specimen is the number of cycles spent prior to crack initiation (or in undetected crack growth). For those specimens in which crack initiation and propagation was studied (see Table 3.8), the period of life spent in crack

---

* The reason that some total lives are shorter than any propagation life shown in Fig. 3.37 is that the propagation life was not measured in all specimens reported; thus the propagation lives for some short total life specimens are missing.

initiation varied from essentially zero cycles to over 38,000 cycles at 0 to +80 ksi and from essentially zero to over 74,000 cycles at 0 to +50 ksi.

As would be expected, the total lives and the number of cycles spent in crack initiation and propagation are smaller at the higher stress level than at the lower stress level. Also, there is a general, though not entirely consistent, correlation between large flaws and short fatigue lives as can be verified by inspection of Table 3.8. However, as noted earlier, it was found that the critical fatigue crack did not always start at the flaw which appeared to be most severe on the radiographs taken prior to testing. Often the fatal crack would start at a defect not evident upon the initial radiograph.

3.3.3 Fracture Mechanics Analysis

From the foregoing observations and the results of several recent studies, (19, 21 - 23) it would seem reasonable that the effect of flaws on the fatigue life of welds could be related to the maximum stress experienced in the material adjacent to the defect, i.e., to the stress intensity associated with the defect. Moreover, it would seem that the type of the defect should have little effect upon the advancement of the fatigue crack, once initiated. Thus, the variation in the fraction of fatigue life spent in crack propagation shown in Fig. 3.37 is independent of the initial flaw type. Once an active fatigue crack has formed, the number of cycles to failure at any given stress level depends only upon the rate at which the crack propagates through filler metal and not upon the type of flaw initiating the crack, *per se*.

The rate at which a fatigue crack will advance has been studied

extensively by Paris, (26) who showed that the rate of crack growth advance per cycle can be related to the range of stress intensity factor by the following equation:

$$\frac{da}{dn} = C(\Delta K)^n \qquad [1]$$

where:

$\frac{da}{dn}$ = rate of crack advance per cycle

C = material constant

n = material constant

ΔK = range of stress intensity factor.

Paris found that C and n remained constant over a wide range of stress intensity factors; other studies (16) have further shown that these constants vary little from one high-strength steel to another.

The range of stress intensity factor, ΔK, is a function of the crack width and stress level. Therefore, for tests conducted at a constant stress range, ΔK becomes a direct function of instantaneous crack length, and the number of cycles of propagation may be expressed as:

$$N = \int_{a_o}^{a_f} \frac{1}{C(\Delta K)^n} \, da \qquad [2]$$

where:

N = cycles spent in advancing the crack from a_o to a_f

a_o = half initial crack size (defect dimension in direction of subsequent crack growth)

a_f = half final crack size.

The number of cycles of repeated stress necessary to advance the crack from an initial flaw size $2a_o$ to a final crack size $2a_f$ can be calculated using Equation [2] if an analytical function for the range of stress

intensity factor can be found and integrated. In those cases where the integration of Equation [2] is difficult, a finite difference technique can be used and the integration performed numerically with the aid of a computer.

$$N = \sum_{a_o}^{a_f} \frac{\Delta a}{C(\Delta K)^n} \qquad [3]$$

where:

Δa = small finite advance of the crack.

Using either Equation [2] or [3] and letting a_f equal half the thickness of the specimen, it is possible to estimate the number of cycles spent in crack propagation during the fatigue life of a weld if the initial flaw size in the through-thickness specimen direction, $2a_o$, is known, the material constants C and n are known, and if an analytical function for the range of stress-intensity factor can be found which fits the geometry and/or boundary conditions of the physical situation.

Although exact solutions for a generalized flaw in a finite body are not available, solutions for simpler cases which bound or closely model most physical situations do exist.

A very simple model for a flaw in a weld, a disc-shaped crack in an infinite body, is shown in Fig. 3.38. The range of stress intensity for a zero-to-tension stress condition (stress perpendicular to the plane of the crack) would be: (26)

$$\Delta K = \frac{2}{\pi} \sigma \sqrt{\pi a} \qquad [4]$$

where:

σ = maximum tensile stress

a = crack radius or half width.

Substituting this function into Equation [2] and integrating:

$$N = \frac{a_f^{(1-\frac{n}{2})} - a_o^{(1-\frac{n}{2})}}{(1 - \frac{n}{2})\ C \left(\frac{2\sigma}{\sqrt{\pi}}\right)^n} \qquad [5]$$

A second model, that of a through crack in a body which is finite in the direction of crack advance is shown in Fig. 3.39. The range of stress intensity for a zero-to-tension stress situation can be expressed as: (27)

$$\Delta K = \sigma\sqrt{\pi a}\ (\sec \frac{\pi a}{2b})^{\frac{1}{2}}, \quad 0 \leq a \leq 0.8b \qquad [6]$$

where:

b = plate half thickness.

Substituting this function (Equation [6]) into Equation [3]:

$$N = \sum_{a_o}^{a_f} \left[\frac{\cos \frac{\pi a}{2b}}{a\ C^n\ \sigma^2\ \pi^{\frac{2}{n}}}\right]^{\frac{n}{2}} \cdot \Delta a \qquad [7]$$

In Fig. 3.40 models of various types of flaws commonly encountered in welds are shown. The through crack of Fig. 3.39, for which Equations [6] and [7] were developed, models the continuous and intermittent linear flaws shown in Figs. 3.40a and 3.40b quite closely; but, it does not adequately model the small, isolated pore. The disc-shaped flaw of Fig. 3.38, for which Equations [4] and [5] were developed, is more realistic for the latter case. One characteristic of both Equations [5] and [7] is that the crack propagation life calculated is very sensitive to the choice of initial flaw size, a_o. A fatigue crack spends the major portion of its propagation life as a very small crack and the accuracy of the solution will therefore depend in large part upon accurately modeling the initial size and geometry of the defect (see Fig. 3.41).

3.3.4 Comparison with Experimental Results

As reasoned above, the initial size (in the direction of subsequent propagation) and, to a lesser extent, the geometry of a flaw should determine the length of the crack propagation period of the fatigue life. The fatigue lives of Table 3.8 and Fig. 3.37 have therefore been replotted as a function of initial flaw size for the two stress levels of 0 to +80 ksi and 0 to +50 ksi in Figs. 3.42 and 3.43. The initial flaw size $2a_o$ in these plots is the initial width of the critical flaw seen on the fracture surface of each specimen. This dimension has been plotted against the total fatigue life, and, for those specimens in which propagation measurements were taken, against the life spent in crack propagation as determined experimentally by radiography. The propagation and total lives measured for a specimen have been connected by a horizontal line, the length of which is the life apparently spent in initiating an active fatigue crack (or in undetected, early crack growth).

Also appearing in Figs. 3.42 and 3.43 are three curves for the life spent in crack propagation, N, which have been calculated using Equations [5] and [7]. The values of C and n used in these calculations are those determined by Barsom, Imhof and Rolfe (16) for HY-130(T) steel using a zero-to-tension stress cycle and one-inch thick wedge-opening-loading (WOL) specimens, conditions which are, with the exception of specimen geometry, similar to those used in the present study.

At 0 to +80 ksi the total lives and, particularly, the propagation lives, lie within a band that straddles the predicted results calculated using the through crack in a finite plate model, Equation [7]. This model represents a condition of severity at least equal to that of the most critical flaw

encountered in this study (continuous lack of fusion, etc., see Fig. 3.40). The fact that some of the specimens exhibited propagation lives less than those predicted by Equation [7] may be explained in part by the limitations of the NDT techniques used to detect crack initiation; i.e., crack extensions of less than about 0.03 in. were generally undetectable on a radiograph, which could result in appreciable error in the estimation of life spent in propagation. It is more difficult to explain why the total lives of some of the test specimens were less than the propagation lives predicted by Equation [7].

A possible explanation for the shorter lives may be that most flaws were not positioned along the centerline of the weld as assumed for Equation [7], but were actually asymmetrically located. The position of the center of the flaw relative to the surface of the specimen is given in Table 3.8. The centers of some flaws are more nearly at the quarter-points of the specimen. With such flaws, the stress intensity factor for the edge nearest the surface of the specimen is greater than that assumed in the calculation of Equation [7] for a 1-in. thick plate. Consequently, a fatigue life shorter than that predicted above could result. The magnitude of this effect can be assessed by bounding the problem with the solution of Equation [7] for a ½-in. thick plate, the assumption being that a flaw of $2a_o$ initial width with its center at 0.25 inches from the surface of a 1-in. plate could be similar to but not worse than a flaw of $2a_o$ initial width at the centerline of a ½-in. plate.

Curves for this latter condition are also plotted in Figs. 3.42 and 3.43; it can be seen that the differences between the solution for a 1-in. and ½-in. thick plate are most pronounced at the larger flaw sizes. For very small flaw sizes the solutions are essentially identical because the effect of

the boundary conditions upon the flaw's initial behavior is small. The solution for the ½-in. plate very nearly bounds all the data.

The smallest defects which have been observed to initiate fatigue cracks were very small pores. The initial geometry and the boundary conditions for these flaws may be conservatively approximated by the disc-shaped crack in an infinite body model assumed in Equation [5]. The difference between the curves for Equation [7] and Equation [5] (in Fig. 3.42) at small flaw sizes reflects the effect of the difference in geometry between point and line flaws. Consequently, the curve for Equation [5] should represent the propagation life of very small isolated pores better than should Equation [7]. As can be seen in Fig. 3.42, the plot of Equation [5] bounds most of the fatigue data and agrees particularly well with the fatigue lives of the smallest (spheroidal) defects initiating fatigue fracture.

The same general remarks apply to the data presented in Fig. 3.43 for tests conducted at 0 to +50 ksi. Few lives were recorded less than that predicted by Equation [7] for a 1-in. plate. The data for the most part lie between the curves for Equation [7] and Equation [5].

The two models used in the fracture mechanics analysis can be seen to bound the data measured at both stress levels, as shown in Fig. 3.37. S-N curves based on various initial flaw widths have been plotted using the results of Equations [5] and [7]. Most of the measured fatigue data lie between the solution of Equation [7] for an initial flaw size $2a_o$ of 0.3 in. and Equation [5] for an initial flaw size $2a_o$ of 0.001 in.

3.4 Acoustic Emission Studies

In a separate phase of the current investigation, a program was

initiated to develop equipment and test procedures for the detection of acoustic emission resulting from plastic deformation and crack propagation in HY-130(T) steel. The relationship between acoustic emission and the stress and strain history for the HY-130(T) base material was studied, for both notched and unnotched tensile specimens. The experimental methods developed were extended to zero-to-tension fatigue tests in which the same equipment was used to detect the onset of crack propagation.

3.4.1 Experimental Procedure

Work by previous investigators of acoustic emission resulting from deformation has shown that this phenomenon can be detected over a very broad band of frequency, (28) a fact which allows the operation of the detection equipment at a very high center frequency; this is advantageous to the conduct of acoustic emission experiments since elaborate soundproofing and acoustic isolation is avoided and most extraneous noises can generally be eliminated with adequate filtering. By narrowing the bandwidth, increased signal to noise (Nyquist) ratio can also be obtained. These two measurement techniques have allowed the development of experimental methods that make acoustic emission useful for failure detection and crack propagation monitoring.

The specimens of HY-130(T) steel were tested in an Instron machine because of its relatively noiseless operation. A ferroelectric transducer placed against the gage section of the specimen detected the emission pulses in the frequency range between 40 kc and 150 kc. The electronic instrumentation used for the detection and recording of acoustic emission data is shown in Fig. 3.44. The data was recorded on magnetic tape and played back into a

strip chart recorder so that a permanent graphical record of emission could be formed.*

Three types of specimens were used: unnotched tensile specimens, single edge-notched specimens, and center-notched fatigue specimens. The basic design for all three types of specimens was the same (see Fig. 3.45), being 24 in. long, .4 in. wide and with a reduced test section of 10 in. in length. The 24 in. length of these specimens was selected to allow the transducer to be as far away from the connecting pins as possible, thereby reducing the pickup of extraneous noise, i.e., emissions from the testing machine and stressed areas around the pins.

To further reduce extraneous noise and emissions, a preloading procedure first used by Dunegan (30) was performed on all of the specimens. This procedure consisted of compression preloading the regions around the pin holes in a specially designed device (see Fig. 3.46). The load imposed was 10 percent higher than the maximum load expected during the test. Any emissions that would normally be expected to originate from the grip region during a test would thus be eliminated due to the Kaiser effect. (31)

3.4.2 Test Results

In Fig. 3.47 are shown plots of acoustic emission pulse count and stress as a function of strain for an HY-130(T) steel unnotched specimen. To obtain this plot, the total number of acoustic emission pulses was recorded every 10 seconds during the test. The results are presented as a rate of emission over ten second periods as a function of strain in the test specimen.

---

* A complete description of the equipment and test procedures used in the investigation is presented in Reference 29.

The results show that the peaks in acoustic emission occurred shortly before and after general yielding has occurred. This was followed by a period of little detectable acoustic emission activity. This behavior continued until failure. At failure a large number of counts were registered over a very short time period. Experiments in attempting to get better recordings of this time period by running a specimen very slowly (less than .02 in. per minute) through fracture produced no improvement in the results.

In Fig. 3.48 are shown plots for acoustic emission and stress as a function of strain for an edge-notched HY-130(T) steel specimen. The plots in this figure can be seen to be quite different from the results for the unnotched specimens. The level of acoustic emission activity built up rapidly and remained at a high level until failure.

Early experiments in monitoring center-notched HY-130(T) specimens in fatigue gave no positive results. The purchase of a low noise amplifier, however, did permit the detection of fatigue crack propagation in the center-notched specimens. The strip chart record and plot of acoustic emissions per cycle versus number of cycles in Fig. 3.49 shows that a definite increase of emission activity was noticed approximately 70 cycles before failure for a specimen subjected to a stress cycle of 0 to +140 ksi. This activity increased only during the loading portion of the stress cycle and ended when unloading commenced.

3.4.3 Discussion of Results

The tests conducted to date have shown that the notched HY-130(T) specimens produced a higher acoustic emission rate and a higher total number of

acoustic emissions than the unnotched material at comparable strains during a monotonic tension test. This agrees quite well with Dunegan's theory (30) that acoustic emissions are caused by microdynamical dislocation activity. This theory and the current data would therefore infer that acoustic emissions are dependent upon plastic strains in the material.

In extending this technique to monitoring fatigue tests using the center-notched specimen, it was expected that a large number of acoustic emissions would occur during the first loadings. This activity would eventually die down as the material work hardened and because of the Kaiser effect. When a fatigue crack has initiated, new material at the tip of the crack would be plastically deformed and acoustic emissions should rise sharply. The amount of deformation that will occur is dependent on the size of the crack, the type of loading to which the test member is subjected, and the orientation of the crack with respect to the principal stresses. The parameter expressive of the interrelationship among these variables is the stress intensity factor at the crack tip. Therefore, since acoustic emission appears to be dependent upon the amount of plastic strain in the material, and the plastic strain can be related to the stress intensity factor, one should expect an increase in acoustic emission with an increase in the stress intensity factor.

Using fracture mechanics it is known that the stress intensity factor K is dependent upon the configuration of loading and body geometry, and has been determined for many cases. For a Griffith crack of length 2a in a plate subjected to a uniaxial tensile stress of σ, the stress intensity factor is:

$$K = \sigma\sqrt{\pi a}$$

The radius (r_y) of the plastic zone originating at the tip of the crack (when the plastic zone is small compared to the crack length) is:

$$r_y = \frac{1}{2\pi} \left(\frac{K}{\sigma_{ys}}\right)^2$$

where σ_{ys} is the material yield stress. It can be seen that an increase in K results in an increase of r_y, which in turn should result in an increase in the number of acoustic emissions. Therefore, as the crack propagates and enlarges ("a" increases) the acoustic emissions detected should increase accordingly.

Using Equation [7] developed in Section 3.3 for predicting the fatigue crack propagation lifetime for a crack in a plate of finite width, it was predicted that crack propagation would begin approximately 90 cycles prior to failure for the center-notched fatigue specimen mentioned in Section 3.4.2. Thus, it would theoretically be possible to detect an increase in emission activity 90 cycles before failure and an increasing acoustic emission rate as the size of the crack increased. As seen in Fig. 3.49, it was possible to detect an increasing emission activity beginning at 70 cycles prior to failure. A closer examination of the emission data showed that not every cycle resulted in the same emission pattern. Instead, alternating cycles were similar. This phenomenon, if not an artifact of testing, should be further studied.

IV. PRELIMINARY STUDIES OF HY-100(T) PLAIN PLATES AND BUTT WELDS

4.1 Fatigue of Plain Plates

To provide a comparison with data from earlier fatigue tests of HY-100 material, four plain-plate specimens were fabricated from the grit-blasted HY-100(T) plate material received for use in the present study (see Tables 2.4 and 2.5). Two specimens were tested at a stress cycle of 0 to +80 ksi and two at 0 to +100 ksi.

The results of these tests are compared in Table 4.1 with the data from the earlier tests of as-rolled HY-100 plate. (5) One of the specimens in the current study, LA-3, failed at a line scribed on the surface of the plate for fabrication purposes, suggesting that the life of the specimen may have been shortened by the presence of the scribe line. The life of LA-3, however, was longer than that for the other specimen tested at the same stress cycle.

The data from the HY-100(T) fatigue tests are plotted in Fig. 4.1 for comparison with the data and S-N curve for HY-100 as-rolled plain plates, including butt weldments that failed away from the weld at the mill-scale surface. (7) At the 0 to +80 ksi stress cycle, the fatigue lives of the grit-blasted plate specimens were about six times the average life of the as-rolled plates. This is consistent with the higher lives experienced with descaled and painted HY-130(T) plates compared to the as-rolled HY-130(T) material (see Table 3.2). Additional tests are required to determine the degree to which this improvement in the fatigue behavior of the HY-100(T) material extends to stresses below 80 ksi.

At the 0 to +100 ksi stress level, the lives of the two grit-blasted plates are seen in Fig. 4.1 to fall within the two standard deviation limits of the S-N curve for the as-rolled material. At stresses approaching the nominal yield strength of the base metal, inelastic deformations would be expected to result in relatively shorter periods spent in crack initiation for both surface treated and as-rolled plates, so that a convergence of the fatigue lives for both types of specimen would be anticipated. Again, additional tests are required to confirm this expected behavior at the higher cyclic stresses.

4.2 Fatigue of Butt Welds

The welding procedure used in the fabrication of the butt-welded specimens for the current series of tests is shown in Fig. 4.2 (McKay covered electrode). The procedure, using 1-in. thick base material, was qualified in accordance with procedures recommended by the U. S. Steel Corporation (9) and those required by the U. S. Navy for fabrication of HY-80 submarine hulls. (10) The qualification tests included the reduced section tension test, side bend test, macroetch specimens, and radiographic inspection; the quantitative results of the tension tests and side bend tests are reported in Table 4.2.

The welding procedure described above was used also in the preparation of test specimens containing intentional defects, except that measures similar to those described in Section 3.2 were taken to deposit specific types and quantities of flaws in the weldments.

4.2.1 Failure at Toe of Weld

Three HY-100(T) butt-welded plate specimens were tested in the as-welded condition; two failed at the toe of the weld and one initiated failure

at internal defects. The test data are reported in Table 4.3. The results of the tests of the two specimens that failed at the toe of the weld are plotted in Fig. 4.3 for comparison with the data and S-N curve for as-welded HY-100 specimens tested in a previous study. (7) The fatigue strengths exhibited by the current test specimens are equivalent to those of the earlier HY-100 weldments; this was to be expected because fatigue crack initiation in these specimens is governed primarily by the geometrical conditions (stress raiser) at the toe of the weld, and is relatively insensitive to slight variations in the composition of the filler metal or base material.

4.2.2 Failure at Internal Defects

The specimens used in this part of the study were tested with the reinforcement removed and the plate surfaces polished to preclude the possibility of fatigue failure initiating at the toe of the weld reinforcement. Six of the seven HY-100(T) butt-welded specimens tested with the reinforcement removed failed at internal defects; in addition, one as-welded specimen, LA-5 (see Table 4.3), also failed at internal flaws and is included in the following discussions. Table 4.4 presents the results of the fatigue tests and includes descriptions of the defects detected in the radiographic inspections and those observed on the fracture surfaces. It is significant that the defect at which failure occurred was not detected in the initial radiographs of five of the seven specimens.

The results of the fatigue tests of the HY-100(T) weldments are plotted in Fig. 4.4 with the data from previous tests (6,7) of similar specimens fabricated with the earlier HY-100 base material. The data for the current tests are within the scatter of the previous test results except for

three specimens that exhibited considerably longer lives at the 0 to +80 ksi stress cycle. As with the HY-130(T) weldments reported in Section 3.2, the wide scatter in the fatigue lives of the HY-100(T) specimens may be attributed to the nature of the defect at the crack initiation site, including the type (geometry) and size of defect, its position relative to other weld flaws and to the surface of the specimen, and the nature of the residual stress field. In this regard, it may be noted that the range of fatigue lives exhibited by the HY-100(T) weldments lies approximately within the scatter band for the HY-130(T) specimens, Fig. 3.8, for both the 0 to +50 ksi and 0 to +80 ksi stress cycles.

Fatigue crack propagation was observed as described in Section 2.3 during the testing of two of the HY-100(T) weldments: LA-10 (tested at 0 to +80 ksi) and LA-11 (at 0 to +50 ksi). The progression patterns of the fatigue cracks are illustrated in Figs. 4.5 and 4.6 for the two specimens; the estimated number of cycles spent in crack propagation is reported in Table 4.5. By comparing the fatigue crack propagation lives of LA-10 and LA-11 with those observed for the HY-130(T) welds tested at equivalent stress levels (Table 3.8), the data are seen to be within the same general range. Although no significant conclusions can be drawn from the results of two tests, the data do appear to offer further support of the observation in Section III that, for cyclic stresses within the nominal elastic range of each of the individual grades of the HY-series steels considered herein, the fatigue behavior of weldments initiating cracking at internal weld defects is strongly influenced by the nature of the defect at the location of initiation, with material characteristics being of only secondary concern.

V. SUMMARY AND CONCLUSIONS

5.1 Studies of HY-130(T) Steel

5.1.1 Fatigue of Plain Plates and Butt Welds

The behavior, under repeated axial loads, of plain plates and butt weldments fabricated using HY-130(T) base material has been studied and the data compared to the test results for similar specimens of HY-80 and HY-100 steel. The results of the current fatigue tests, conducted at a stress cycle of zero-to-tension, have indicated the following:

For the HY-130(T) material, surface condition was found to have a marked effect on the fatigue resistance of the plain plate specimens. The fatigue lives of polished plates and plates with descaled (grit-blasted) and painted surfaces were essentially the same; at a stress cycle of 0 to +80 ksi, the average life of the plates with treated surfaces was four times the average for plates with mill-scale intact.

Within the range of lives from approximately 10^4 to 10^6 cycles, the fatigue behavior of the as-rolled plain plate specimens (mill-scale intact) was similar for the HY-80, HY-100 and HY-130(T) steels; the combined data for the three steels can be adequately described by a single S-N curve within this life range.

The fatigue lives of HY-130(T) butt weldments (as-welded) in which crack initiation occurred at the toe of the weld showed little scatter. The time to initiation of fatigue cracking appears to be governed primarily by the surface geometry at the toe of the weld, and is relatively independent of differences between the two welding processes (GMA and SMA) used in the fabrication of the weldments.

For maximum cyclic stresses above approximately 50 ksi, the fatigue behavior of the butt weldments of the HY-80, HY-100 and HY-130(T) steels exhibiting toe-initiated failures could be represented by a single S-N curve. For these combined data, the reductions in fatigue strength relative to the behavior of the plain plate specimens were most pronounced at the longer lives reflecting, in part, the earlier initiation of fatigue cracking in the welds at the stress raiser provided by the toe of the reinforcement. At 500,000 cycles, the average fatigue strength of the welded specimens was 27.5 ksi, in comparison to the 50 ksi fatigue strength of the plain plates; at 20,000 cycles, the fatigue strength of the welds increased to almost 90 percent of the 100 ksi average fatigue strength of the plain plates, which is indicative of a proportionately longer and similar life fraction spent in crack propagation for both specimen types at the higher stresses.

Wide variations in fatigue life at all test stress levels were exhibited by the HY-130(T) butt-welded specimens in which cracking initiated at internal weld discontinuities. The scatter in lives could not be explained solely on the basis of the type of weld defect initiating failure, nor could it be attributed to differences in the weld metal composition or the welding process. Further, the one- or two-dimensional characteristics of the defect which are commonly used as the basis for radiographic NDT acceptance standards (viz., defect length measured parallel to the weld axis, or total area of defect) were found to be largely inappropriate for estimating the total life expectancy of a weldment with internal flaws. The test data have indicated, however, that the fraction of the total life spent in (macroscopic) crack propagation could be estimated with reasonable reliability if the through-thickness dimension (width) of the crack-initiating defect, the position of

the defect relative to the specimen surface, and the nominal cyclic stress were known.

5.1.2 Crack Initiation and Propagation

Measurements were made of the point at which observable (by radiography) fatigue cracks began to propagate from the boundaries of internal weld defects in HY-130(T) weldments. The results have shown that a large fraction of the total fatigue lives of these specimens is often spent in crack propagation and, particularly at the higher stress levels and for the more severe defects, the crack propagation period may in fact constitute almost the entire fatigue life of the specimen.

The results of the experimental portions of this study have been compared with the propagation lives calculated using the concepts and equations of fracture mechanics. The data agree well with these theories and several conclusions may be drawn from the results:

1. The effect of flaw width (dimension in the through-thickness direction) and the ratio of flaw width to the plate thickness are dominant in controlling the length of the period spent in crack propagation at a specific stress level.
2. The position of the flaw relative to the centerline of the weld is an important parameter in determining the propagation life. Larger flaws positioned off the centerline of the weld should propagate to failure more rapidly than ones located in exactly the middle of the plate. For very small flaws this is not as important an effect.
3. For very small flaws, where the finiteness of the plate does

not affect the flaw during its early stages of crack propagation, the actual geometry of the flaw, i.e., whether it is elongated or spherical, is influential in determining the propagation life. For flaws which are large relative to the plate thickness, the geometry of the flaws influences the propagation life only to a minor extent.

Further study and more refined experimental techniques will be required to determine more accurately the period of life spent in initiating an active fatigue crack and the role of flaw size, flaw geometry and stress level in determining that life.

Until such time as the factors controlling this initiation period are better understood and permit the length of that period to be predicted, the fatigue lives of weldments failing at internal flaws may be estimated by neglecting the crack initiation period and using the concepts of fracture mechanics to (empirically) predict the number of cycles spent in crack propagation and, hence, the minimum expected total life. Furthermore, from the demonstrated sensitivity of the propagation life to initial width of the flaw, it would seem that the fatigue life of a weldment in service should be assumed to be no better than that resulting from the largest flaw (through-thickness dimension) which may be permitted or remain undetected by the post fabrication nondestructive inspection standards used.

5.1.3 Acoustic Emission Study

The results of preliminary studies of the acoustic emission characteristics of HY-130(T) steel indicate that there is a definite difference in acoustic emissions from notched and unnotched specimens in a static tension

test. These results agree with the belief that acoustic emissions have a definite correlation with internal dislocation activity. In addition, the results obtained from monitoring a specimen subjected to fatigue cycling indicate that acoustic emission monitoring may be used effectively to detect the onset of crack propagation and, therefore, is a potentially valuable tool for in-service nondestructive testing of structures subject to fatigue. Further studies in this area should be undertaken to provide additional information regarding the capabilities and limitations of this inspection technique.

5.2 Studies of HY-100(T) Steel

Preliminary studies of the fatigue behavior of plain plates and butt weldments of HY-100(T) steel have been conducted. These studies have included examination of the fatigue lives of welded specimens containing internal weld defects, together with measurements of the separate stages of initiation and propagation of cracks originating at the internal flaws. The results of the tests, conducted at a zero-to-tension stress cycle, have indicated the following:

As with the HY-130(T) material, surface treatment was found to improve the fatigue behavior of the HY-100(T) plain plate specimens. At a stress cycle of 0 to +80 ksi, the average fatigue life of two plates with grit-blasted surfaces was approximately six times the average life of HY-100 as-rolled plates (mill-scale intact). The improvement in behavior resulting from this surface treatment apparently decreases, however, at cyclic stresses approaching the yield strength of the steel.

Butt-welded HY-100(T) specimens exhibiting fatigue crack initiation at the toe of the weld reinforcement had lives equivalent to those obtained

for similar weldments fabricated using an earlier grade of HY-100 steel. Furthermore, as noted above, these lives were within the same range as the lives exhibited by comparable welds in HY-80 and HY-130(T) steel in which fatigue cracking also initiated at the toe of the weld.

Butt-welded specimens (including those fabricated with the HY-100(T) and the earlier HY-100 base plate material) exhibited considerable scatter in fatigue lives in tests where crack initiation occurred at internal weld defects. The wide variations in life were comparable to those exhibited by similar specimens of HY-130(T) steel; this suggests that the same geometric variables, including defect configuration and position, are primarily responsible for the crack initiation and propagation characteristics of both materials within the range of cyclic stresses studied. Comparisons of the crack propagation lives of two HY-100(T) butt-welded specimens with similar measurements for HY-130(T) weldments were found to offer support to the conclusions of other investigators that the rate of crack propagation is approximately the same for each of the three high-strength steels considered herein.

LIST OF REFERENCES

1. Sahgal, R. K., and Munse, W. H., "Fatigue Behavior of Axially Loaded Weldments in HY-80 Steel," Civil Engineering Studies, Structural Research Series No. 204, University of Illinois, Urbana, Illinois, September 1960.

2. Hartmann, A. J., and Munse, W. H., "Fatigue Behavior of Welded Joints and Weldments in HY-80 Steel Subjected to Axial Loadings," Civil Engineering Studies, Structural Research Series No. 250, University of Illinois, Urbana, Illinois, July 1962.

3. Zimmerman, J. E., Jr., and Munse, W. H., "Fatigue Behavior of Defective Welded Joints in HY-80 Steel Subjected to Axial Loadings," Civil Engineering Studies, Structural Research Series No. 252, University of Illinois, Urbana, Illinois, July 1962.

4. Hartmann, A. J., Bruckner, W. H., Mooney, J., and Munse, W. H., "Effect of Weld Flaws on the Fatigue Behavior of Butt-Welded Joints in HY-80 Steel," Civil Engineering Studies, Structural Research Series No. 275, University of Illinois, Urbana, Illinois, December 1963.

5. Munse, W. H., Bruckner, W. H., Hartmann, A. J., Radziminski, J. B. Hinton, R. W., and Mooney, J. L., "Studies of the Fatigue Behavior of Butt-Welded Joints in HY-80 and HY-100 Steel," Civil Engineering Studies, Structural Research Series No. 285, University of Illinois, Urbana, Illinois, November 1964.

6. Munse, W. H., Bruckner, W. H., Radziminski, J. B., Hinton, R. W., and Leibold, J. W., "Fatigue of Plates and Weldments in HY-100 and HY-130/150 Steels," Civil Engineering Studies, Structural Research Series No. 300, University of Illinois, Urbana, Illinois, December 1965.

7. Radziminski, J. B., Hinton, R. W., Meinheit, D. F., Osman, H. A., Bruckner, W. H., and Munse, W. H., "Fatigue of Plates and Weldments in High Strength Steels," Civil Engineering Studies, Structural Research Series No. 318, University of Illinois, Urbana, Illinois, February 1967.

8. Radziminski, J. B., Lawrence, F. V., Mukai, S., Panjwani, P. N., Johnson, R., Mah, R., and Munse, W. H., "Low Cycle Fatigue of HY-130(T) Butt Welds," Civil Engineering Studies, Structural Research Series No. 342, University of Illinois, Urbana, Illinois, December 1968.

9. Porter, L. F., Rathbone, A. M., *et al.*, "The Development of an HY-130(T) Steel Weldment," Applied Research Laboratory Report No. 39.018-001 (64), U. S. Steel Corporation, Monroeville, Pa., July 1966.

10. NAVSHIPS Specification No. 0900-006-9010, "Fabrication, Welding and Inspection of HY-80 Submarine Hulls," Naval Ship Engineering Center, Navy Department, Washington, D. C., June 1966.

11. Reemsnyder, H. S., "Procurement and Analysis of Structural Fatigue Data," *Journal of the Structural Division*, ASCE, Vol. 95, No. ST7, Proc. Paper 6693, July 1969, pp. 1533-1551.

12. Schwab, R. C., and Gross, M. R., "Fatigue Properties of 5 Ni-Cr-Mo-V, HY-130/150 Steel," MEL R&D Phase Report 365/65, U. S. Navy Marine Engineering Laboratory, Annapolis, Md., October 1965.

13. Haak, R. P., Loginow, A. W., and Rolfe, S. T., "Rotating-Beam Fatigue Studies of Experimental HY-130/150 and HY-180/210 Steels," Applied Research Laboratory Report No. 40.018-001(32), U. S. Steel Corporation, Monroeville, Pa., December 1964.

14. Haaijer, G., "Design Data for High-Yield-Strength Alloy Steel," *Journal of the Structural Division*, ASCE, Vol. 92, No. ST4, Proc. Paper 4887, August 1966, pp. 31-49.

15. Crooker, T. W. and Lange, E. A., "Low Cycle Fatigue Crack Propagation Resistance of Materials for Large Welded Structures," *Fatigue Crack Propagation, ASTM STP 415*, Am. Soc. Testing Matls. 1967, pp. 94-126.

16. Barsom, J. M., Imhof, E. J., Jr., and Rolfe, S. T., "Fatigue-Crack Propagation in High-Strength Steels," Applied Research Laboratory Report No. 39.018-007(27), U. S. Steel Corporation, Monroeville, Pa., December 1968.

17. "Guide for Interpretation of Non-Destructive Tests of Welds in Ship Hull Structures," Ship Structure Committee Report SSC-177, Prepared by National Academy of Sciences - National Research Council, Washington, D. C., September 1966.

18. Enis, A. and Telford, R. T., "Gas Metal-Arc Welding of HY-130(T) Steel," *Welding Journal*, Vol. 47, No. 6, June 1968, Research Supplement, pp. 271s-278s.

19. Burdekin, F. M., Harrison, J. D., and Young, J. G., "The Effect of Weld Defects with Special Reference to BWRA Research," *Welding Research Abroad*, Welding Research Council, Vol. XIV, No. 7, August - September 1968. Reprinted from the *Australian Welding Journal*, January 1968.

20. Schijve, J., "Significance of Fatigue Cracks in Micro-Range and Macro-Range," *Fatigue Crack Propagation, ASTM STP 415*, Am. Soc. Testing Matls., 1967, pp. 415-457.

21. Harrison, J. D., "The Analysis of Fatigue Results for Butt Welds with Lack of Penetration Using a Fracture Mechanics Approach," *Fracture*, Proceedings of the Second International Conference on Fracture, Brighton, April 1969.

22. Fisher, J. W., Frank, K. H., Hert, M. A., and McNamer, B. M., "Effect of Weldments on the Fatigue Strength of Steel Beams," Fritz Engineering Laboratory, Department of Civil Engineering, Lehigh University, September 1969.

23. Sinclair, G. M. and Rolfe, S. T., "Analytical Procedure for Relating Subcritical Crack Growth to Inspection Requirements," Applied Research Laboratory Report No. 39.018-007(26), U. S. Steel Corporation, Monroeville, Pa., January 1969.

24. Miller, G. A., "The Dependence of Fatigue Crack Growth Rate on the Stress Intensity Factor and the Mechanical Properties of Some High-Strength Steels," Trans. ASM, Vol. 61, 1968.

25. NAVSHIPS Specification No. 0900-006-3010, "Ultrasonic Inspection Procedure and Acceptance Standards for Production and Repair Welds," Naval Ship Engineering Center, Navy Department, Washington, D. C., January 1966.

26. Paris, P. C. and Sih, G. C., "Stress Analysis of Cracks," *Fracture Toughness Testing and Its Applications, ASTM STP 381*, Am. Soc. Testing Matls., 1965.

27. Feddersen, C. E., Discussion to "Plane Strain Crack Toughness Testing of High Strength Metallic Materials," by Brown, W. F., and Srawley, J. E., *Plain Strain Crack Toughness Testing of High Strength Metallic Materials, ASTM STP 410*, Am. Soc. Testing Matls., 1967.

28. Dunegan, H. L. and Harris, D. O., "Acoustic Emission: A New Nondestructive Testing Tool," Lawrence Radiation Laboratory, January 1968.

29. Mah, R., "Acoustic Emission from Deformed Metals," Master's Thesis Submitted to the Graduate College, University of Illinois, Urbana, Illinois, 1970.

30. Dunegan, H. L., Harris, D. O., and Tatro, C. A., "Fracture Analysis by Use of Acoustic Emission," *Engineering Fracture Mechanics*, Vol. 1, 1968, pp. 105-122.

31. Kaiser, J., "Untersuchungen über das Auftreten non Geranschen beim Zugnersuch," Ph.D., Technischen Hochschule, München, 1950.

TABLE 2.1

CHEMICAL COMPOSITION OF HY-130(T) BASE METAL

(Data Supplied by U. S. Steel Corporation)

Heat Number	5P2456	5P2004
Fatigue Specimen Designation	ND	NE
Chemical Composition, percent		
C	0.10	0.11
Mn	0.84	0.88
P	0.007	0.003
S	0.004	0.006
Si	0.24	0.35
Ni	4.92	4.95
Cr	0.54	0.53
Mo	0.50	0.50
V	0.08	0.08
Ti	0.04	--
Cu	0.06	0.07

TABLE 2.2

MECHANICAL PROPERTIES OF HY-130(T) BASE METAL

(Data Supplied by U. S. Steel Corporation)

Heat Number	Fatigue Specimen Designation	Plate Thickness (inches)	Properties in Longitudinal Direction				
			Yield Strength* (ksi)	Tensile Strength (ksi)	Elong. in 2 inches (percent)	Reduction in Area (percent)	Charpy V-Notch (ft-lbs @ 0°F)
5P2456†	ND	1	140.4	149.2	20.0	64.4	83
5P2004†	NE	1	141.6	152.0	20.0	63.8	90

*0.2 percent offset.

†Plates received descaled and one coat painted.

TABLE 2.3

CHEMICAL COMPOSITION OF ELECTRODES FOR WELDING HY-130(T) PLATES*

Manufacturer	Linde Division, Union Carbide Corporation			McKay Company	
Electrode Designation	Linde 140			McKay 14018	
Electrode Type	1/16" bare-electrode wire			5/32", 3/16" covered electrodes	
Heat Number	106140			1P1375	
Lot Number		291085	272485	21475†	
Batch Number		1149	9908	3167	3166
Chemical Composition (percent)		5/32"	3/16"	5/32"	3/16"
C	0.11	0.083	0.078	0.077	0.81
S	0.007	0.004	0.007	0.003	0.004
P	0.008	0.004	0.005	0.003	0.003
Mn	1.72	1.98	2.00	1.91	1.85
Si	0.36	0.47	0.46	0.42	0.39
Ni	2.49	2.12	2.02	2.08	1.92
Cr	0.72	0.68	0.75	0.71	0.73
Mo	0.88	0.44	0.45	0.43	0.43
V	0.01	--	--	--	--
Cu	0.08	--	--	--	--

* Data supplied by manufacturer.

† Lot 21475 used on McKay-welded specimens up to ND-46, except ND-38. Combination of Batch No. 1149 and Batch No. 3166 used on other McKay-welded specimens.

TABLE 2.4

CHEMICAL COMPOSITION OF HY-100(T) BASE METAL
(Data supplied by U.S. Steel Corporation)

Heat Number	5P3524	N15423
Fatigue Specimen Designation	LA*	HY
Chemical Composition, percent		
C	0.10	0.20
Mn	0.79	0.30
P	0.005	0.010
S	0.011	0.014
Si	0.28	0.21
Ni	3.36	3.00
Cr	0.90	1.67
Mo	0.41	0.50
V	0.09	-
Ti	-	-
Cu	-	0.11

*Manufacturer's designation for steel: HY-110

TABLE 2.5

MECHANICAL PROPERTIES OF HY-100(T) BASE METAL

(Data supplied by U.S. Steel Corporation)

Heat Number	Fatigue Specimen Designation	Plate Thickness (inches)	Properties in Longitudinal Direction				
			Yield Strength* (ksi)	Tensile Strength (ksi)	Elong. in 2 inches (percent)	Reduction in Area (percent)	Charpy V-Notch (ft-lbs @ 0°F)
5P3524†	LA	1	110	124	22.0	68.4	98
N15423††	HY	3/4	110.0	127.5	23.0	71.1	83

*0.2 percent offset.

†Plates received grit blasted. Manufacturer's designation for steel: HY-110

††Plates received as-rolled; used in previous study(5)

TABLE 2.6

CHEMICAL COMPOSITION OF ELECTRODES FOR WELDING HY-100(T) PLATES

(Data Supplied by Manufacturer)

Manufacturer		McKay Company
Electrode Designation		12018
Electrode Type		Coated Electrode
Heat Number		-
CHEMICAL COMPOSITION	C	.07
	S	.022
	P	.015
	Mn	1.50
	Si	.40
	Ni	2.00
	Cr	.45
	Mo	.40

TABLE 3.1

RESULTS OF FATIGUE TESTS OF HY-130(T) PLAIN PLATE SPECIMENS

Specimen Number*	Surface Condition	Stress Cycle (ksi)	Life (cycles)	Location of Failure
NA-8	As-Rolled**	0 to +100.0	26,800	At mill scale surface in test section
NA-7	As-Rolled	0 to +100.0	21,000	At mill scale surface in test section
NA-1	As-Rolled	0 to + 80.0	64,200	At radius of test section
NA-2	As-Rolled	0 to + 80.0	60,900	At mill scale surface in test section
NC-13	As-Rolled	0 to + 80.0	59,800	At mill scale surface in test section
NA-5	As-Rolled	0 to + 80.0	51,100	At polished edge of specimen test section
NC-14	As-Rolled	0 to + 80.0	50,500	At mill scale surface in test section
NA-10	As-Rolled	0 to + 50.0	1,247,800+	Failure in pull-head
NA-6	As-Rolled	0 to + 50.0	712,000+	Failure in pull-head
NA-4	As-Rolled	0 to + 50.0	515,000± ***	At mill scale surface in test section
NA-9	As-Rolled	0 to + 50.0	345,500	At mill scale surface in test section
NA-3	As-Rolled	0 to + 50.0	280,900	At radius of test section
NA-11	Polished	0 to +100.0	176,000	At radius of test section
NA-14	Polished	0 to +100.0	110,500	At radius of test section
NA-13	Polished	0 to + 80.0	304,300	At radius of test section
NA-15	Polished	0 to + 80.0	208,800	At two locations on polished edge of test section
NE-1	Descaled & Painted	0 to + 80.0	330,800	At polished edge in test section
NE-5	Descaled & Painted	0 to + 80.0	252,700	At radius of test section
ND-3	Descaled & Painted	0 to + 80.0	249,000	At radius of test section
ND-2	Descaled & Painted	0 to + 80.0	187,800	At a corner in test section

*Specimens designated by prefix NA, NC and ND were tested in earlier studies (6-8)

**Mill-scale intact on specimen surfaces.

***Cycle counter on fatigue machine broke during test-failure occurred between 484,000 and 627,000 cycles.

TABLE 3.2

FATIGUE OF HY-130(T) PLAIN PLATES -
STRESS CYCLE: 0 to +80 ksi

Mill-Scale Intact		Polished		Descaled and Painted	
Specimen No.	Life, Cycles	Specimen No.	Life, Cycles	Specimen No.	Life, Cycles
NA-1	64,200	NA-13	304,300	NE-1	330,800
NA-2	60,900	NA-15	208,800	NE-5	252,700
NC-13	59,800			ND-3	249,000
NA-5	51,100			ND-2	187,800
NC-14	50,500				
Avg.	57,300	Avg.	256,500	Avg.	255,100

TABLE 3.3

RESULTS OF NDT EXAMINATION AND FATIGUE TESTS OF HY-130(T) TRANSVERSE BUTT WELDS IN THE AS-WELDED CONDITION[a]

FAILURE AT TOE OF WELD

Specimen Number	Welding Procedure (see Ref. 8)	Radiographic Examination			Stress Cycle (ksi)	Life (cycles)
		Defect Description	Defect Area (percent)	Rating		
NC-32	P130(T)-USS-A	Sound weld	--	P	0 to +80.0	25,800
NC-33	P130(T)-USS-A	Sound weld	--	P	0 to +80.0	19,600
ND-23	P130(T)-USS-A	Sound weld	--	P	0 to +80.0	16,300
NC-38	P130(T)-L140-A	Sound weld	--	P	0 to +80.0	29,100
NC-39	P130(T)-L140-A	Sound weld	--	P	0 to +80.0	21,000
NC-45	P130(T)-M140-A	Sound weld	--	P	0 to +80.0	25,800
NC-36	P130(T)-USS-A	Weld undercut, 0.03" deep x 0.4" long	--	F[b]	0 to +60.0	115,300
NC-42	P130(T)-L140-A	Sound weld[c]	--	P	0 to +60.0	70,000
NC-41	P130(T)-L140-A	Sound weld[c]	--	P	0 to +60.0	69,200
NC-50	P130(T)-L140-A	Single pore, 0.04" d.	0.041	P	0 to +60.0	56,200
NC-34	P130(T)-USS-A	Porosity cluster	0.33	F	0 to +50.0	526,100
NC-49	P130(T)-M140-A	Sound weld	--	P	0 to +50.0	119,500
NC-35	P130(T)-USS-A	Single pore, 0.04" d.	0.037	P	0 to +58.0	138,200[d]

[a] Data from previous study[8].

[b] Visual inspection rating.

[c] Weld originally contained surface crack 1-1/4" long; area repaired by grinding to sound metal and rewelding.

[d] Failure initiated on surface of base metal removed from toe of weld.

TABLE 3.4

COMPARISON OF FATIGUE STRENGTHS OF
PLAIN PLATES AND BUTT WELDS

Combined Data for HY Series Steels

Type of Specimen	Fatigue Life, Cycles	Fatigue Strength, ksi	Percent of Plain Plate Fatigue Strength
Plain Plate, mill scale intact	20,000	100	-
	50,000	82	-
	100,000	71	-
	200,000	61	-
	500,000	50	-
	2,000,000	37.5	-
Butt Weld, as-welded (failure at toe of weld)	20,000	86	86
	50,000	62	76
	100,000	48.5	68
	200,000	38	62
	500,000	27.5	55
	2,000,000	(16.5)[a]	44

[a] Estimated.

TABLE 3.5

RESULTS OF NDT EXAMINATION AND FATIGUE TESTS OF HY-130(T)
TRANSVERSE BUTT WELDS WITH REINFORCEMENT REMOVED

Specimen Number	Welding Procedure[a] (see Figs.3.6,3.7)	Radiographic Examination: Defect Description	Radiographic Examination: Defect Area (percent)	Rating	Stress Cycle (ksi)	Life (cycles)	Location of Failure
ND-27	P130(T)-L140-A	Sound weld	---	P	0 to +80.0	86,300	In weld metal
ND-43	P130(T)-L140-A	Intermittent lack of fusion, 0.25", 0.16" long	---	F	0 to +80.0	28,900	At lack of penetration, 0.7" long; & at single pore, 0.04" d.
ND-41†	P130(T)-L140-A	Lack of fusion, 0.3" long, & irreg. shaped void, 0.26" x 0.14"	1.55	F	0 to +80.0	9,030	At intermittent lack fo fusion, 0.94" total length; secondary crack at irreg. shaped void 0.3" x 0.2"
ND-36†	P130(T)-L140-A	Lack of fusion, 0.25" long; & 3 dispersed pores, 0.04", 0.05" d.	0.214	F	0 to +80.0	6,600	At lack of fusion, 0.35" long
ND-44†	P130(T)-L140-A	Intermittent lack of fusion, 0.12", 0.08" long	---	P	0 to +80.0	5,800	At intermittent lack of fusion, 0.4" total length
ND-37†	P130(T)-L140-A	Lack of fusion, 0.16" long; & porosity, pores 0.01" to 0.03" d.	0.198	P	0 to +80.0	5,600	At intermittent lack of fusion, 0.45" total length
ND-40†	P130(T)-L140-A	Elongated void 0.6" x 0.06"	1.3	F	0 to +80.0	5,380	At irreg. shaped void, 0.6" x 0.10"
ND-42	P130(T)-L140-A	Lack of fusion, 0.18" long; & pore, 0.03" d.	0.033	F	0 to +80.0	4,450	At intermittent lack of fusion, 0.58" total length
NE-10††	P130(T)-L140-A	4 dispersed pores, 0.03" - 0.05" d.	0.22	P	0 to +80.0	3,250	At intermittent lack of fusion, 0.96" total length
NE-9	P130(T)-L140-A	4 dispersed pores, 0.02" - 0.04" d.	0.173	P	0 to +80.0	1,760	At intermittent lack of fusion, 0.74" total length; & at minute porosity
ND-39	P130(T)-L140-A	Lack of fusion, 0.5" long; & 3 irreg. shaped voids, 0.35" x 0.08", 0.18" x 0.1", 0.08" x 0.06"	1.8	F	0 to +80.0	1,500	At intermittent lack of fusion, 1.17" total length; & at 2 irreg. shaped voids, 0.34" x 0.16", 0.2" x 0.08"
ND-33	P130(T)-L140-A	Sound weld	---	P	0 to +80.0	133,000+	Crack through half of width at radius of test section, test not completed
ND-46†	P130(T)-M140-A	2 irreg. shaped voids, 0.2" x 0.1", 0.08" x 0.06"	0.90	P	0 to +80.0	42,800	At intermittent slag, 0.18" total length; & at 2 pores, 0.03", 0.02"d
ND-47††	P130(T)-M140-A	Slag deposit, 0.05" x 0.04"	0.076	P	0 to +80.0	10,400	At slag deposit, 0.06" long
ND-45††	P130(T)-M140-A	Irreg. shaped void, 0.22" x 0.1"	0.80	P	0 to +80.0	6,750	At slag deposit, 0.22" long
ND-38††	P130(T)-M140-A	Slag deposits, 0.06" x 0.04" (2); & 3 pores, 0.02" d.	0.239	P	0 to +80.0	5,700	At slag deposit, 0.06" long
NE-8†	P130(T)-M140-A	4 dispersed pores, 0.03", 0.02"d.; & at slag deposits, 0.08" x 0.06", 0.04" x 0.03", 0.04" x 0.05"	0.406	P	0 to +80.0	4,970	At slag deposit, 0.44" long; & at 2 pores, 0.02" d.
ND-34	P130(T)-M140-A	Sound weld	---	P	0 to +80.0	158,600	At radius of test section
NE-7†	P130(T)-M140-A	Slag deposits, 0.1" d, 0.08" d, 0.04" d, & 0.03" x 0.02"; & porosity cluster, 16 pores 0.01" to 0.04" d.	1.54	F	0 to +80.0	2,870	At slag deposits, 0.12" x 0.09", 0.04" x 0.02", 0.01" d.; & at 2 pores 0.01" d., 0.02" d.
NE-11††	P130(T)-M140-A	2 cracks ⊥ weld axis, 0.50" long; & slag deposit 0.52" x 0.06"	1.53	F	0 to +80.0	4,830	At pore, 0.01" d.; secondary crack at 3 pores, 0.01" d.
NE-12††	P130(T)-M140-A	2 cracks ⊥ weld axis, 0.54", 0.48" long; & lack of fusion, 0.38" long	---	F	0 to +80.0	4,400	At slag deposit, 0.50" x 0.08"; secondary crack at pore, 0.06" d.

a. Welding procedures altered to intentionally introduce specific weld defects.

† Specimen subjected to periodic radiographic examination during cycling.

†† Specimen subjected to periodic radiographic examination during cycling, & to ultrasonic inspection before cycling and after radiographic indication of fatigue cracking.

TABLE 3.6

RESULTS OF NDT EXAMINATION AND FATIGUE TESTS OF HY-130(T) TRANSVERSE BUTT WELDS WITH REINFORCEMENT REMOVED[a] -- FAILURE AT INTERNAL DEFECTS

Specimen Number	Welding Procedures[b] (see Refs. 7,8)	Radiographic Examination			Stress Cycle (ksi)	Life (cycles)	Location of Failure
		Defect Description	Defect Area (percent)	Rating			
ND-9	P130(T)-USS-A	Sound weld	---	P	0 to +80.0	170,000	In weld metal
ND-6	P130(T)-USS-A	Sound weld	---	P	0 to +80.0	95,300	At minute dispersed porosity, <0.01" d.
ND-26	P130(T)-USS-A	2 pores, 0.04" d.	0.121	P	0 to +80.0	95,000	At lack of fusion, 0.10" long.
ND-22	P130(T)-USS-A	Sound weld	---	P	0 to +80.0	69,000	In weld metal
ND-24	P130(T)-USS-A	2 pores, 0.07", 0.02" d.	0.238	P	0 to +80.0	17,800	At lack of fusion, 0.25" long;& at irreg. shaped void, 0.35" x 0.03"
ND-13	P130(T)-L140-A	4 dispersed pores, 0.01" to 0.03" d.	0.66	P	0 to +80.0	110,000	At single pore, 0.03" d.
ND-11	P130(T)-L140-A	Sound weld	---	P	0 to +80.0	4,300	At intermittent lack of fusion, 1.05" total length
ND-16	P130(T)-M140-A	Crack, 0.20" long ⊥ weld axis	---	F	0 to +80.0	6,200	At elongated slag deposit, 0.3" long
ND-25	P130(T)-USS-A	6 dispersed pores, 0.02" to 0.05" d.	0.15	P	0 to +50.0	651,900	At 3 separate pores, 0.02", 0.03", 0.05" d.
ND-8	P130(T)-USS-A	Lack of fusion, 0.38" long	---	F	0 to +50.0	59,500	At lack of fusion, 0.97" long
ND-21	P130(T)-USS-A	Irreg. shaped voids, 0.45" x 0.12", 0.1" x 0.06"; crack, 0.12" long; & 2 pores, 0.04" d.	1.5	F	0 to +50.0	43,800	At void, 0.35" x 0.2"
ND-20	P130(T)-USS-A	Lack of penetration, 0.76" long; & irreg. shaped void, 0.24" x 0.1"	0.61	F	0 to +50.0	36,000	At lack of penetration, 0.3" long; & at irreg. shaped void, 0.2"x0.1"
ND-12	P130(T)-L140-A	Lack of penetration, 0.4" long; & 2 pores, 0.04", 0.02" d.	0.048	F	0 to +50.0	219,200	At lack of penetration, 0.52" long
ND-28	P130(T)-L140-A	6 dispersed pores, 0.02" to 0.05" d.	0.18	P	0 to +50.0	72,300	At intermittent lack of fusion, 0.5" total length
ND-10	P130(T)-L140-A	Intermittent lack of fusion, 0.3" long; & 2 pores, 0.04" d.	0.072	P	0 to +50.0	27,500	At intermittent lack of fusion 0.65" total length
ND-18	P130(T)-M140-A	Crack, 0.4" long ⊥ weld axis; & slag deposit 0.35" x 0.15"	1.23	F	0 to +50.0	83,800	At slag deposit, 0.55" long
ND-17	P130(T)-M140-A	2 cracks, 0.35", 0.3" long ⊥ weld axis; & elongated slag, 0.95" long	---	F	0 to +50.0	71,300	At 2 cracks ⊥ weld axis; secondary crack at slag deposit, 0.95" long
ND-19	P130(T)-M140-A	Crack, 0.3" long ⊥ weld axis; & slag deposit, 0.4" x 0.15"	1.45	F	0 to +50.0	52,000	At slag deposit, 0.7" long
ND-14	P130(T)-M140-A	Porosity, pores 0.02" to 0.04" d.	0.22	P	0 to +50.0	33,500	At porosity cluster, 0.38% area reduction
ND-15	P130(T)-M140-A	Porosity, pores 0.01" to 0.10" d.	0.94	F	0 to +50.0	32,400	At porosity cluster, 0.92% area reduction
NC-22	P150-AX140-D	Porosity, pores 0.01" to 0.08" d.	1.78	F	0 to +80.0	9,500	At dispersed pores, 0.02", 0.04" 0.045", 0.05" d.
NC-21	P150-AX140-D	Lack of fusion, 0.5" long; & single pore, 0.07" d.	0.21	F	0 to +80.0	3,900	At lack of fusion, 0.9" long
NC-23	P150-AX140-D	Lack of fusion, 0.6" long; & porosity, pores 0.01" to 0.05" d.	0.29	F	0 to +50.0	21,000	In weld metal at linear discontinuity, 3.5" long
NC-20	P150-AX140-D	Porosity, pores 0.02" to 0.05" d.	0.41	F	0 to +50.0	6,600	In weld metal at linear discontinuity, 2.4" long
NC-19	P150-AX140-D	Porosity, pores 0.01" to 0.05" d.	0.75	F	0 to +43.0	2,272,500	At single, isolated pore, 0.08" d.

a. Data from previous studies [7,8]

b. Welding procedures altered to intentionally introduce specific weld defects.

TABLE 3.7

RESULTS OF NDT EXAMINATION AND FATIGUE TESTS OF HY-130(T) TRANSVERSE BUTT WELDS IN THE AS-WELDED CONDITION[a] -- FAILURE AT INTERNAL DEFECTS

Specimen Number	Welding Procedure (see Refs. 7,8)	Radiographic Examination: Defect Description	Defect Area (percent)	Rating	Stress Cycle (ksi)	Life (cycles)	Location of Failure
ND-30	P130(T)-USS-A	Single pore, 0.03" d.	0.038	P	0 to +100.0	4,100	In weld metal
ND-29	P130(T)-L140-A	Sound weld	---	P	0 to +100.0	6,150	At lack of fusion, 0.09" long
ND-31	P130(T)-M140-A	Crack, 0.35" long ⊥ weld axis; & weld undercut, 0.02" deep x 0.25" long	---	F	0 to +100.0	3,150	At crack perpendicular to weld axis; & at single pore, 0.02" d.
NC-31	P130(T)-USS-A	Sound weld	---	P	0 to +80.0	14,700	At lack of fusion, 1.0" long
NC-46	P130(T)-M140-A	Sound weld	---	P	0 to +80.0	22,000	At 2 isolated pores < 0.01" d.
NC-44	P130(T)-M140-A	Sound weld	---	P	0 to +80.0	9,000	At lack of fusion; 0.09" long; & at single pore, 0.02" d.
ND-1	P130(T)-M140-A	Weld undercut, 0.02" deep x 0.08" long	---	P	0 to +80.0	6,200	At lack of fusion, 0.08" long
NC-40	P130(T)-L140-A	Sound weld	---	P	0 to +60.0	12,300	At intermittent lack of fusion, 0.6" total length
ND-4	P130(T)-M140-A	Sound weld	---	P	0 to +60.0	57,500	At lack of fusion, 0.05" long; & at single pore, < 0.01" d.
NC-48	P130(T)-M140-A	Sound weld	---	P	0 to +60.0	27,000	At lack of fusion, 0.09" long
ND-5	P130(T)-M140-A	Sound weld	---	P	0 to +60.0	19,900	At lack of fusion, 0.14" long
NC-47	P130(T)-M140-A	Sound weld	---	P	0 to +60.0	18,400	In weld metal at linear discontinuity, 0.10" long
NC-43	P130(T)-L140-A	Lack of fusion, 0.16" long	---	P	0 to +50.0	52,000	At lack of fusion, 0.06" long
NC-15	P150-AX140-D	Porosity, pores 0.01" to 0.03" d.	0.07	P	0 to +50.0	34,200	At 5 dispersed pores, 0.02" (2), 0.03" (2), .04" d.
NC-11	P150-AX140-D	Porosity, pores 0.02" to 0.04" d.	0.12	P	0 to +50.0	14,800	In weld metal at linear discontinuity 1.63" long
NC-12	P150-AX140-D	Sound weld	---	P	0 to +50.0	12,400	In weld metal at linear discontinuities, 1.4", 0.7" long
NB-3	P150-X150-B	Sound weld	---	P	0 to +50.0	6,900	At lack of fusion, 2.75" long
NC-4	P150-AX140-C	Porosity, pores 0.01" to 0.06" d.	1.26	F	0 to +80.0	13,400	At lack of fusion, 0.66" long; & at 4 pores, 0.02", 0.04"(2), 0.06" d
NC-5	P150-AX140-C	Porosity, pores 0.02" to 0.04" d.	0.28	P	0 to +80.0	10,600	At lack of fusion, 2.25" long
NC-3	P150-AX140-C	Porosity, pores 0.01" to 0.06" d.	1.20	F	0 to +80.0	5,400	At lack of fusion, 0.82" long; & at dispersed pores
NC-7	P150-AX140-D	Porosity, pores 0.03" & 0.11" d.	0.44	F	0 to +80.0	9,900	In weld metal
NC-6	P150-AX140-D	Sound weld	---	P	0 to +80.0	4,050	In weld metal at 2 parallel linear discontinuities, each 1.30" long
NB-6	P150-X150-A	Porosity, pores 0.01" to 0.05" d.	0.914	F	0 to +80.0	19,900	At 3 dispersed pores, 0.025", 0.02", 0.015" d.
NB-7	P150-X150-A	Sound weld	---	P	0 to +80.0	5,100	At lack of fusion
NB-8	P150-X150-A	Single pore, 0.03" d.	0.031	P	0 to +80.0	3,000	At lack of fusion, 2.25" long
NB-4	P150-X150-B	Single pore, 0.06" d.	0.122	P	0 to +80.0	10,100	At lack of fusion, 0.32" long; & at several dispersed minute pores
NB-2	P150-X150-B	Sound weld	---	P	0 to +80.0	2,200	At lack of fusion, 0.45" long
NB-9	P150-X150-B	Sound weld	---	P	0 to +80.0	10,100	At lack of fusion, 0.23" long

a. Data from previous studies (7,8)

TABLE 3.8

RESULTS OF FATIGUE CRACK INITIATION AND PROPAGATION STUDY OF HY-130(T) TRANSVERSE BUTT WELDS CONTAINING INTENTIONAL WELD DEFECTS

Specimen Number	Welding Procedure	Stress Cycle (ksi)	Crack Propagation Life (Cycles)	Total Life (Cycles)	Defect Type (a)	Defect Length (in.)	Defect Width (in.)	Defect Position (in. from surface)
ND-8	P130(T)-USS-A	0-50	14,500	59,500	L	.97	.05	.50
ND-21	P130(T)-USS-A	0-50	16,300	43,800	V	.35	.20	.40
ND-20	P130(T)-USS-A	0-50	31,000	36,000	LP	.30	.06	.38
ND-12	P130(T)-L140-A	0-50	<44,200	219,200	LP	.52	.04	.50
ND-28	P130(T)-L140-A	0-50	+ (b)	72,300	L	.50	.125	.28
ND-10	P130(T)-L140-A	0-50	22,500	27,500	L	.65	.05	.37
ND-18	P130(T)-M140-A	0-50	23,800	83,800	S	.55	.05	.46
ND-17	P130(T)-M140-A	0-50	43,800	71,300	S	.95	.10	.36
ND-19	P130(T)-M140-A	0-50	34,500	52,000	S	.70	.07	.36
ND-14	P130(T)-M140-A	0-50	15,000	33,500	P	.175	.175	.27
ND-15	P130(T)-M140-A	0-50	25,400	32,400	P	.08	.08	.26
ND-25	P130(T)-M140-A	0-50	+	651,900	P	.05	.05	.50
ND-9	P130(T)-USS-A	0-80	+	170,000	P	<.001	<.001	.44
ND-6	P130(T)-USS-A	0-80	9,300	95,300	P	<.001	<.001	.50
ND-26	P130(T)-USS-A	0-80	+	95,000	L	.10	.05	.20
ND-22	P130(T)-USS-A	0-80	+	69,000	P	<.001	<.001	.38
ND-24	P130(T)-USS-A	0-80	+	17,800	V	.35	.025	.32
ND-13	P130(T)-L140-A	0-80	+	110,000	P	.03	.03	.35
ND-11	P130(T)-L140-A	0-80	+	4,300	L	1.05	.12	.28
ND-16	P130(T)-M140-A	0-80	+	6,200	S	.30	.02	.40
ND-27	P130(T)-L140-A	0-80	+	86,300	P	<.001	<.001	.50
ND-43	P130(T)-L140-A	0-80	+	28,900	P	.04	.04	.50
ND-41	P130(T)-L140-A	0-80	2,530	9,030	L	.94	.175	.33
ND-36	P130(T)-L140-A	0-80	6,100	6,600	L	.35	.16	.30
ND-44	P130(T)-L140-A	0-80	4,550	5,800	L	.40	.08	.29
ND-37	P130(T)-L140-A	0-80	4,600	5,600	L	.45	.10	.36
ND-40	P130(T)-L140-A	0-80	2,380	5,380	V	.6	.10	.50
ND-42	P130(T)-L140-A	0-80	+	4,450	L	.58	.10	.35
NE-10	P130(T)-L140-A	0-80	2,250	3,250	L	.96	.05	.35
NE-9	P130(T)-L140-A	0-80	+	1,760	L	.74	.08	.29
ND-39	P130(T)-L140-A	0-80	+	1,500	L	1.17	.20	.41
ND-46	P130(T)-M140-A	0-80	4,850	42,850	S	.18	.05	.25
ND-47	P130(T)-M140-A	0-80	4,950	10,400	S	.06	.05	.32
ND-45	P130(T)-M140-A	0-80	5,730	6,750	S	.22	.08	.35
ND-38	P130(T)-M140-A	0-80	5,200	5,700	S	.06	.04	.24
NE-8	P130(T)-M140-A	0-80	3,220	4,970	S	.44	.02	.50
NE-7	P130(T)-M140-A	0-80	2,620	2,870	S	.12	.09	.40
NE-11	P130(T)-M140-A	0-80	3,230	4,830	P	.01	.01	.22
NE-12	P130(T)-M140-A	0-80	2,900	4,400	S	.50	.08	.41

a.
S = Slag
P = Porosity
V = Void
L = Lack of fusion
LP = Lack of penetration

b.
+ : Not measured

TABLE 4.1

RESULTS OF FATIGUE TESTS OF HY-100(T) PLAIN PLATE SPECIMENS

Specimen Number[a]	Surface Condition	Stress Cycle (ksi)	Life (cycles)	Location of Failure
HY-4	As Rolled[b]	0 to +80.0	46,400	At radius of test section
HY-6	As Rolled	0 to +80.0	57,100	At mill scale surface near radius of test section
HY-7	As Rolled	0 to +76.5	81,200	At mill scale surface near radius of test section
HY-5	As Rolled	0 to +50.0	546,300	At radius of test section
HY-2	As Rolled	0 to +50.0	253,100	At radius of test section
HY-3	As Rolled	0 to +50.0	180,000	At mill scale surface near radius of test section
LA-17	Grit Blasted	0 to +100.0	70,000	At radius of test section
LA-4	Grit Blasted	0 to +100.0	43,000±[c]	At radius of test section
LA-3	Grit Blasted	0 to +80.0	532,500	At polished edge at scribe line
LA-2	Grit Blasted	0 to +80.0	402,000	At polished edge of test section

a. Specimens prefixed HY designate HY-100 steel plates tested in earlier study.[5]

b. Mill scale intact on specimen surfaces.

c. Microswitch failed to turn off machine; failure occurred between 38,000 and 48,000 cycles.

TABLE 4.2

RESULTS OF WELD QUALIFICATION TESTS OF HY-100(T) WELDMENTS

Reduced Section Tension Tests

Electrode Designation	Welding Procedure	Ultimate Tensile Strength, ksi	Area Reduction	Location of Fracture
McKay M12018	P110-M12018-A	131.0	51.3%	Base Metal

Side Bend Tests*

Electrode Designation	Welding Procedure	Total Angle	Maximum Load, lbs.	Remarks
McKay M12018	P110-M12018-A	180°	9000	no cracks
"	"	180°	9000	no cracks
"	"	180°	9260	no cracks
"	"	180°	9340	no cracks

*Bend test radius: 2t

TABLE 4.3

RESULTS OF NDT EXAMINATION AND FATIGUE TESTS OF HY-100(T)
TRANSVERSE BUTT WELDS IN THE AS-WELDED CONDITION

Specimen Number	Welding Procedure (see Fig. 4.2)	Radiographic Examination			Stress Cycle (ksi)	Life (cycles)	Location of Failure
		Defect Description	Defect Area (percent)	Rating			
LA-5	P110-M12018-A	Sound Weld	--	P	0 to +80.0	19,000	At lack of fusion, 0.06" long; & at porosity, pores $\leq$0.01" d.
LA-6	P110-M12018-A	Sound Weld	--	P	0 to +80.0	16,300	At toe of weld
LA-9	P110-M12018-A	Sound Weld	--	P	0 to +50.0	93,500	At toe of weld

TABLE 4.4

RESULTS OF NDT EXAMINATION AND FATIGUE TESTS OF HY-100(T)
TRANSVERSE BUTT WELDS WITH REINFORCEMENT REMOVED

Specimen Number	Welding Procedure[a] (see Fig. 4.2)	Radiographic Examination			Stress Cycle (ksi)	Life (cycles)	Location of Failure
		Defect Description	Defect Area (percent)	Rating			
LA-8	P110-M12018-A	Sound Weld	--	P	0 to +80.0	176,900	At slag deposit, 0.08" x 0.025"
LA-14	P110-M12018-A	Sound Weld	--	P	0 to +80.0	109,600	At single pore, 0.02"d, adjacent to specimen surface
LA-12	P110-M12018-A	2 pores ~0.01"d.	0.008	P	0 to +80.0	101,700	At irreg. shaped void w/slag, 0.05" x 0.02"
LA-7	P110-M12018-A	Sound Weld	--	P	0 to +80.0	>12,000 <22,000(b)	At intermittent lack of fusion and slag, 0.56" total length
LA-10†	P110-M12018-A	Irreg. shaped slag deposit, approx. 0.15" x 0.15"	0.98	P	0 to +80.0	3,400	At lack of fusion, 0.26" long; & at slag deposit 0.25" x 0.33"
LA-13	P110-M12018-A	2 pores, ~0.01"d.	0.008	P	0 to +50.0	>2,194,800	In specimen pull-head
LA-11†	P110-M12018-A	Irreg. shaped slag deposit, approx. 0.29" x 0.04"	0.33	F	0 to +50.0	135,900	At slag deposit, 0.37" x 0.05"

[a] Welding procedure altered to intentionally introduce specific weld defects in several specimens.

[b] Cycle counter malfunction - failure occurred between 12,000 cycles and estimated 22,000 cycles.

† Specimen subjected to periodic radiographic examination during cycling.

TABLE 4.5

RESULTS OF FATIGUE CRACK INITIATION AND PROPAGATION STUDY
OF HY-100(T) TRANSVERSE BUTT WELDS CONTAINING INTENTIONAL WELD DEFECTS

Specimen Number	Welding Procedure	Stress Cycle (ksi)	Crack Propagation Life (cycles)	Total Life (cycles)	Defect Type[a]	Defect Length (in.)	Defect Width (in.)	Defect Position (in. from surface)
LA-10	P110-M12018-A	0 to +80.0	1,950	3,400	S	0.25	0.33	0.4
LA-11	P110-M12018-A	0 to +50.0	21,900	135,900	S	0.37	0.05	0.5

a. S = slag

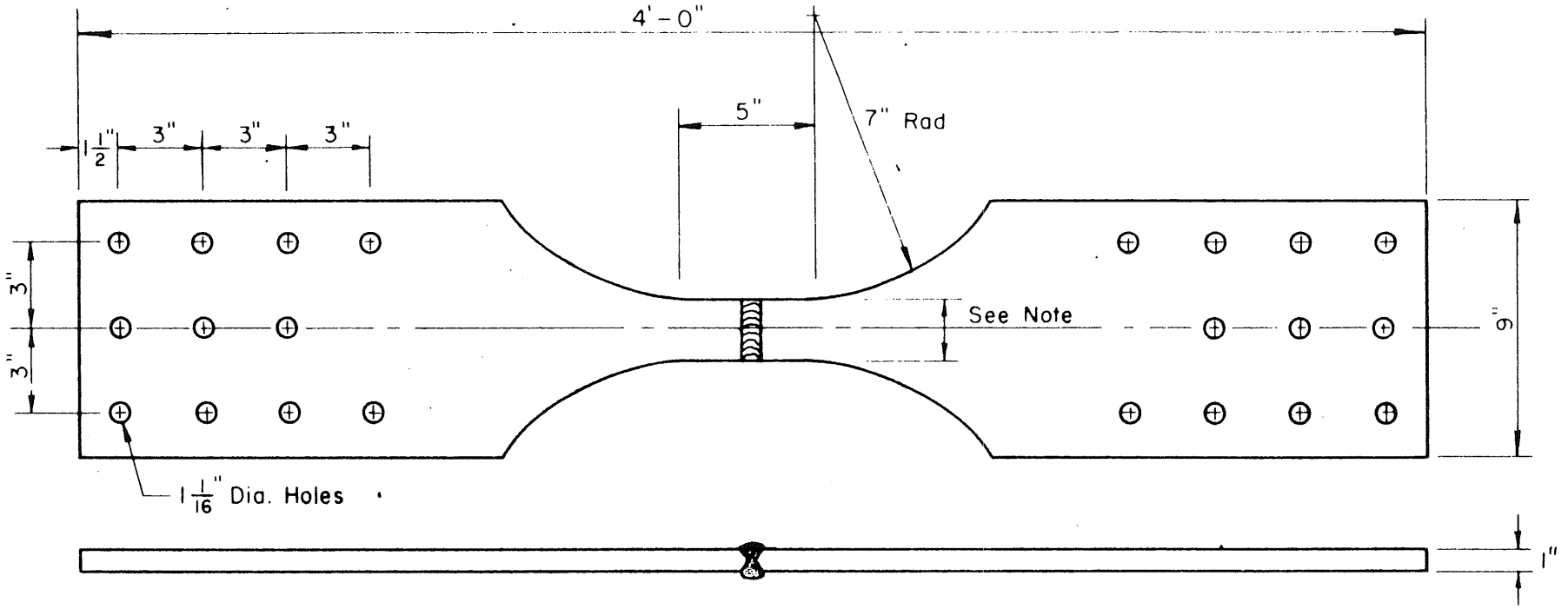

Note:

3 1/4" for tests conducted at maximum stress up to 60 ksi

2" for tests conducted at maximum stress = 80 ksi

FIG. 2.1 DETAILS OF FATIGUE TEST SPECIMENS

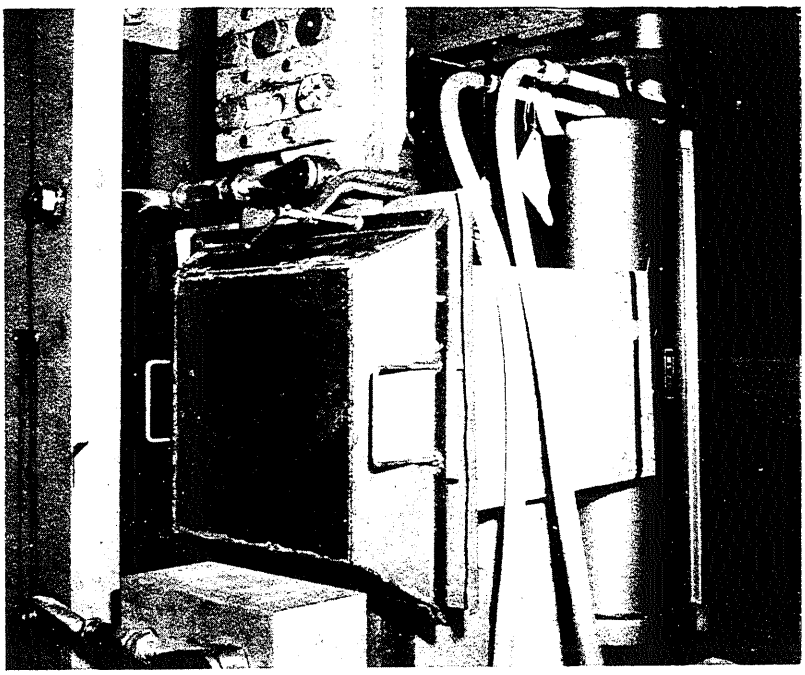

a) Equipment and Lead Shield In Position

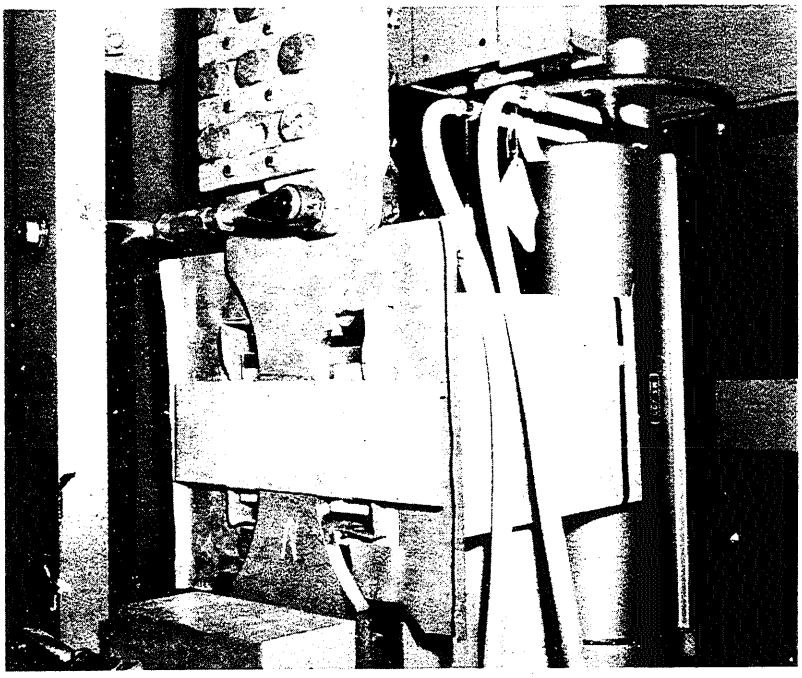

b) Specimen and X-Ray Film Holder

FIG. 2.2 SETUP FOR RADIOGRAPHIC STUDY OF CRACK PROPAGATION

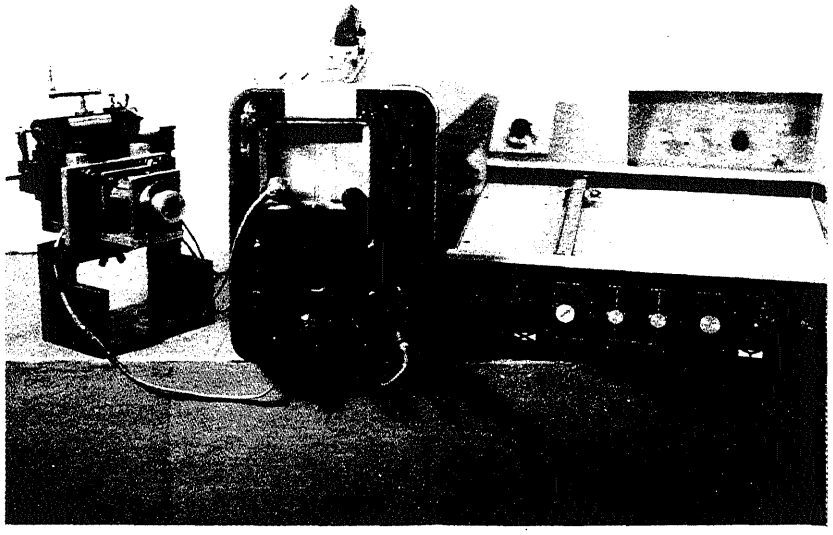

a) Probe Support, Detector And X-Y Recorder

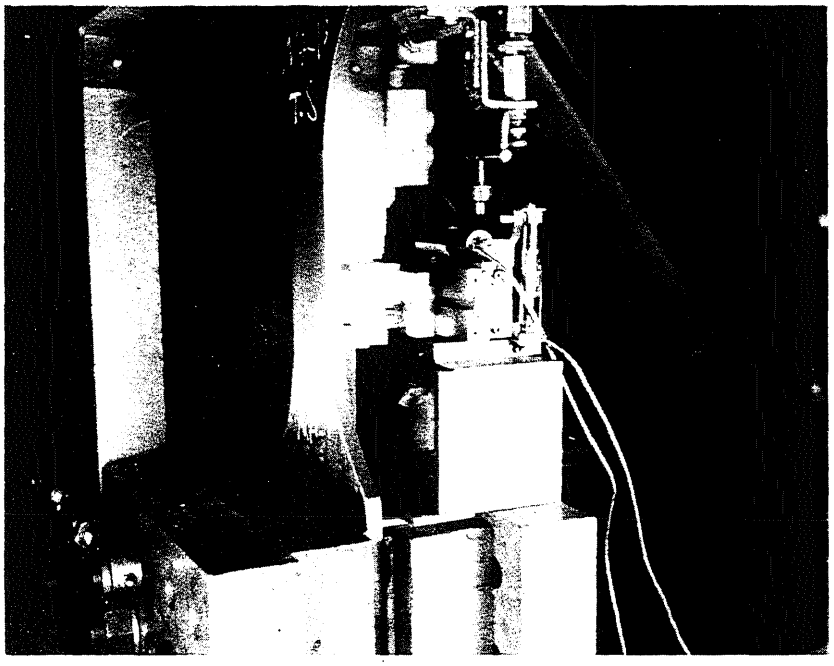

b) Unit In Position For Testing

FIG. 2.3 ULTRASONIC TESTING EQUIPMENT

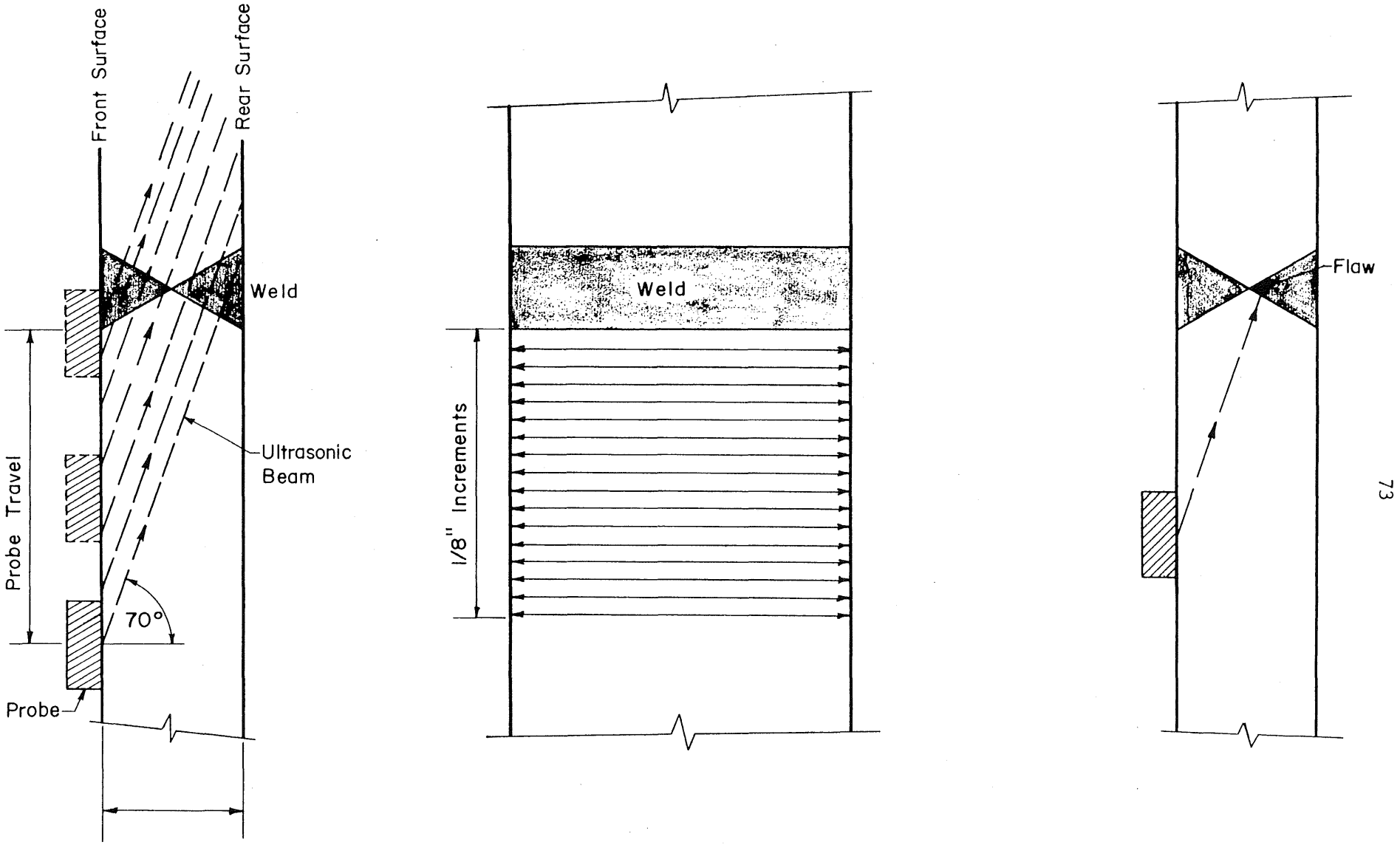

FIG. 2.4 SCANNING PROCEDURE FOR ULTRASONIC EXAMINATION

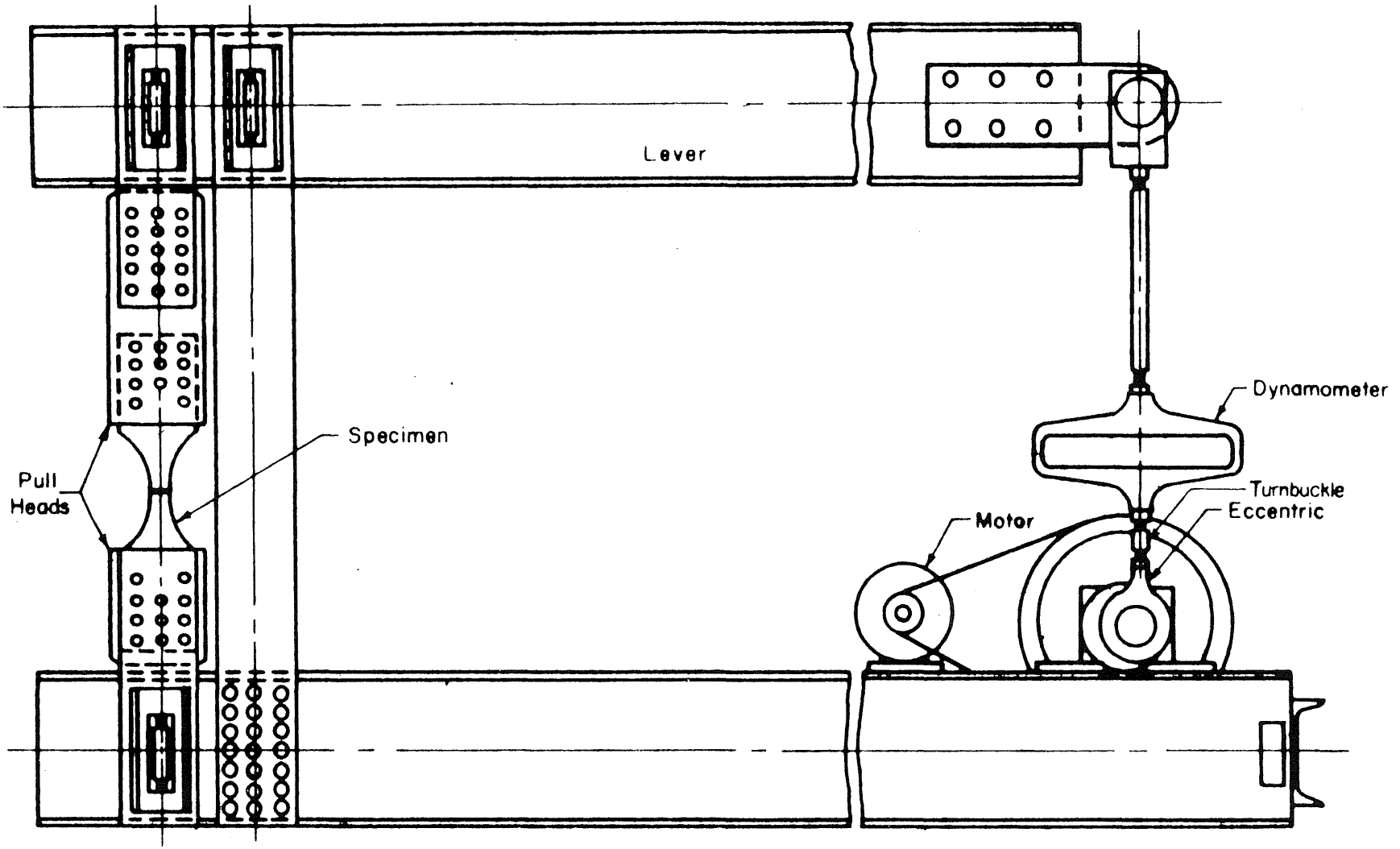

FIG. 2.5 ILLINOIS' FATIGUE TESTING MACHINE AS USED FOR AXIAL LOADING OF WELDED JOINTS

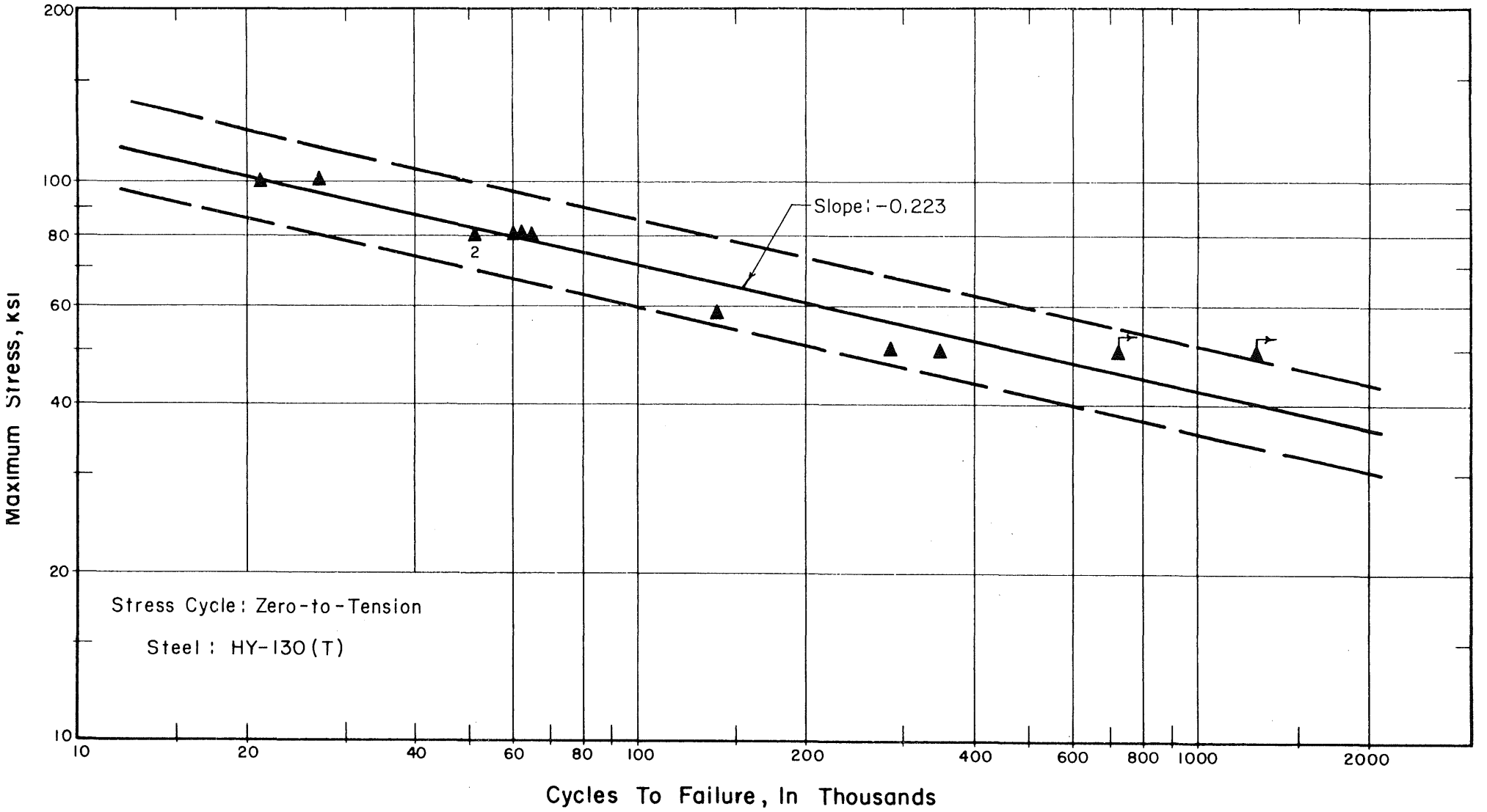

FIG. 3.1 FATIGUE TEST RESULTS AND S-N CURVE FOR HY-130(T) PLAIN PLATE SPECIMENS WITH MILL-SCALE INTACT

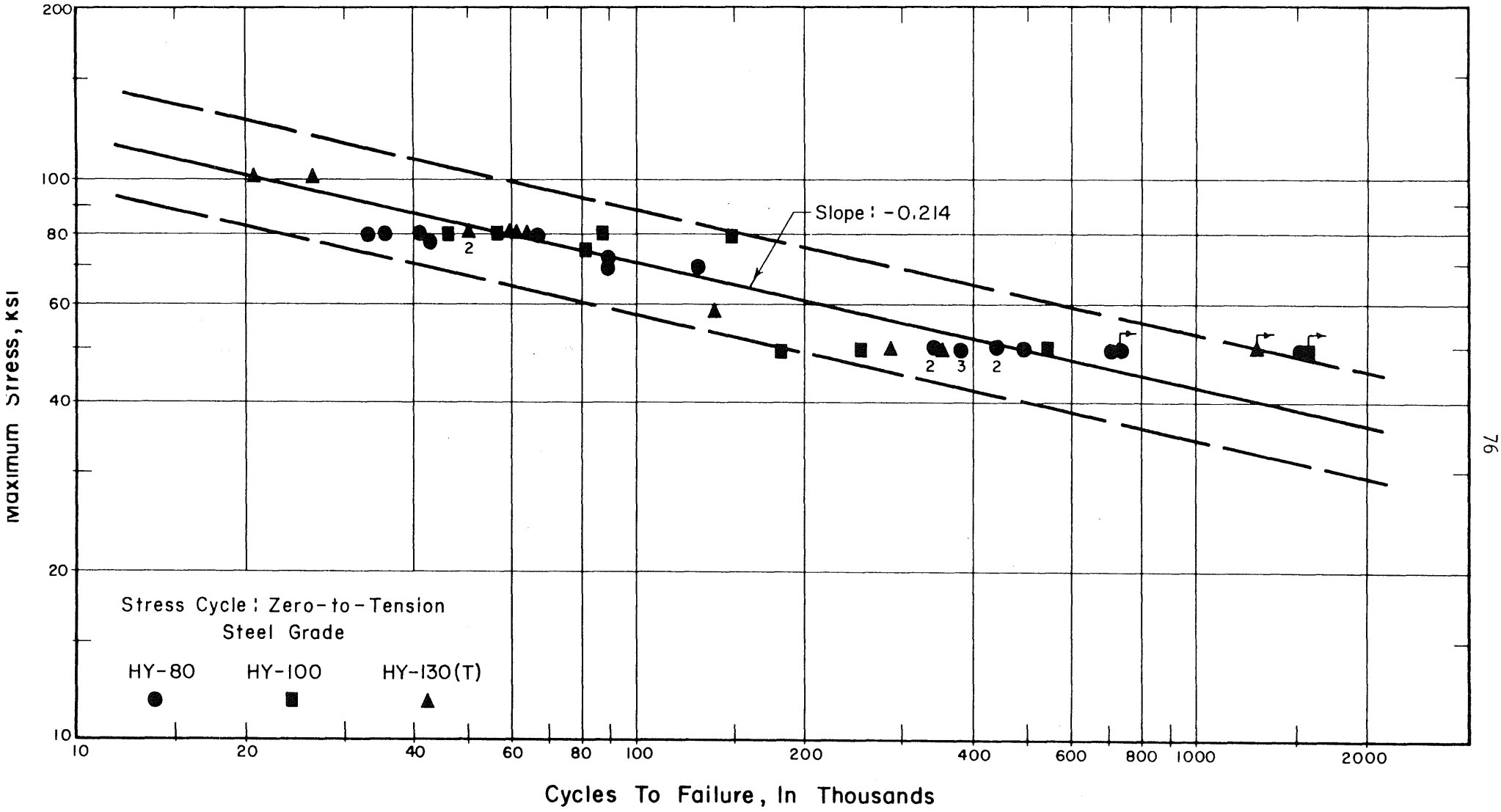

FIG. 3.2 FATIGUE TEST RESULTS AND S-N CURVE FOR PLAIN PLATE SPECIMENS WITH MILL-SCALE INTACT - ALL HY SERIES STEELS

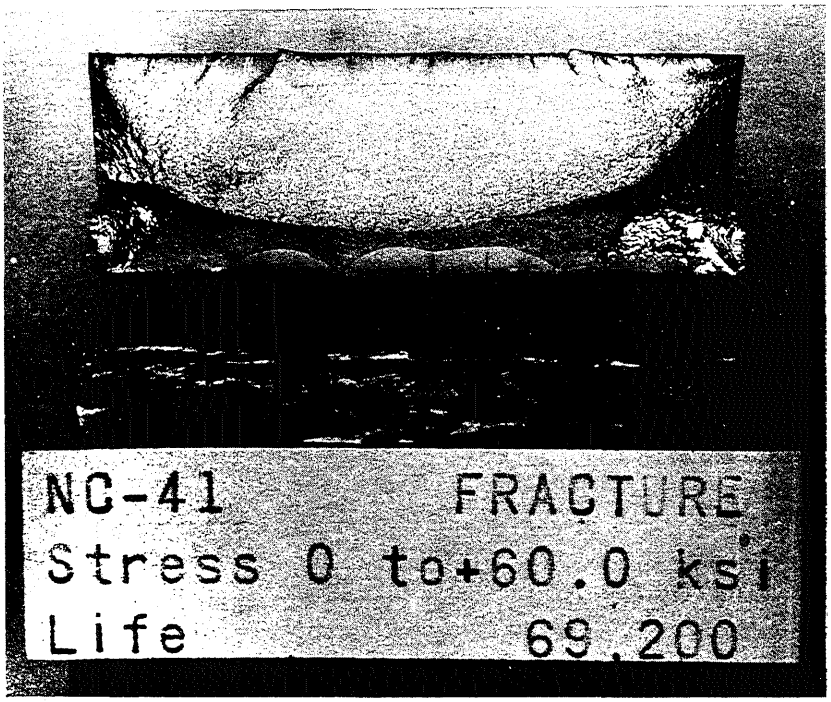

FIG. 3.3 FRACTURE SURFACE OF HY-130(T) BUTT-WELDED SPECIMEN EXHIBITING FATIGUE CRACK INITIATION AT TOE OF WELD

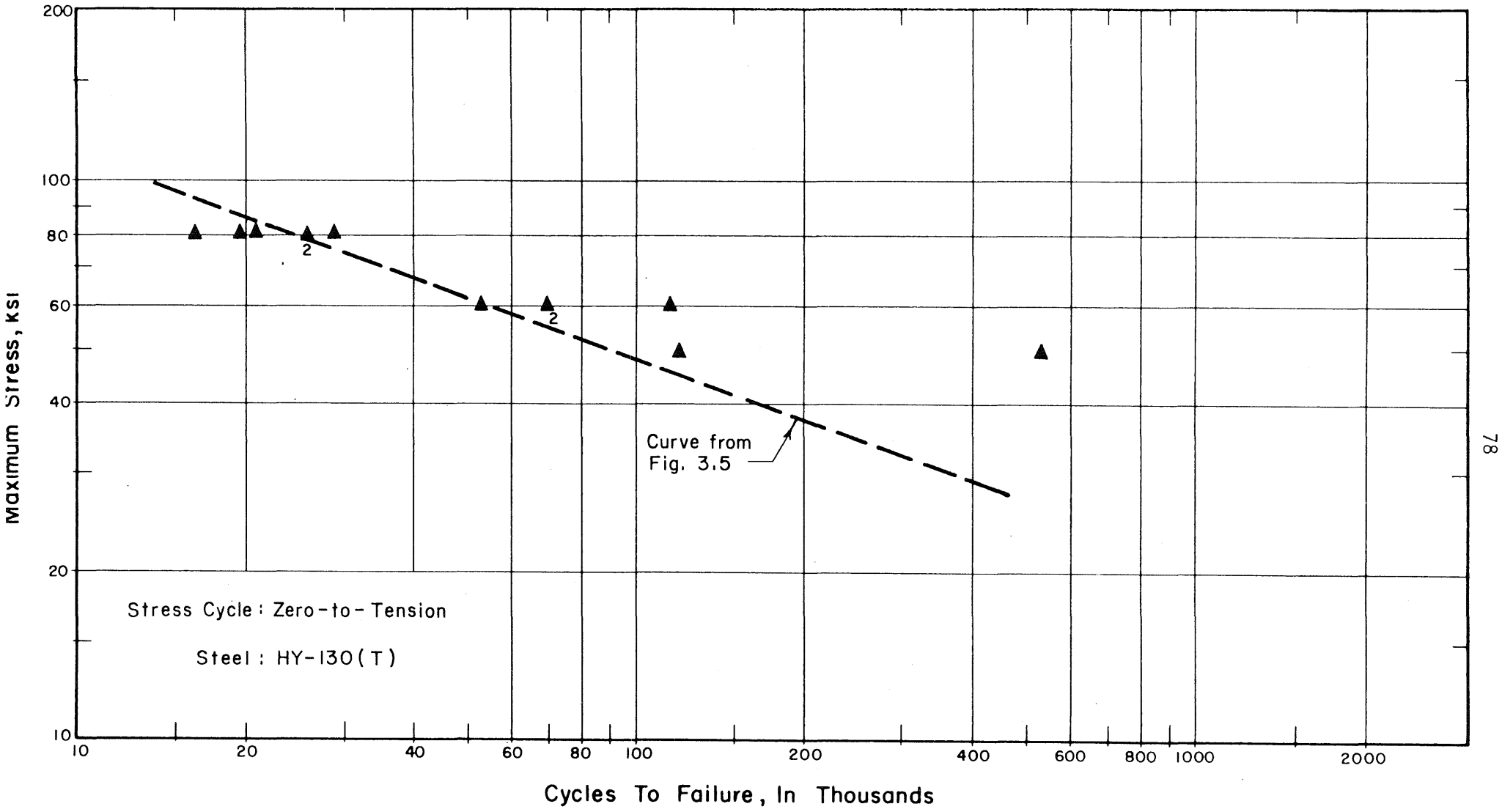

FIG. 3.4 FATIGUE TEST RESULTS FOR HY-130(T) TRANSVERSE BUTT WELDS (AS-WELDED) INITIATING FAILURE AT TOE OF WELD

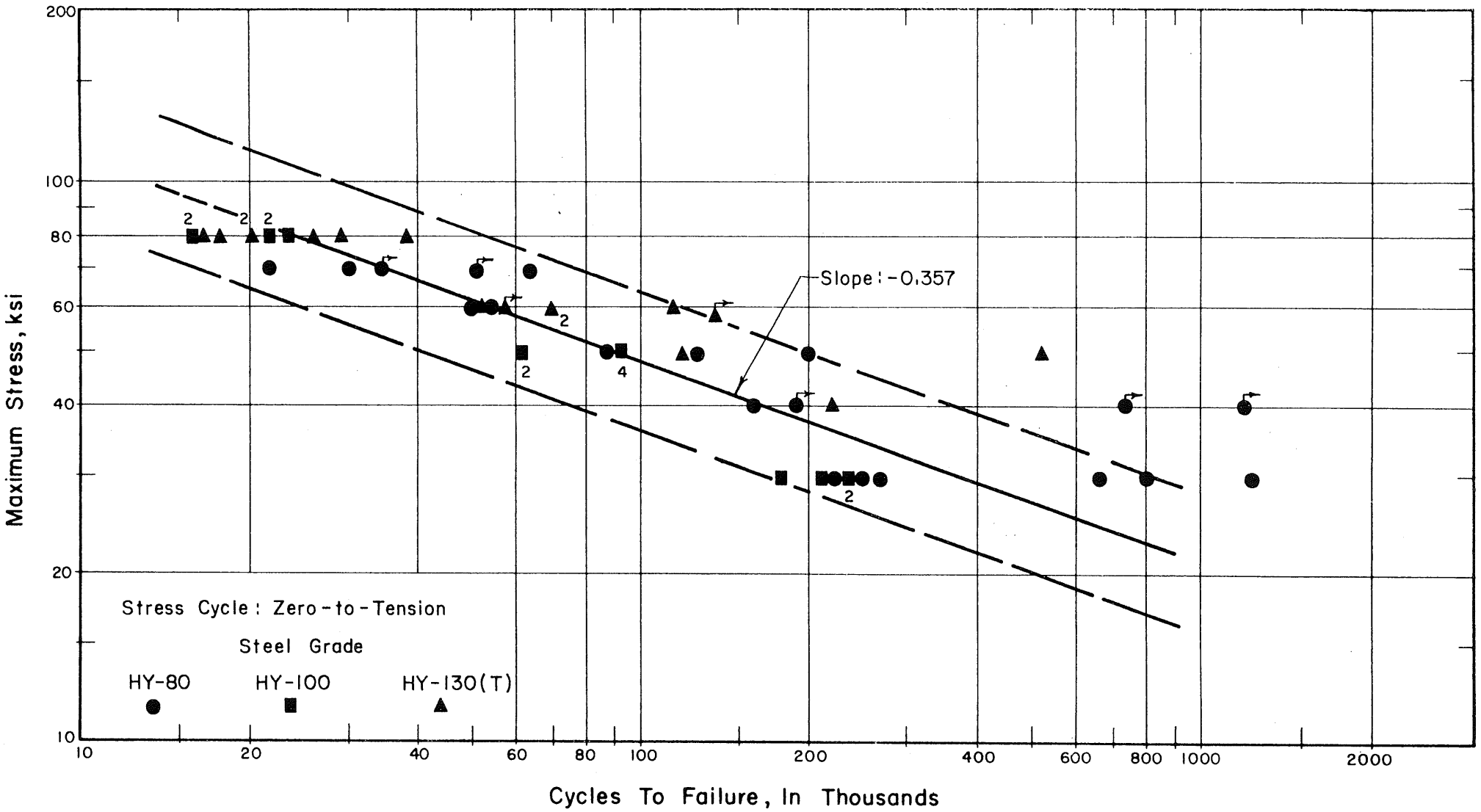

FIG. 3.5 FATIGUE TEST RESULTS AND S-N CURVE FOR TRANSVERSE BUTT WELDS (AS-WELDED) INITIATING FAILURE AT TOE OF WELD — ALL HY SERIES STEELS

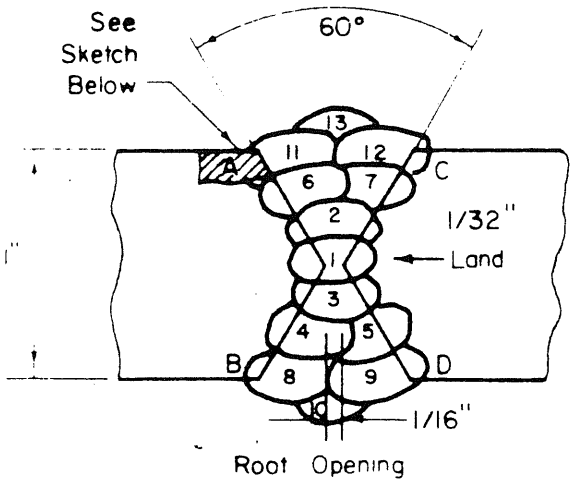

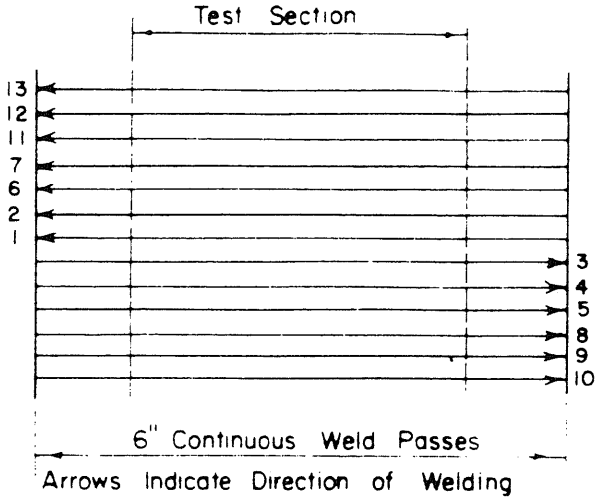

Pass	Voltage Volts	Current, amps	Rate of Travel, in./min.
1	27.5	285	13
2	29	320	13
3	29	325	13
4,5	29	330	13.5
6-13	29	320	13.5

Welding Wire : Linde 140

Electrode Size: 1/16"
Polarity: DC Reversed
Preheat Temperature: 225°F
Interpass Temperature: 225°F
Heat Input: 45,000 joules/in. (Maximum)
All welding in Flat Position
Underside of Pass 1 Ground With Carbide Wheel After Placing Pass 2

Shielding Gas: 98 % Argon
2 % Oxygen

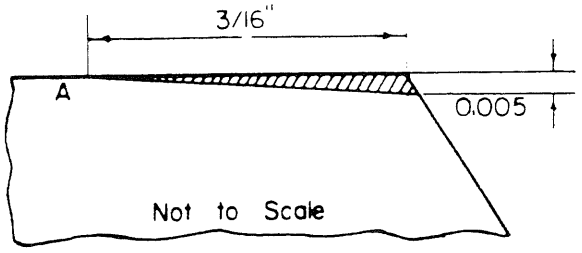

Preparation of Joint Before Welding:
Cross Hatched Area Removed by Milling on Corners A, B, C, D.
Beveled Joint Surfaces Filed and Cleaned With Acetone

FIG. 3.6 WELDING PROCEDURE P130(T)-L140-A

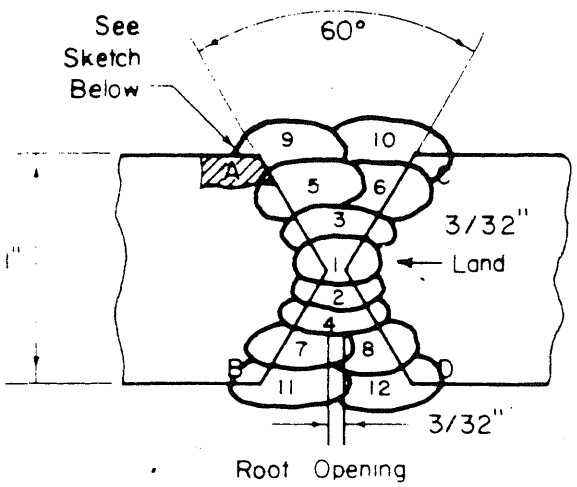

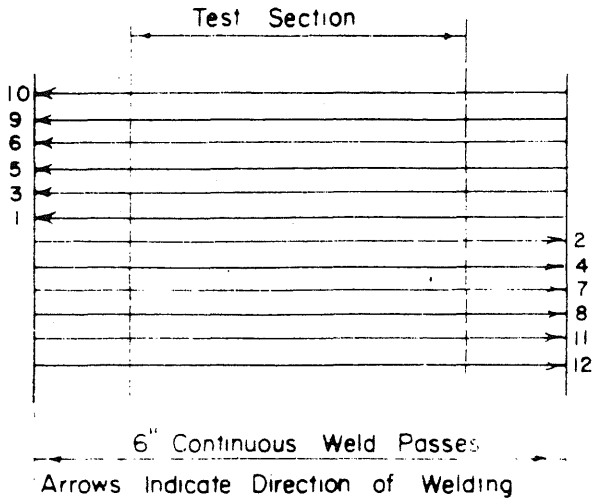

Pass	Electrode Size, in.	Current, amps	Rate of Travel, in./min.
1	5/32	150	6
2	5/32	170	6
3	3/16	200	7.5
4-12	3/16	210	8

Welding Wire : Mc Kay 14018

Voltage: 22 Volts
Polarity: DC Reversed
Preheat Temperature: 200°F
Interpass Temperature: 200°F
Heat Input: 37, 500 joules/in. (Maximum)
All Welding in Flat Position
Underside of Pass 1 Ground With Carbide Wheel Before Placing Pass 2

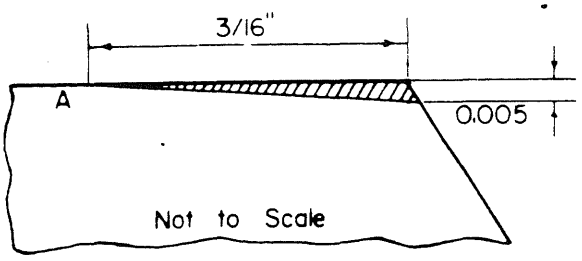

Preparation of Joint Before Welding:

Cross Hatched Area Removed by Milling on Corners A, B, C, D.

Beveled Joint Surfaces Filed and Cleaned With Acetone

FIG. 3.7 WELDING PROCEDURE P130(T)-M140-A

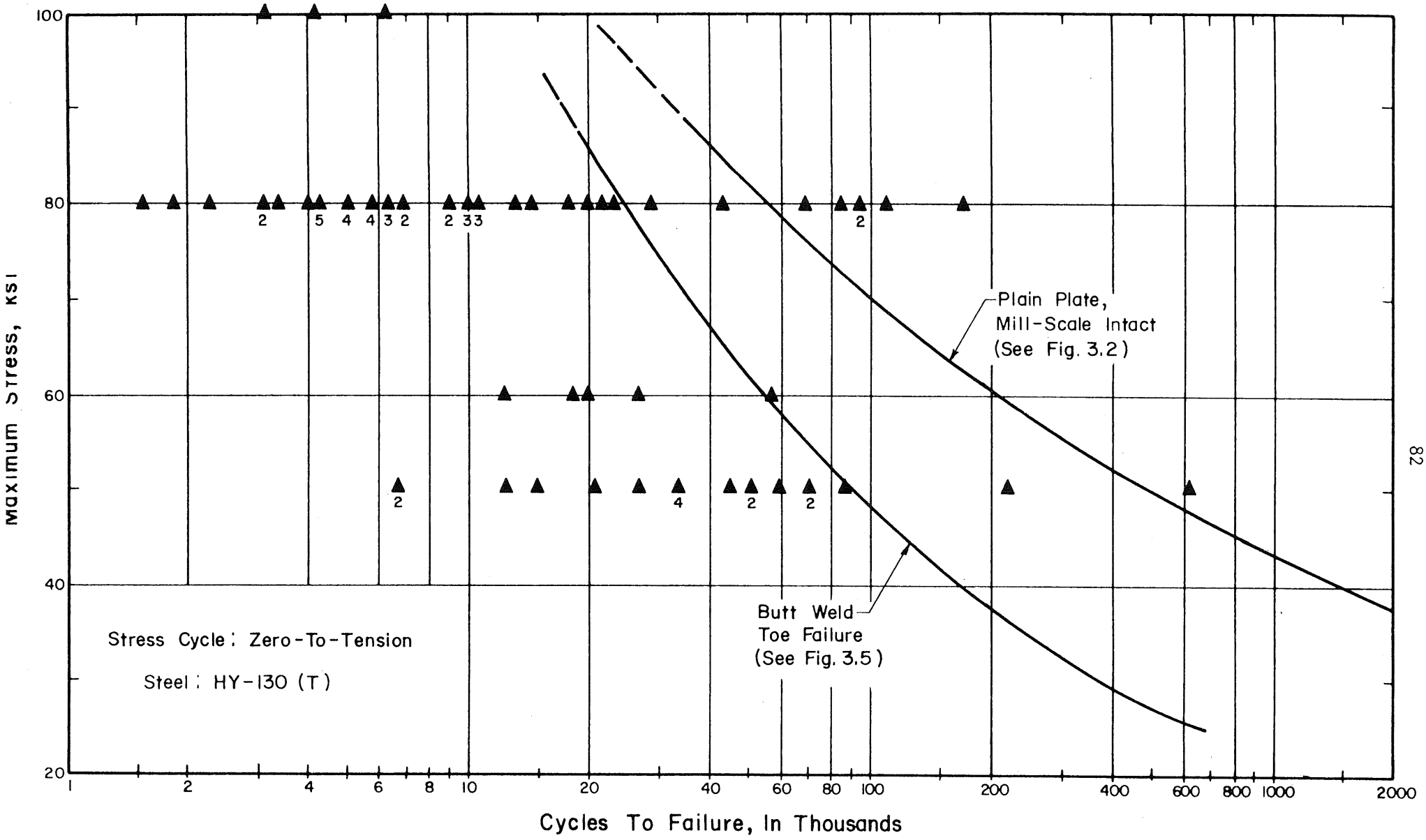

FIG. 3.8 FATIGUE TEST RESULTS FOR HY-130 (T) BUTT-WELDED SPECIMENS EXHIBITING CRACK INITIATION AT INTERNAL WELD DISCONTINUITIES

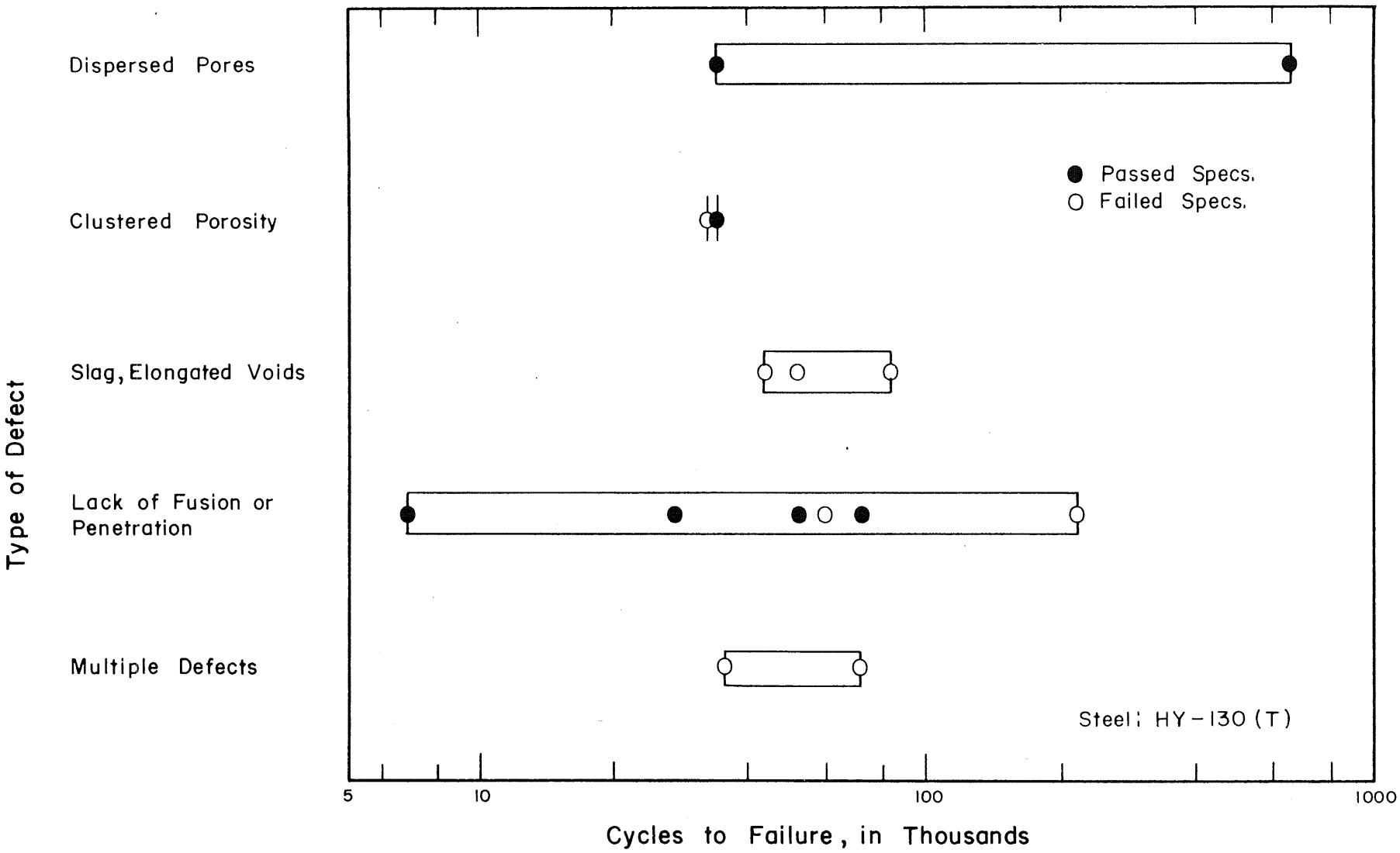

FIG. 3.9 INFLUENCE OF TYPE OF DEFECT ON FATIGUE BEHAVIOR OF HY-130 (T) BUTT-WELDED SPECIMENS. STRESS CYCLE: 0 TO +50 ksi

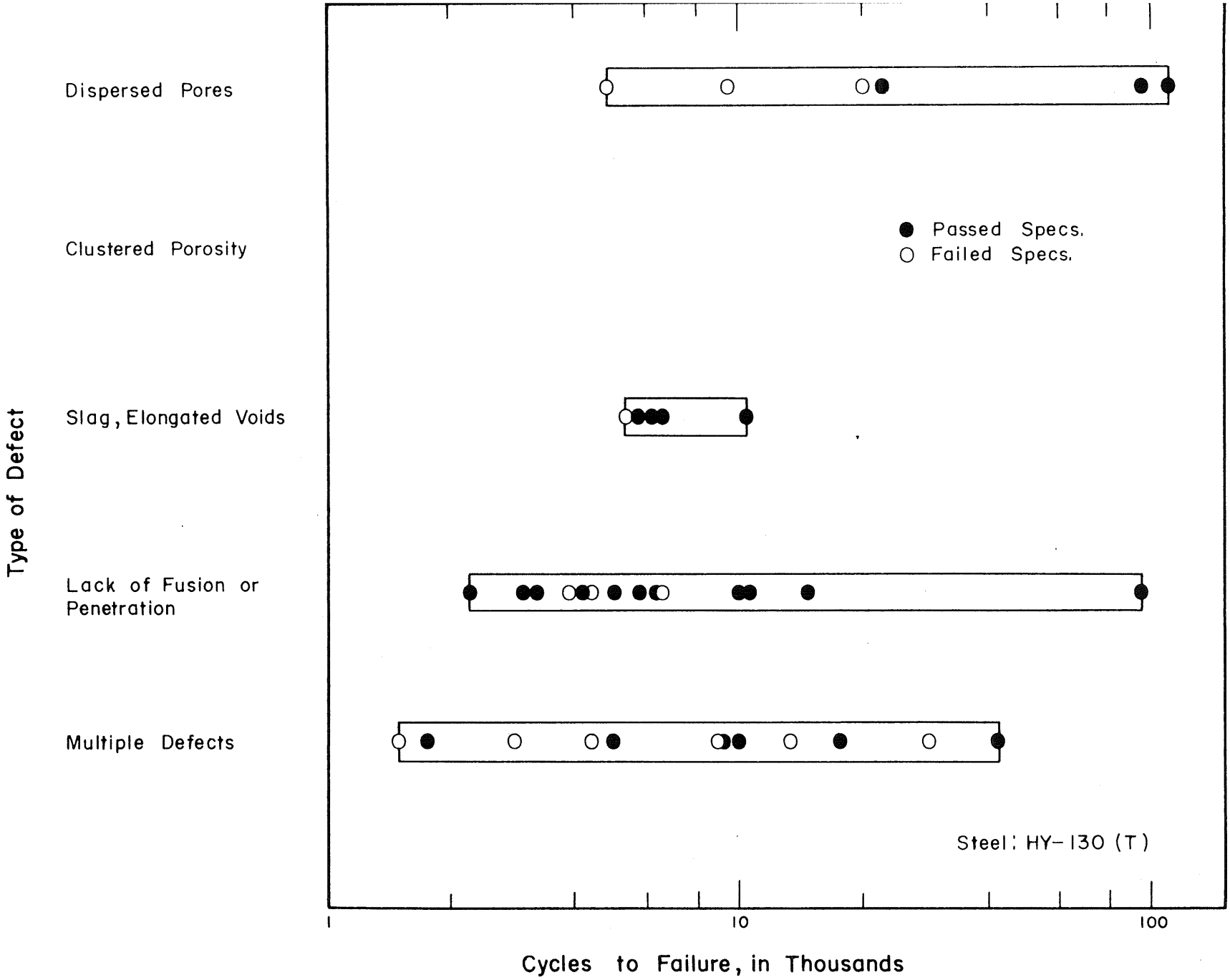

FIG. 3.10 INFLUENCE OF TYPE OF DEFECT ON FATIGUE BEHAVIOR OF HY-130(T) BUTT-WELDED SPECIMENS. STRESS CYCLE: 0 TO + 80 ksi

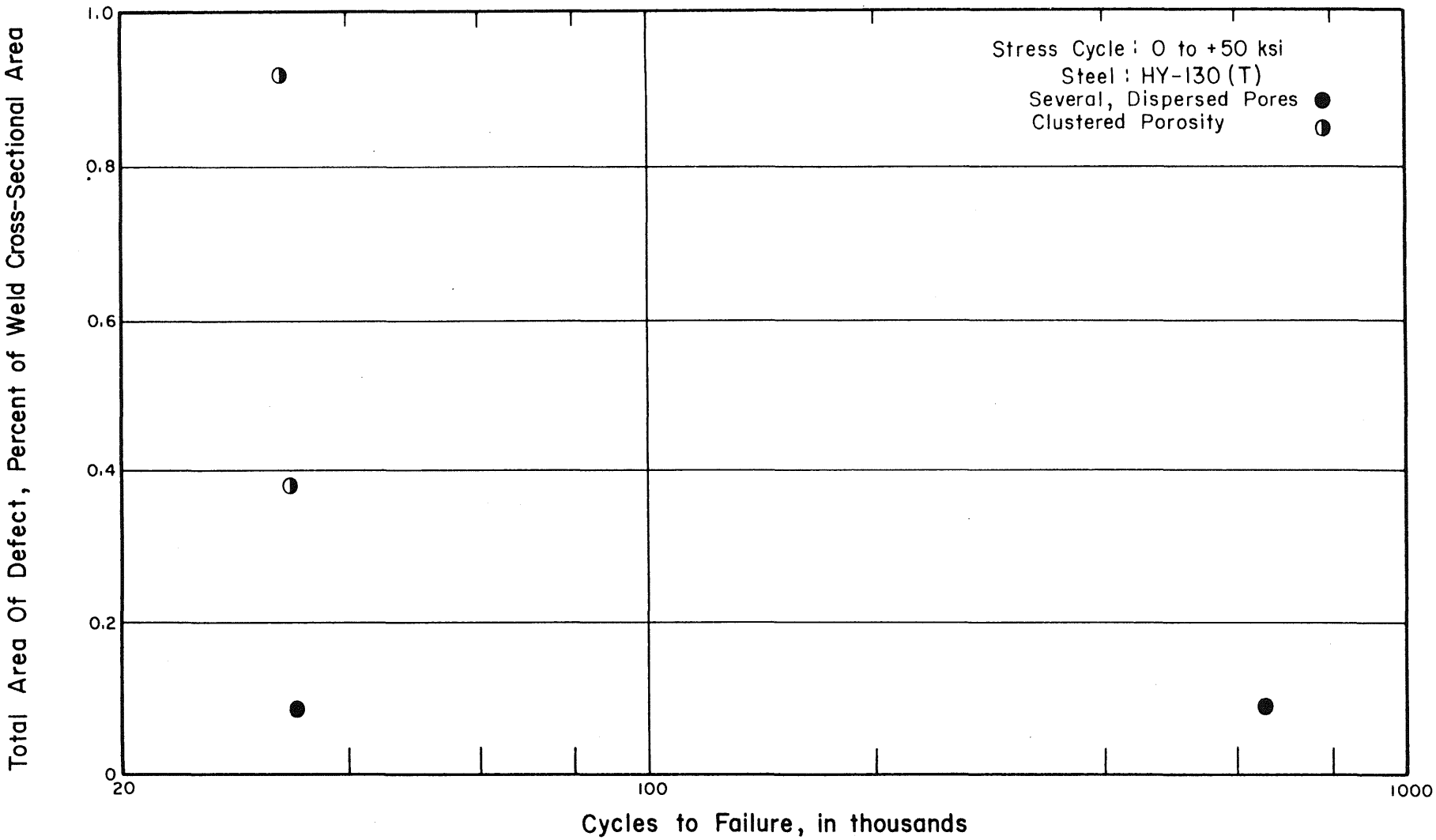

FIG. 3.11 VARIATION IN FATIGUE LIFE WITH TOTAL DEFECT AREA FOR SPECIMENS INITIATING FAILURE AT POROSITY — STRESS CYCLE : 0 TO +50 ksi

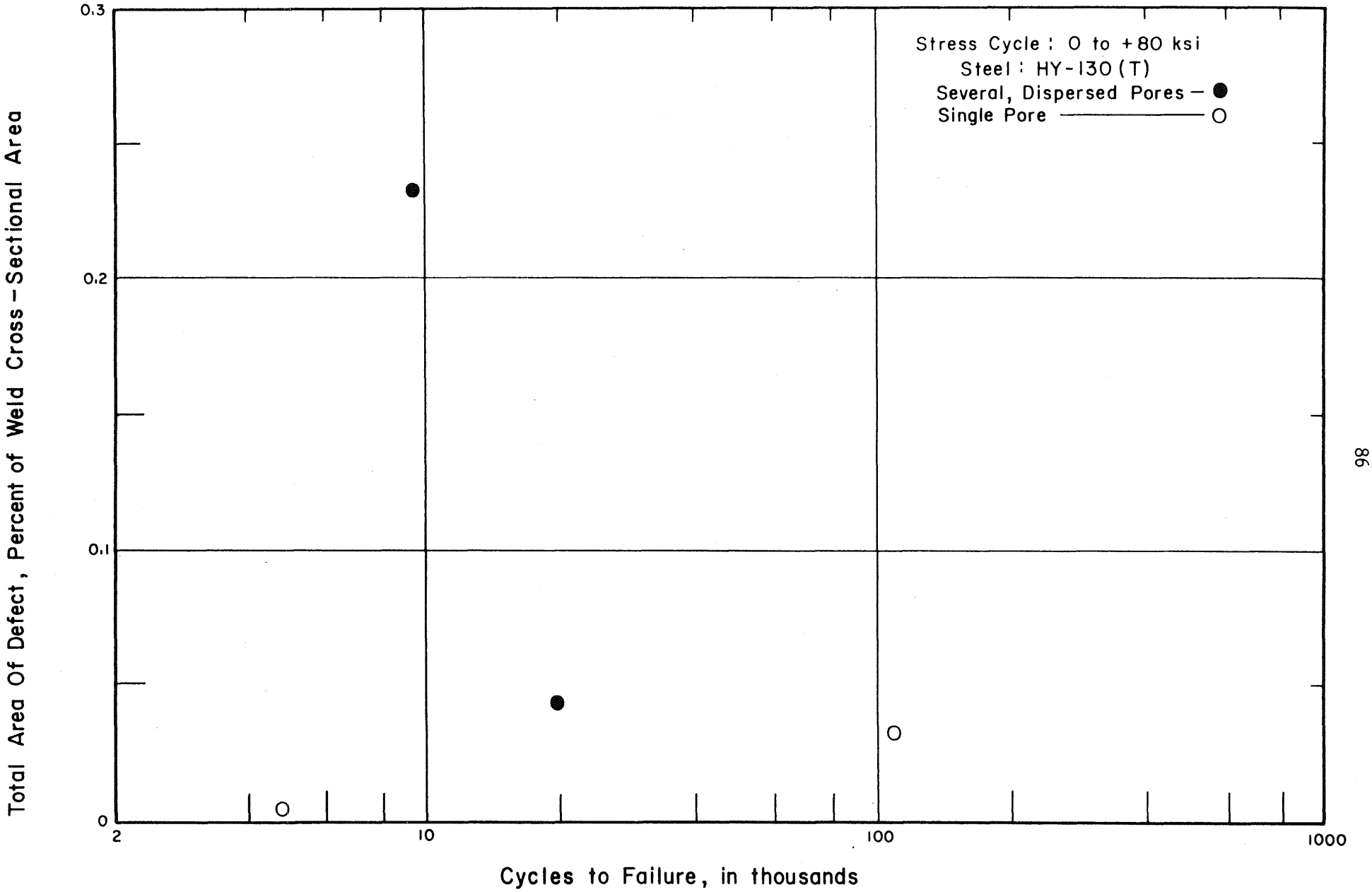

FIG. 3.12 VARIATION IN FATIGUE LIFE WITH TOTAL DEFECT AREA FOR SPECIMENS INITIATING FAILURE AT POROSITY—STRESS CYCLE : 0 TO +80 ksi

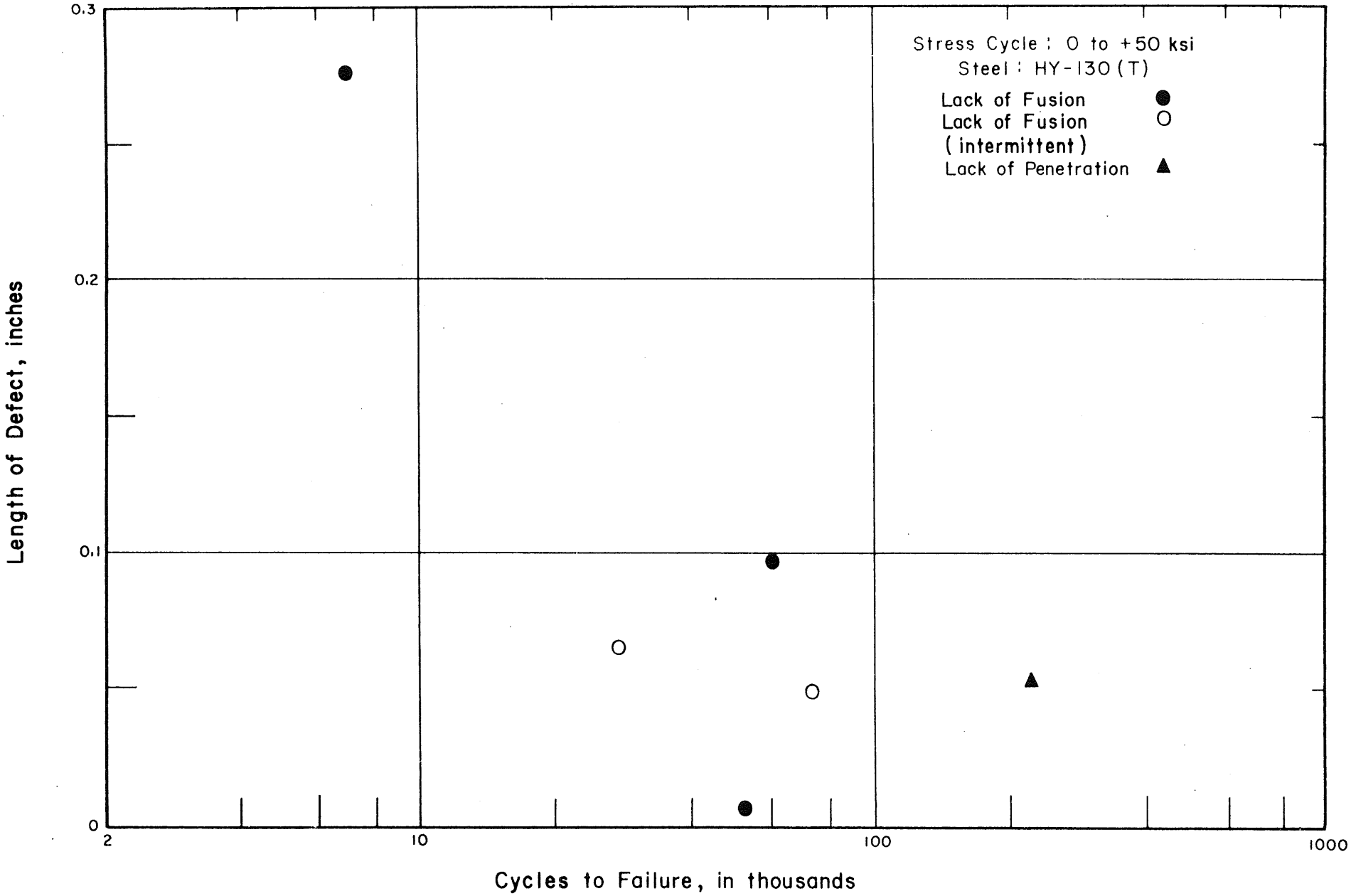

FIG. 3.13 VARIATION IN FATIGUE LIFE WITH DEFECT LENGTH FOR SPECIMEN INITIATING FAILURE AT LACK OF FUSION OR LACK OF PENETRATION — STRESS CYCLE : 0 TO +50 ksi

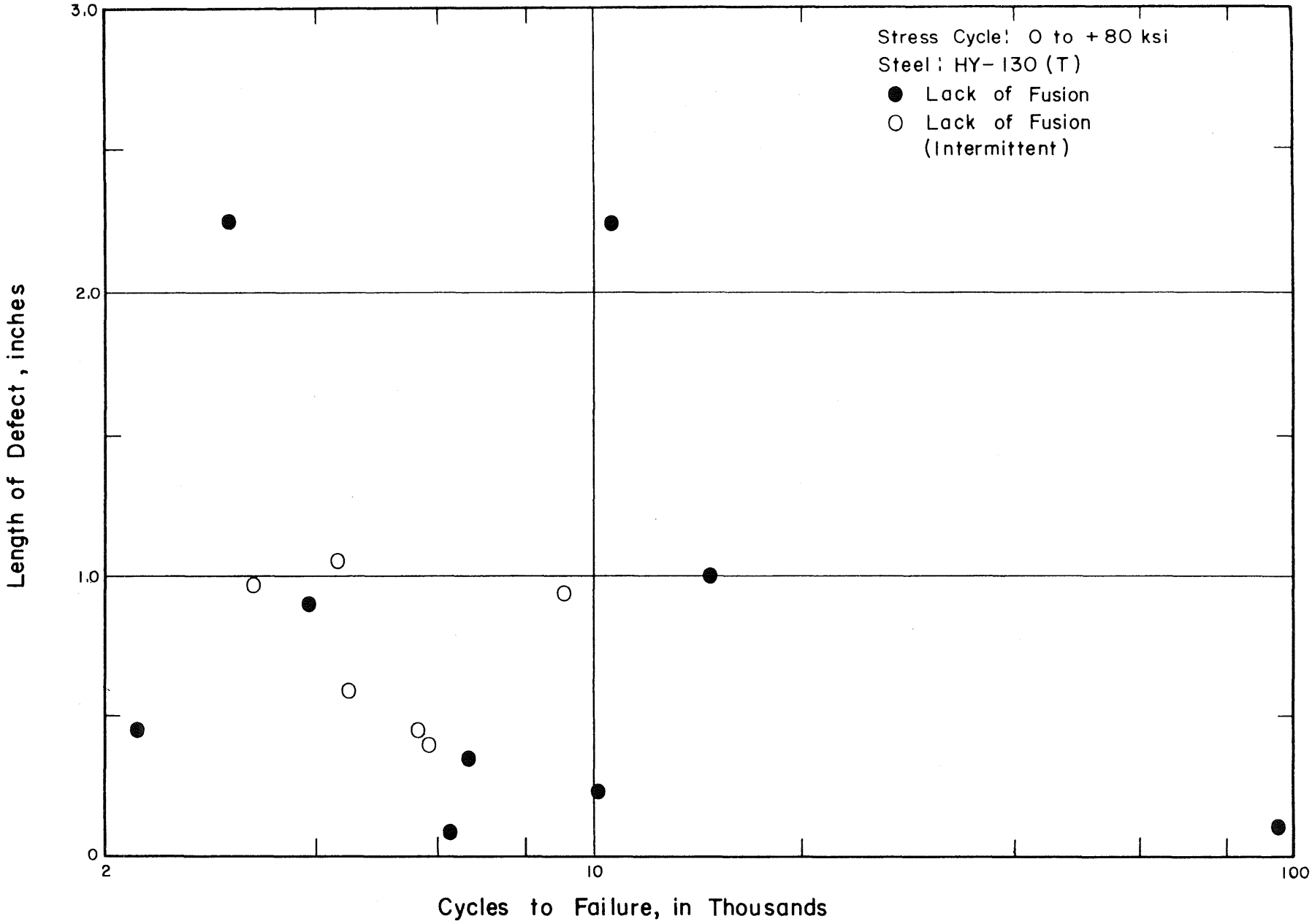

FIG. 3.14 VARIATION IN FATIGUE LIFE WITH DEFECT LENGTH FOR SPECIMENS INITIATING FAILURE AT LACK OF FUSION OR LACK OF PENETRATION STRESS CYCLE : 0 TO +80 ksi

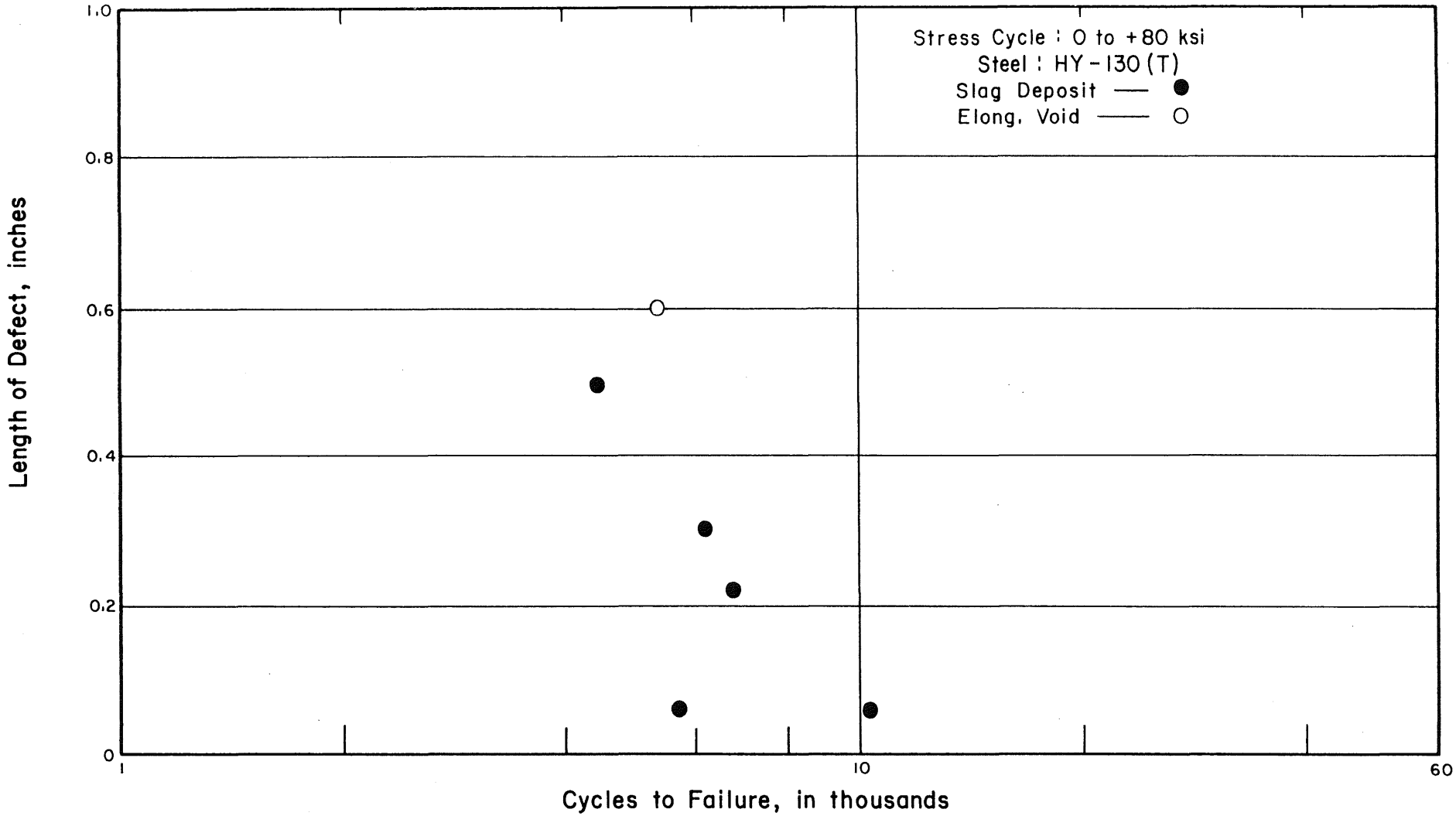

FIG. 3.15 VARIATION IN FATIGUE LIFE WITH DEFECT LENGTH FOR SPECIMENS INITIATING FAILURE AT SLAG OR ELONGATED VOIDS – STRESS CYCLE : 0 TO +80 ksi

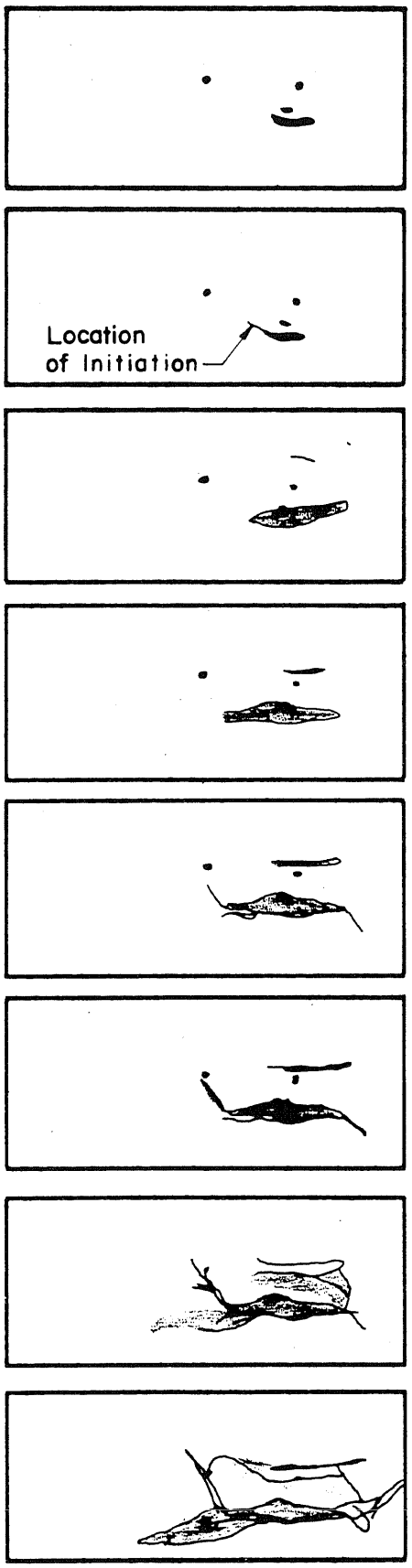

Number of Cycles

N = 0

N = 1000

N = 2000

N = 3280 (Fatigue Crack Visible on Specimen Surface)

N = 5000

N = 5500

N = 6000

N = 6500 (Fatigue Crack Through Plate Thickness)

FIG. 3.16 TRACINGS OF RADIOGRAPHS TAKEN DURING FATIGUE TEST OF SPECIMEN ND-36

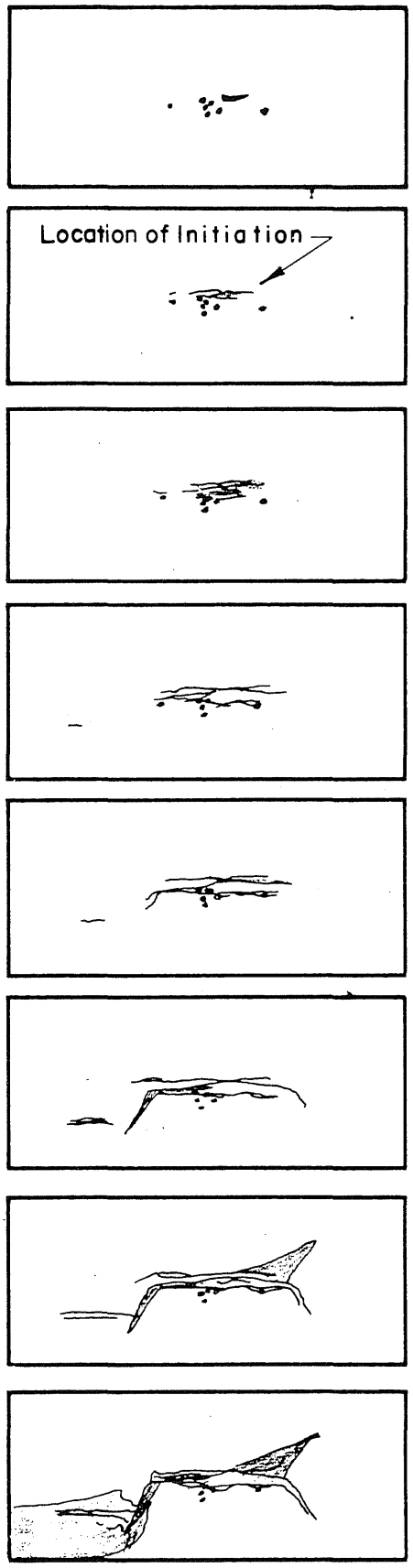

FIG. 3.17 TRACINGS OF RADIOGRAPHS TAKEN DURING FATIGUE TEST OF SPECIMEN ND-37

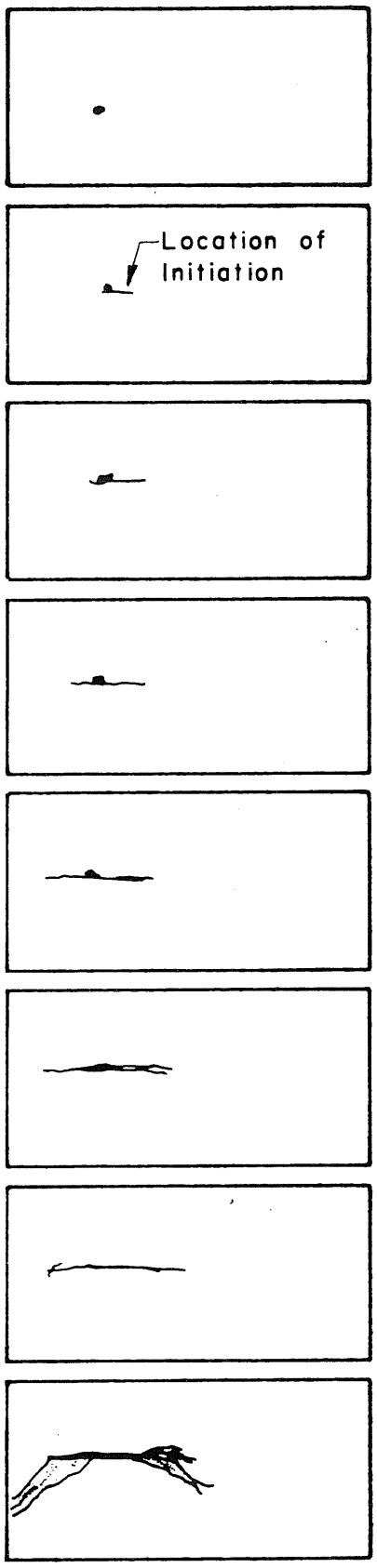

Number of Cycles

N = 0

N = 1000

N = 2000

N = 2500

N = 3460 (Fatigue Crack Visible on Specimen Surface)

N = 4500

N = 5000

N = 5500 (Fatigue Crack Through Plate Thickness)

FIG. 3.18 TRACINGS OF RADIOGRAPHS TAKEN DURING FATIGUE TEST OF SPECIMEN ND-38

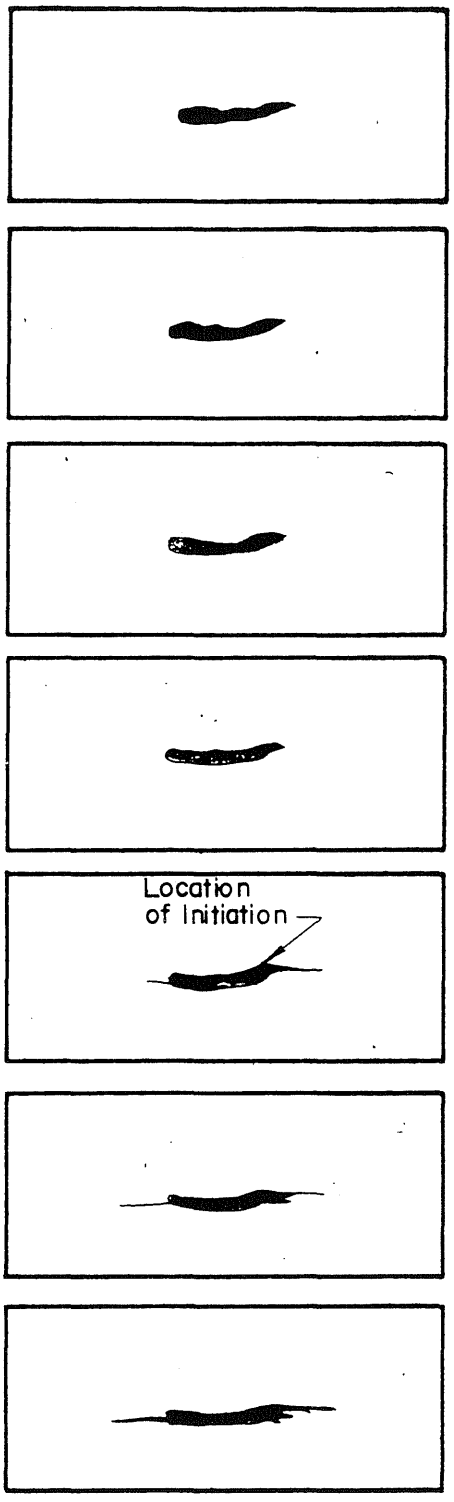

Number of Cycles

N = 0

N = 500

N = 1000

N = 2000

N = 4000

N = 4500 (Fatigue Crack Visible on Specimen Surface)

N = 5000 (Fatigue Crack Through Plate Thickness)

FIG. 3.19 TRACINGS OF RADIOGRAPHS TAKEN DURING FATIGUE TEST OF SPECIMEN ND-40

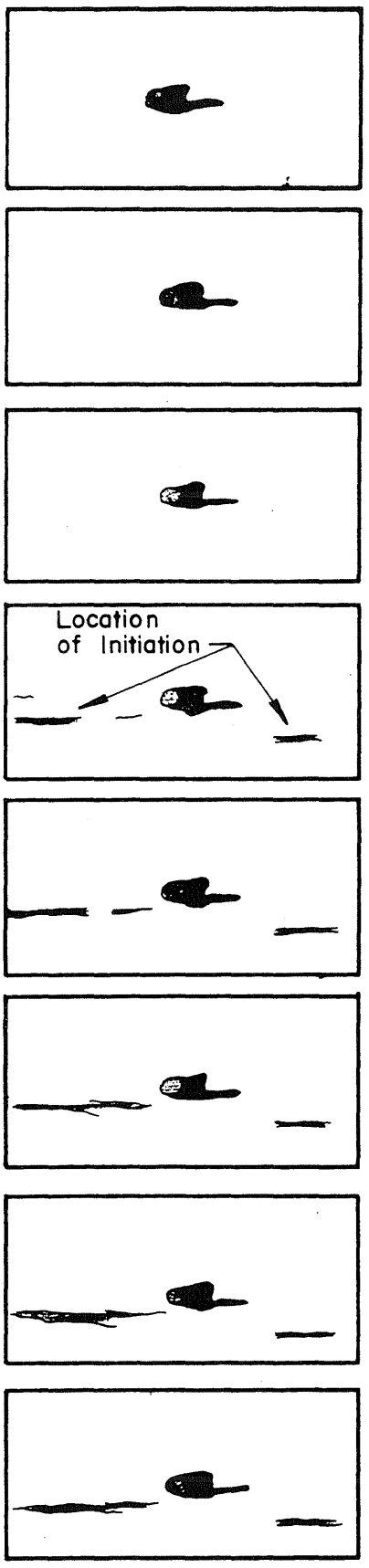

Number of Cycles

N = 0

N = 3000

N = 6000

N = 7000

N = 7500

N = 8000

N = 8500

N = 8770 (Fatigue Crack Visible on Specimen Surface)

FIG. 3.20 TRACINGS OF RADIOGRAPHS TAKEN DURING FATIGUE TEST OF SPECIMEN ND-41

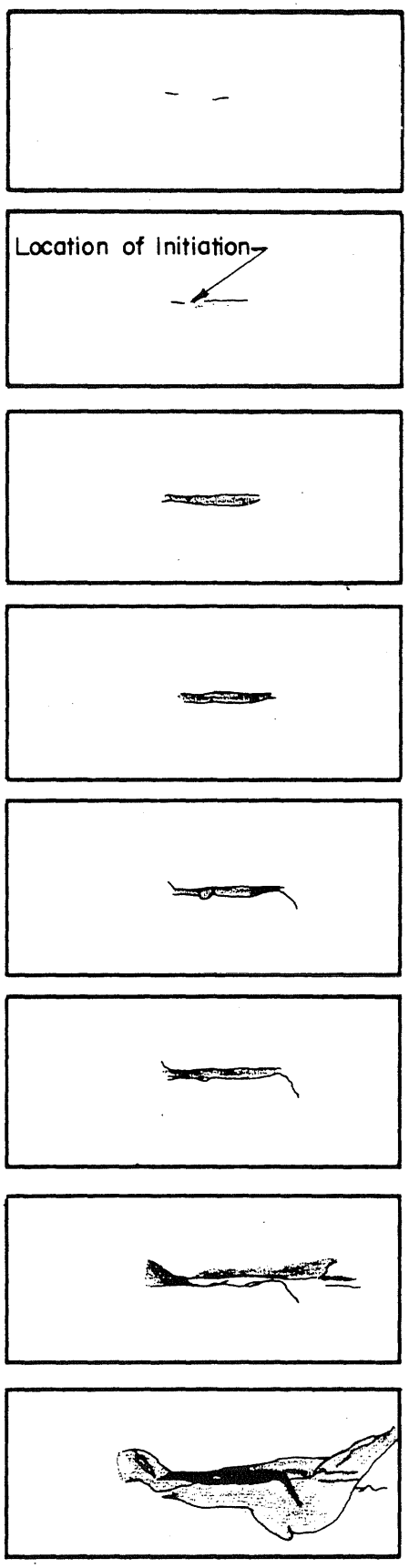

FIG. 3.21 TRACINGS OF RADIOGRAPHS TAKEN DURING FATIGUE TEST OF SPECIMEN ND-44

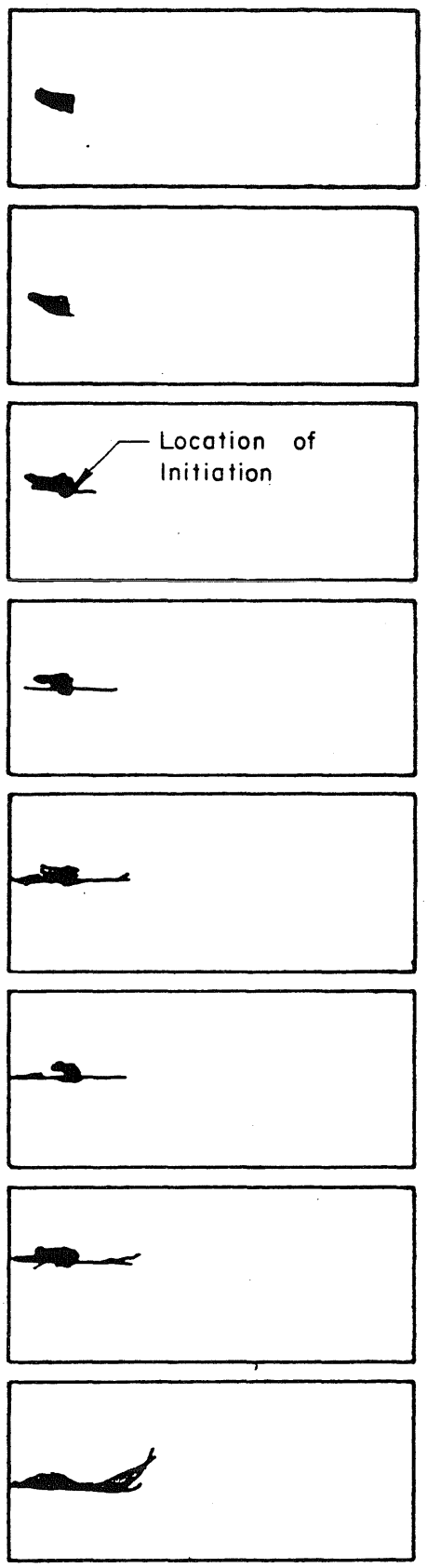

Number of Cycles

N = 0

N = 2040

N = 3000

N = 3890 (Fatigue Crack Visible on Specimen Surface)

N = 5000

N = 5500

N = 6000

N = 6500 (Fatigue Crack Through Plate Thickness)

FIG. 3.22 TRACINGS OF RADIOGRAPHS TAKEN DURING FATIGUE TEST OF SPECIMEN ND-45

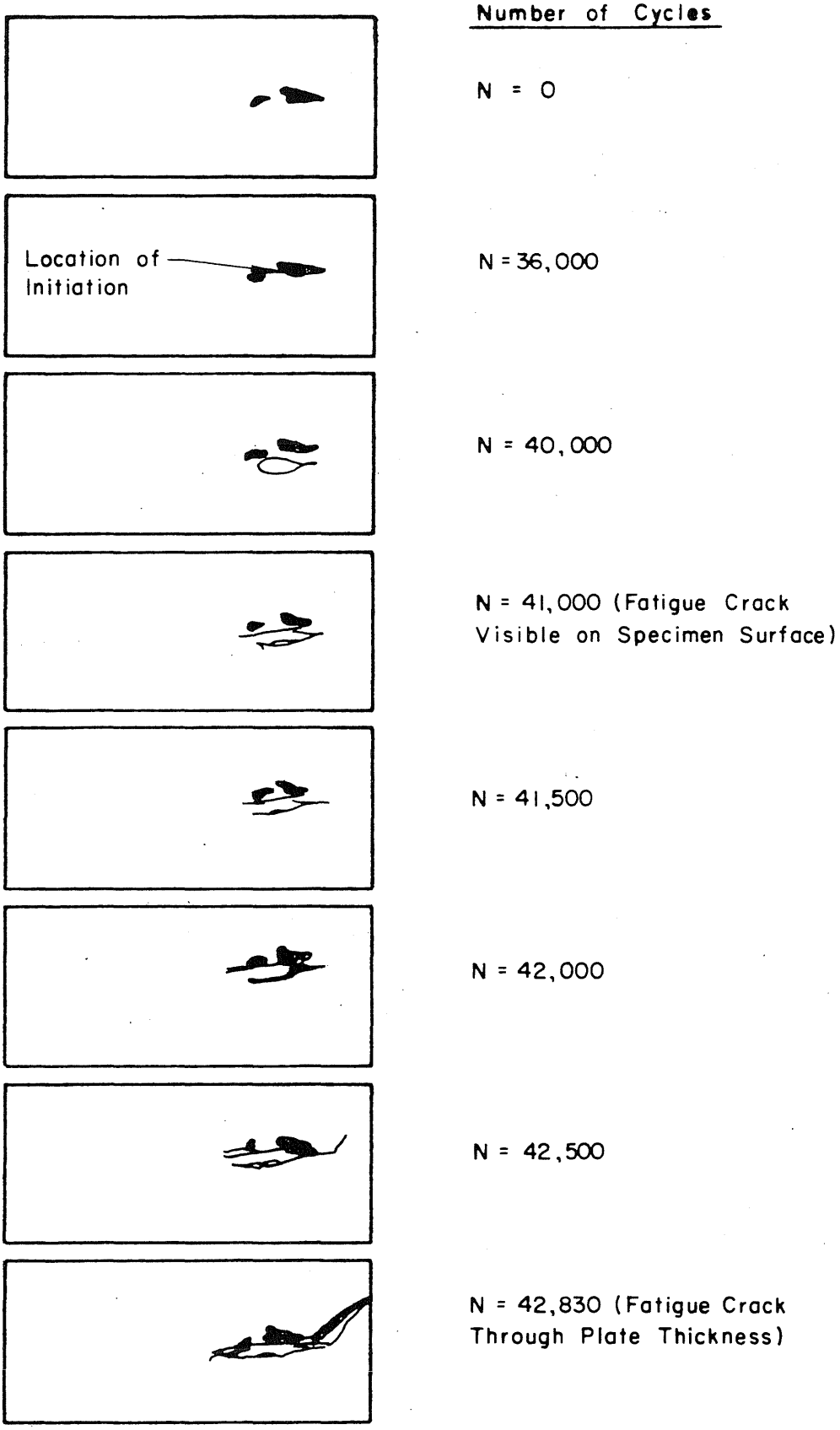

FIG. 3.23 TRACINGS OF RADIOGRAPHS TAKEN DURING FATIGUE TEST OF SPECIMEN ND-46

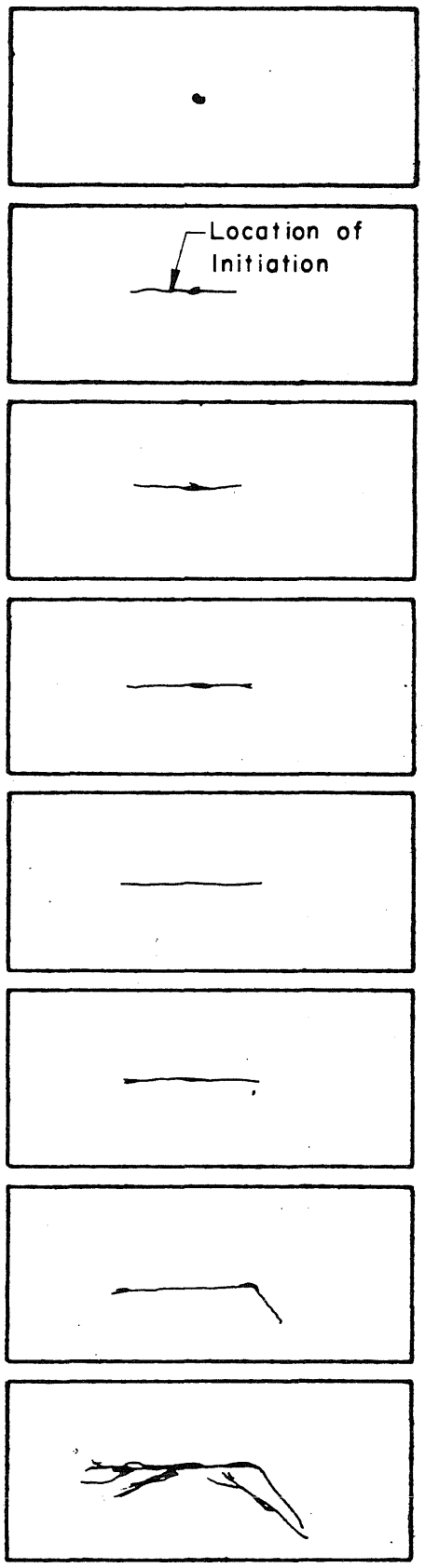

Number of Cycles

N = 0

N = 6900

N = 7350 (Fatigue Crack Visible on Specimen Surface)

N = 8300

N = 8800

N = 9300

N = 9800

N = 10,300 (Fatigue Crack Through Plate Thickness)

FIG. 3.24 TRACINGS OF RADIOGRAPHS TAKEN DURING FATIGUE TEST OF SPECIMEN ND-47

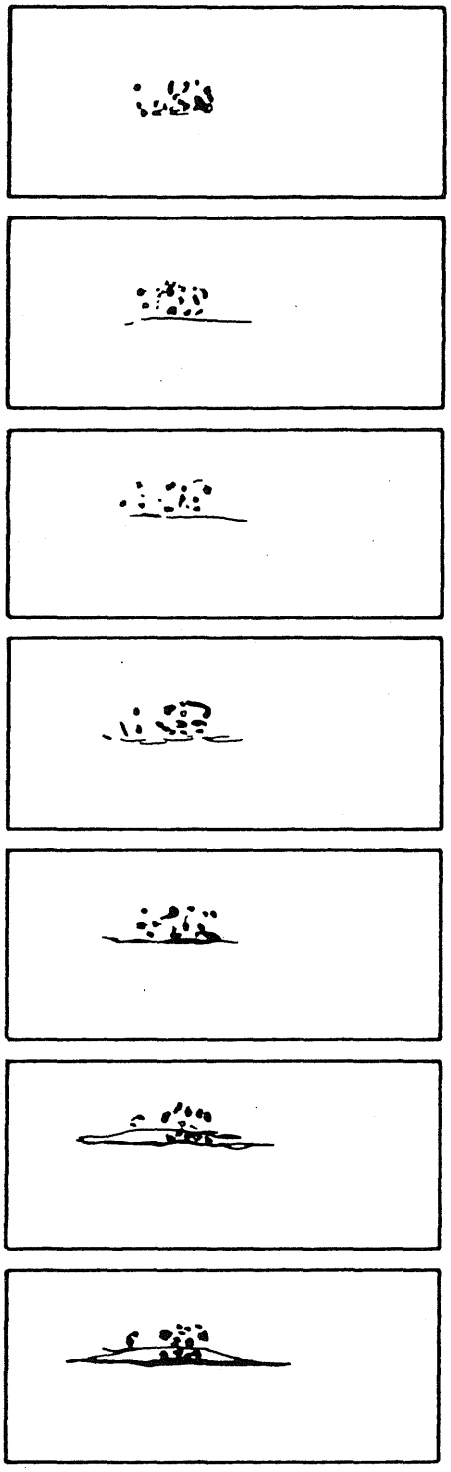

FIG. 3.25 TRACINGS OF RADIOGRAPHS TAKEN DURING FATIGUE TEST OF SPECIMEN NE-7

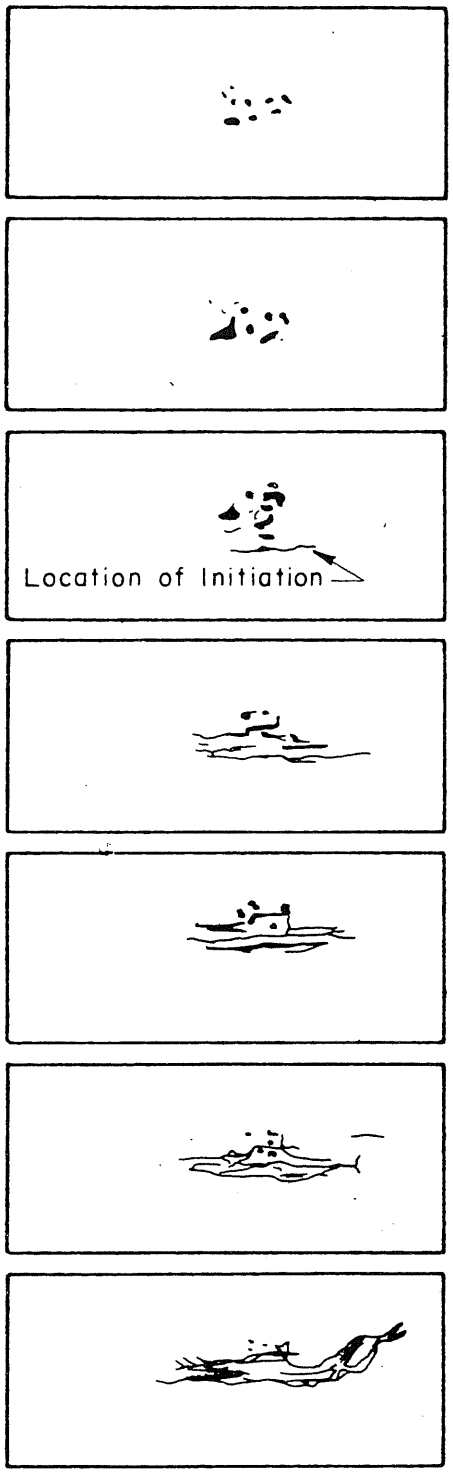

FIG. 3.26 TRACINGS OF RADIOGRAPHS TAKEN DURING FATIGUE TEST OF SPECIMEN NE-8

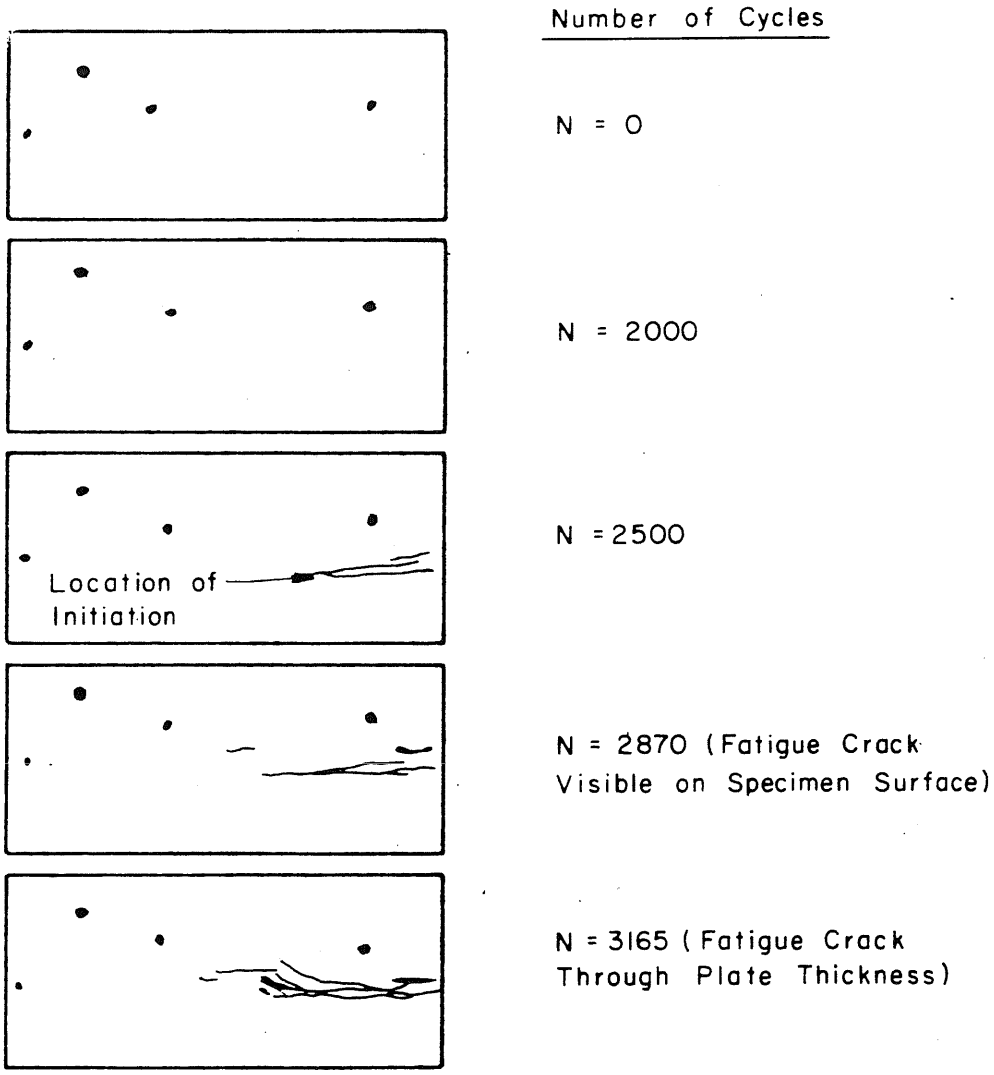

FIG. 3.27 TRACINGS OF RADIOGRAPHS TAKEN DURING FATIGUE TEST OF SPECIMEN NE-10

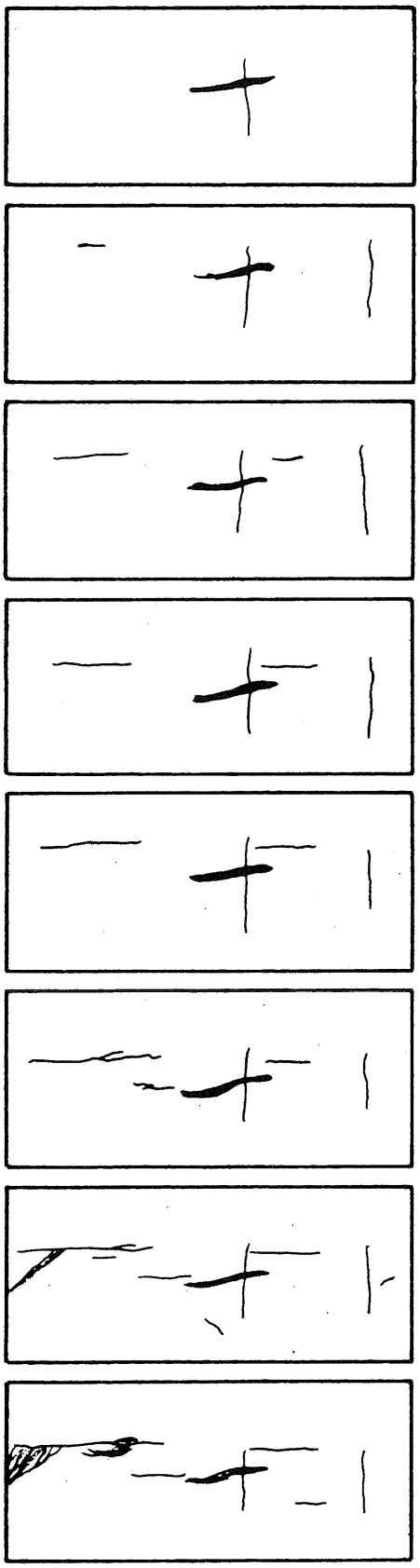

FIG. 3.28 TRACINGS OF RADIOGRAPHS TAKEN DURING FATIGUE TEST OF SPECIMEN NE-11

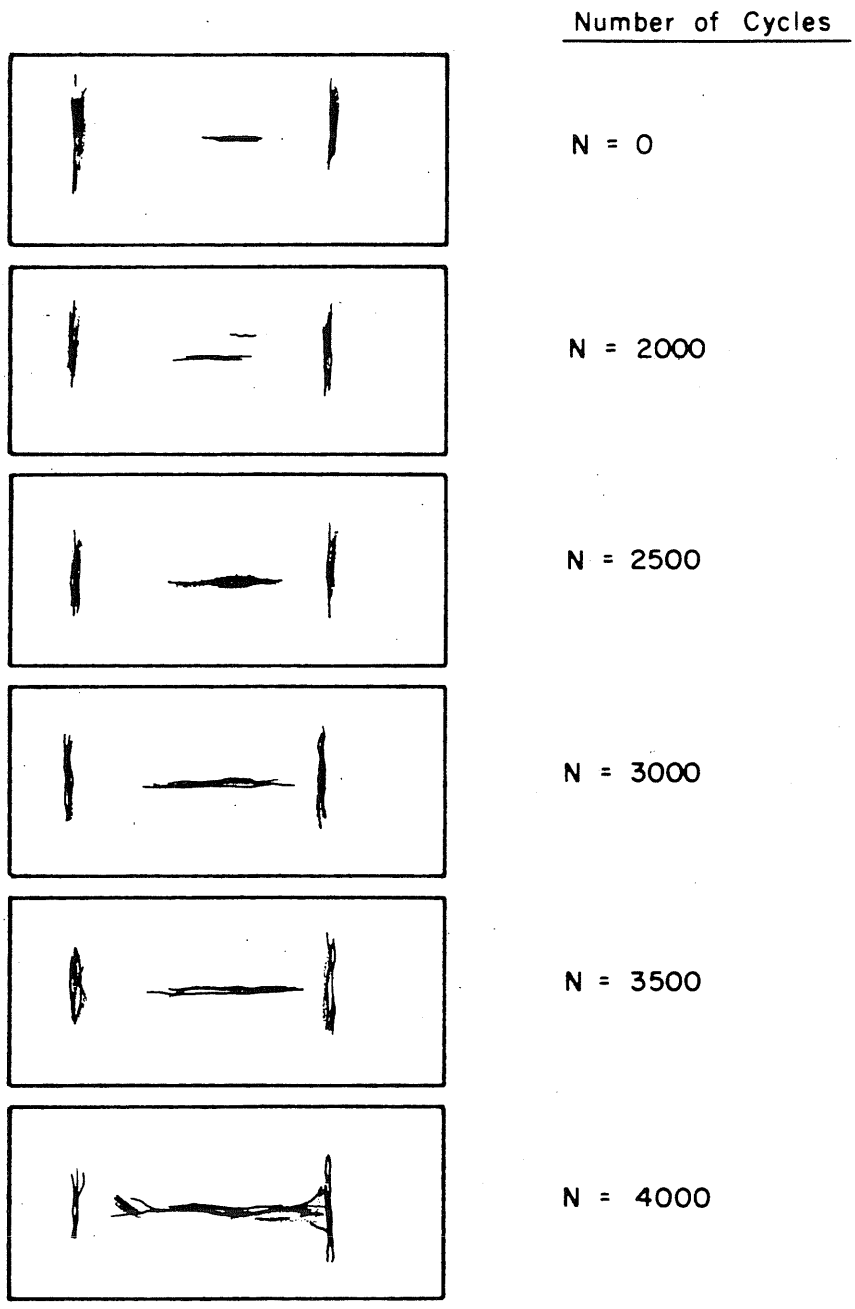

FIG. 3.29 TRACINGS OF RADIOGRAPHS TAKEN DURING FATIGUE TEST OF SPECIMEN NE-12

SPECIMEN ND-38

Stress Cycle: 0 to + 80.0 ksi

Key

Fracture Surface

1) Internal weld flaws visible on fracture surface
2) Extent of fatigue crack propagation at intersection with surface

Ultrasonic Readings

1) Location and extent of responses as indicated on detector scope
2) a. Number designation corresponds to magnitude of peak response as indicated on detector scope
   b. Letter designation corresponds to vertical location on specimen surface

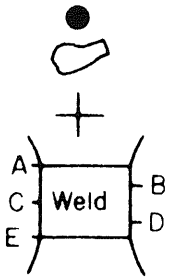

(a)

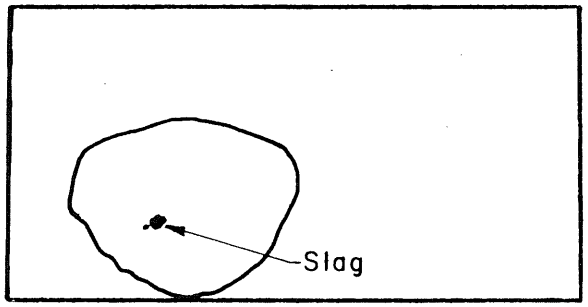

Fracture Surface

(b)

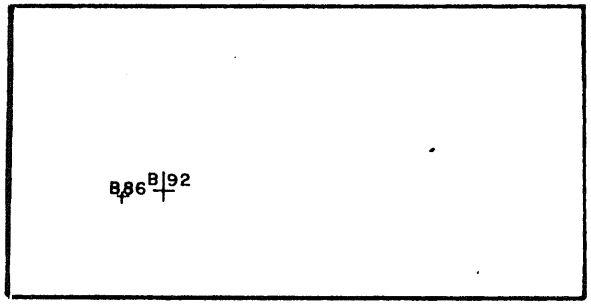

Ultrasonic Indications

0 Cycles

FIG. 3.30 FRACTURE SURFACE, AND ULTRASONIC INDICATIONS RECORDED FOR SPECIMEN ND-38

SPECIMEN ND-38 (Cont.)

(c)

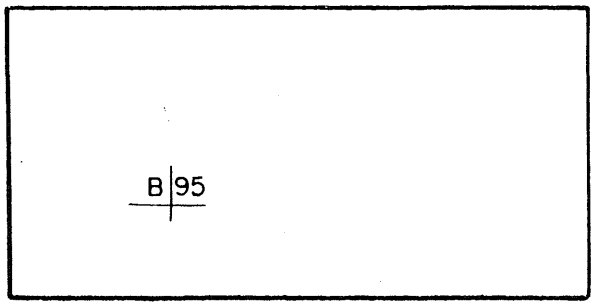

Ultrasonic Indications

1000 Cycles

FIG. 3.30 (cont.) FRACTURE SURFACE, AND ULTRASONIC INDICATIONS RECORDED FOR SPECIMEN ND-38

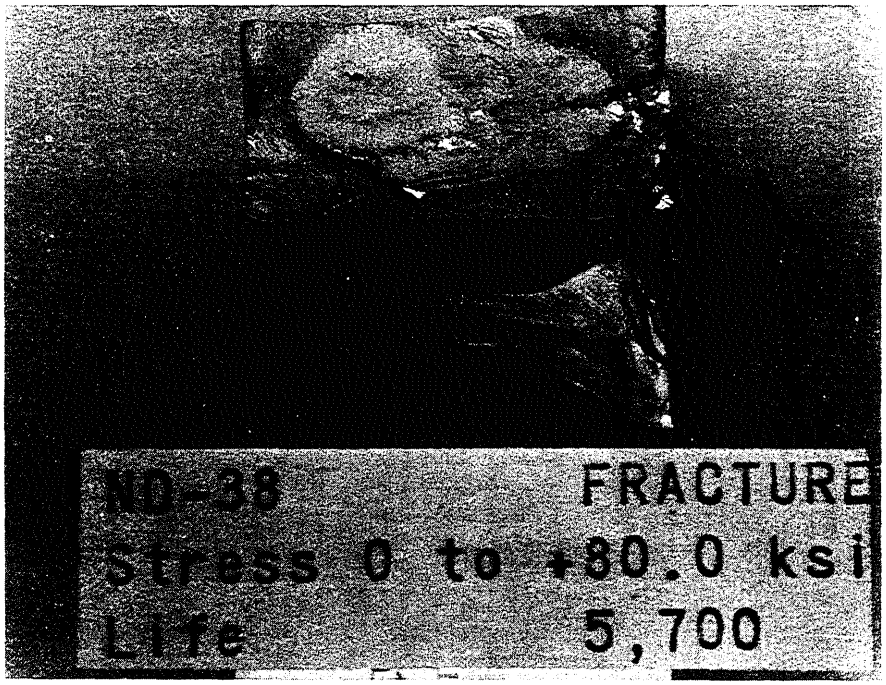

Photograph Of Fracture Surface

FIG.3.30(cont.) FRACTURE SURFACE, AND ULTRASONIC INDICATIONS RECORDED FOR SPECIMEN ND-38

SPECIMEN ND-45

Stress Cycle: 0 to + 80.0 ksi

Key

Fracture Surface

1) Internal weld flaws visible on fracture surface
2) Extent of fatigue crack propagation at intersection with surface

Ultrasonic Readings

1) Location and extent of responses as indicated on detector scope
2) a. Number designation corresponds to magnitude of peak response as indicated on detector scope
   b. Letter designation corresponds to vertical location on specimen surface

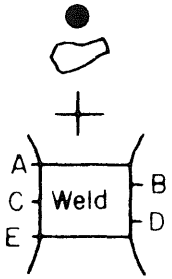

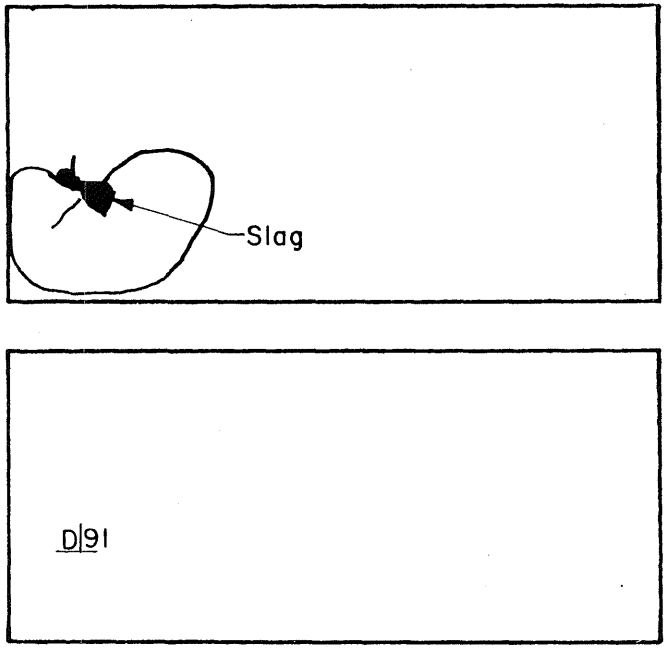

FIG. 3.31 FRACTURE SURFACE, AND ULTRASONIC INDICATIONS RECORDED FOR SPECIMEN ND-45

SPECIMEN ND-45 (Cont.)

(c)

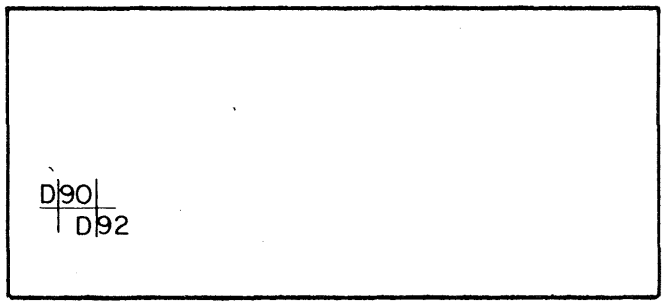

Ultrasonic Indications

2040 Cycles

FIG. 3.31 (cont.) FRACTURE SURFACE, AND ULTRASONIC INDICATIONS RECORDED FOR SPECIMEN ND-45

Photograph Of Fracture Surface

FIG. 3.31 (cont.) FRACTURE SURFACE, AND ULTRASONIC INDICATIONS RECORDED FOR SPECIMEN ND-45

SPECIMEN ND-47

Stress Cycle: 0 to + 80.0 ksi

Key:

Fracture Surface

1) Internal weld flaws visible on fracture surface
2) Extent of fatigue crack propagation at intersection with surface

Ultrasonic Readings

1) Location and extent of responses as indicated on detector scope
2) a. Number designation corresponds to magnitude of peak response as indicated on detector scope
   b. Letter designation corresponds to vertical location on specimen surface

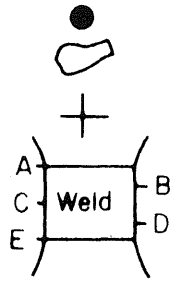

(a)

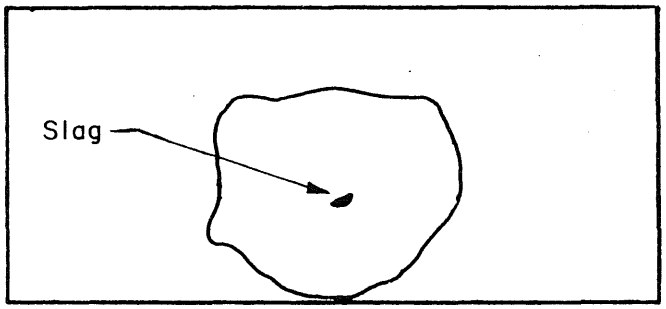

Fracture Surface

(b)

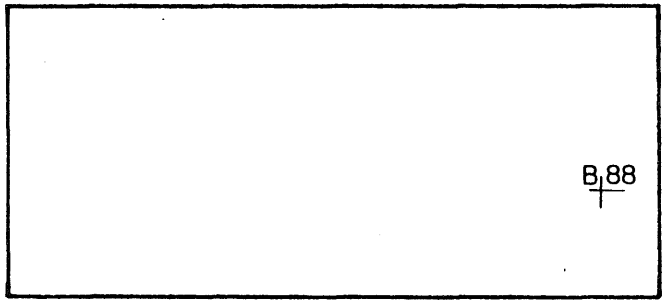

Ultrasonic Indications

0 Cycles

FIG. 3.32 FRACTURE SURFACE, AND ULTRASONIC INDICATIONS RECORDED FOR SPECIMEN ND-47

SPECIMEN ND-47 (Cont.)

(c)

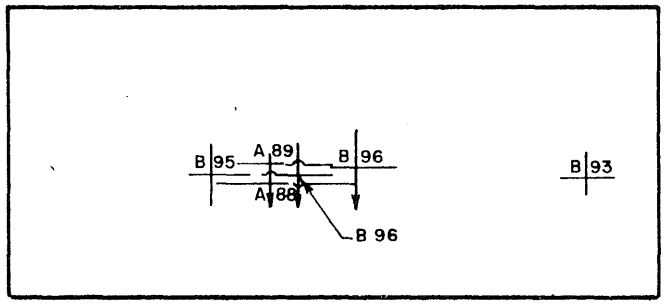

Ultrasonic Indications

6900 Cycles

FIG. 3.32 (cont.) FRACTURE SURFACE, AND ULTRASONIC INDICATIONS RECORDED FOR SPECIMEN ND-47

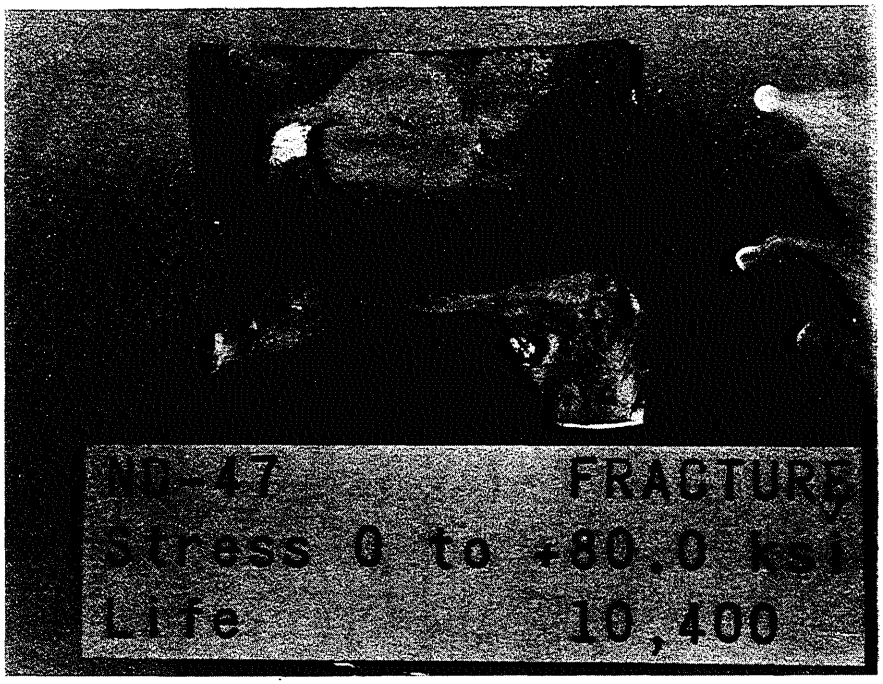

Photograph Of Fracture Surface

FIG.3.32 (cont.) FRACTURE SURFACE, AND ULTRASONIC INDICATIONS RECORDED FOR SPECIMEN ND-47

SPECIMEN NE-7

Stress Cycle: 0 to + 80.0 ksi

Key:

Fracture Surface

1) Internal weld flaws visible on fracture surface
2) Extent of fatigue crack propagation at intersection with surface

Ultrasonic Readings

1) Location and extent of responses as indicated on detector scope
2) a. Number designation corresponds to magnitude of peak response as indicated on detector scope
   b. Letter designation corresponds to vertical location on specimen surface

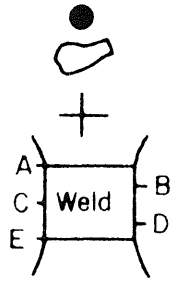

(a)

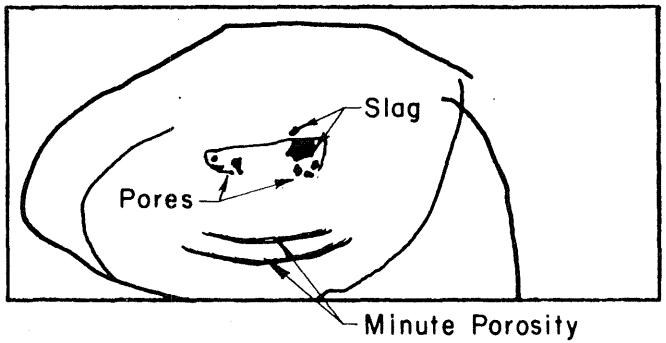

Fracture Surface

(b)

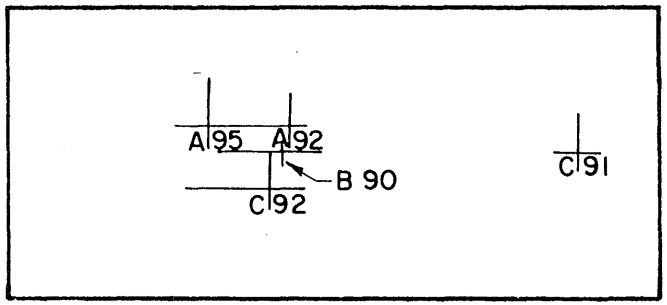

Ultrasonic Indications

0 Cycles

FIG. 3.33 FRACTURE SURFACE, AND ULTRASONIC INDICATIONS RECORDED FOR SPECIMEN NE-7

(c)

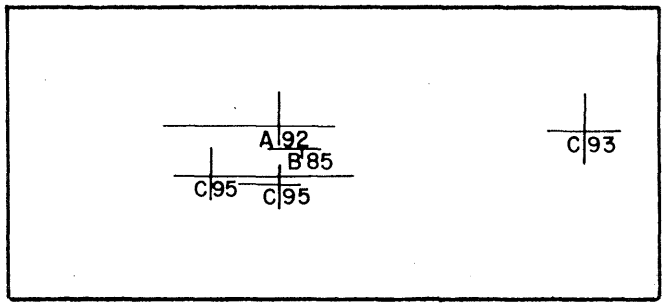

Ultrasonic Indications

500 Cycles

FIG. 3.33 (cont.) FRACTURE SURFACE, AND ULTRASONIC INDICATIONS RECORDED FOR SPECIMEN NE-7

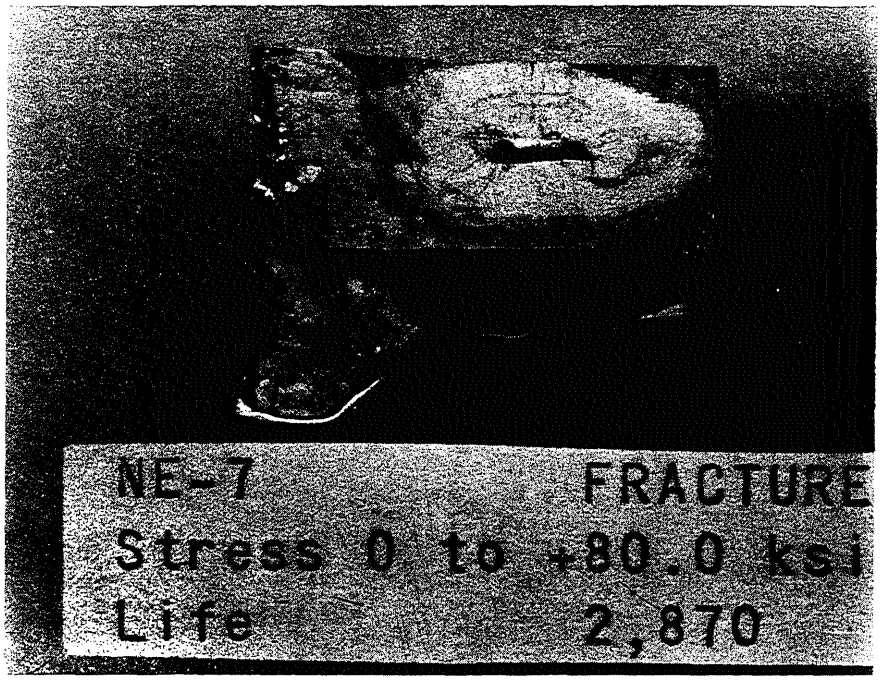

Photograph Of Fracture Surface

FIG.3.33(cont.) FRACTURE SURFACE, AND ULTRASONIC INDICATIONS RECORDED FOR SPECIMEN NE-7

SPECIMEN NE-10

Stress Cycle: 0 to + 80.0 ksi

Key:

Fracture Surface

1) Internal weld flaws visible on fracture surface
2) Extent of fatigue crack propagation at intersection with surface

Ultrasonic Readings

1) Location and extent of responses as indicated on detector scope
2) a. Number designation corresponds to magnitude of peak response as indicated on detector scope
   b. Letter designation corresponds to vertical location on specimen surface

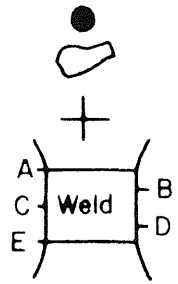

(a)

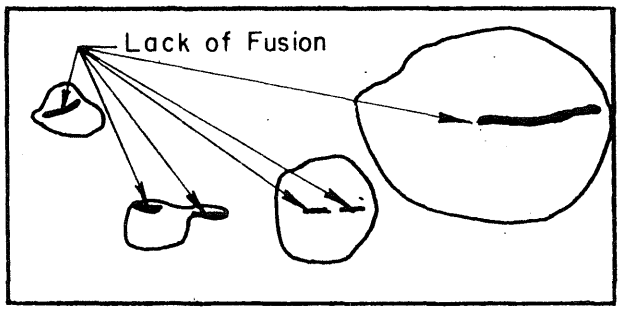

Fracture Surface

(b)

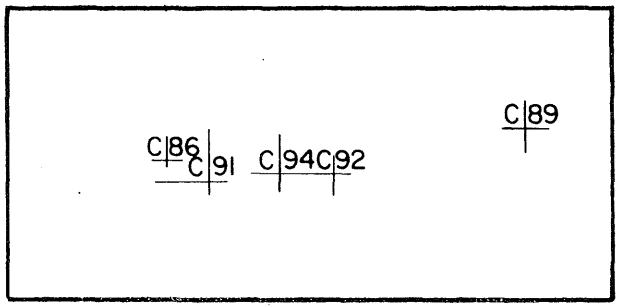

Ultrasonic Indications

0 Cycles

FIG. 3.34 FRACTURE SURFACE, AND ULTRASONIC INDICATIONS RECORDED FOR SPECIMEN NE-10

SPECIMEN NE-10 (Cont.)

(c)

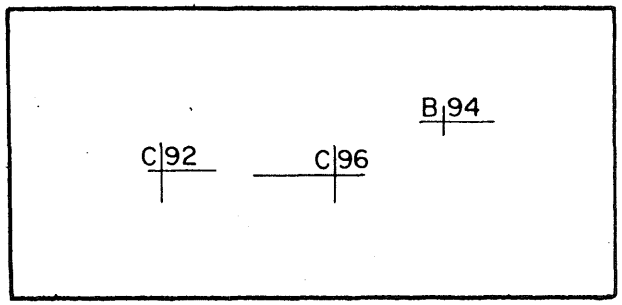

Ultrasonic Indications

2000 Cycles

FIG. 3.34 (cont.) FRACTURE SURFACE, AND ULTRASONIC INDICATIONS RECORDED FOR SPECIMEN NE-10

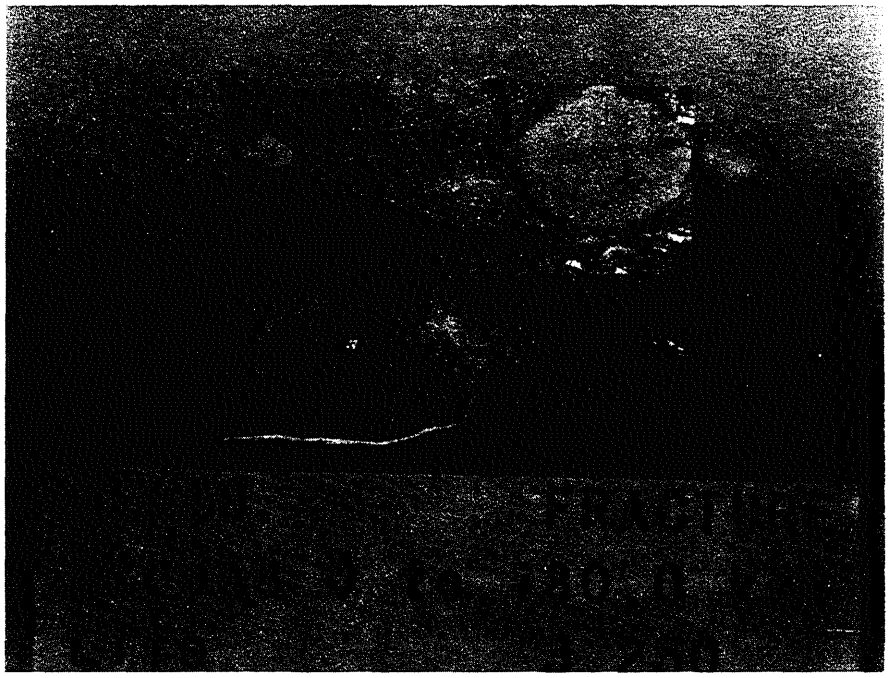

Photograph Of Fracture Surface

FIG.3.34 (cont.) FRACTURE SURFACE, AND ULTRASONIC INDICATIONS RECORDED FOR SPECIMEN NE-10

SPECIMEN NE-11

Stress Cycle: 0 to + 80.0 ksi

Key:

Fracture Surface

1) Internal weld flaws visible on fracture surface
2) Extent of fatigue crack propagation at intersection with surface

Ultrasonic Readings

1) Location and extent of responses as indicated on detector scope
2) a. Number designation corresponds to magnitude of peak response as indicated on detector scope
   b. Letter designation corresponds to vertical location on specimen surface

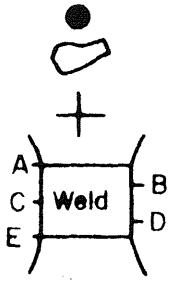

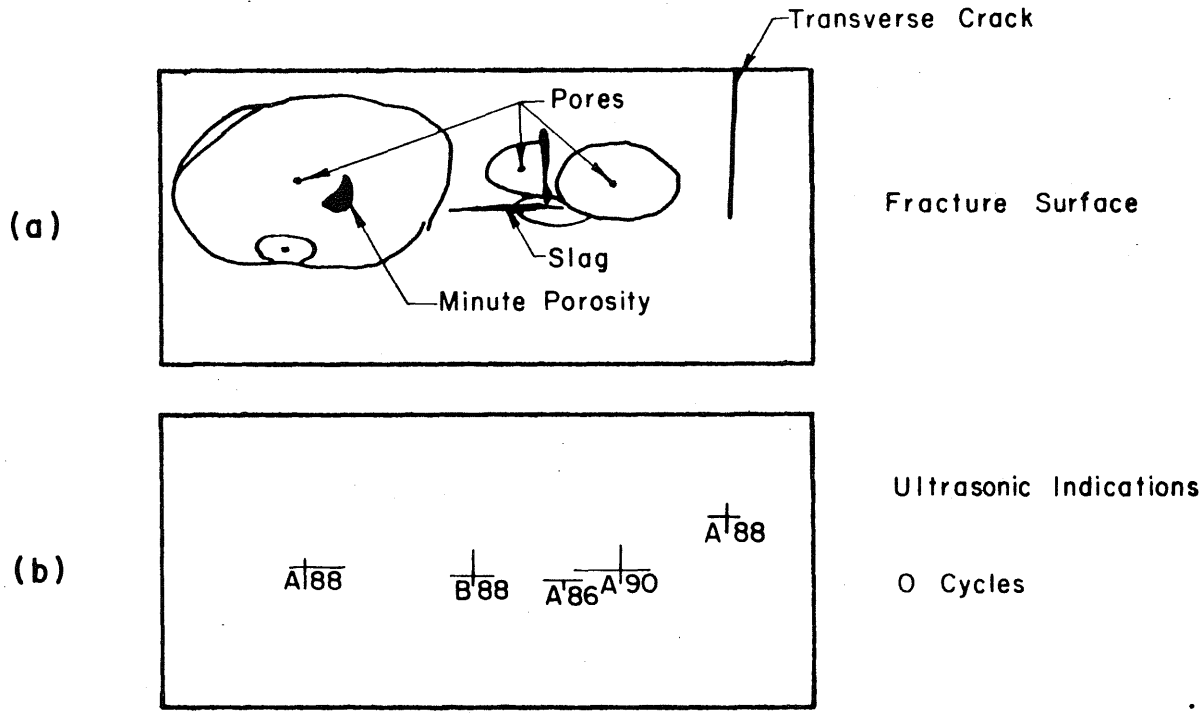

FIG. 3.35 FRACTURE SURFACE, AND ULTRASONIC INDICATIONS RECORDED FOR SPECIMEN NE-11

SPECIMEN NE-11 (Cont.)

(c)

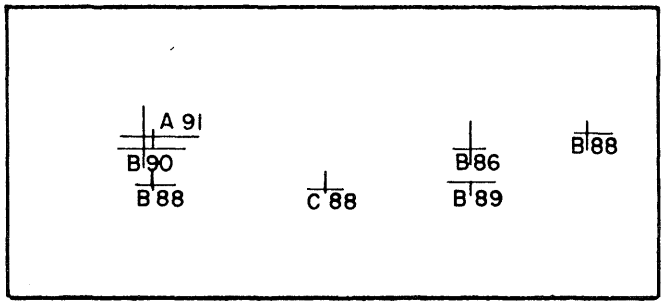

Ultrasonic Indications

2000 Cycles

FIG. 3.35 (cont.) FRACTURE SURFACE, AND ULTRASONIC INDICATIONS RECORDED FOR SPECIMEN NE-11

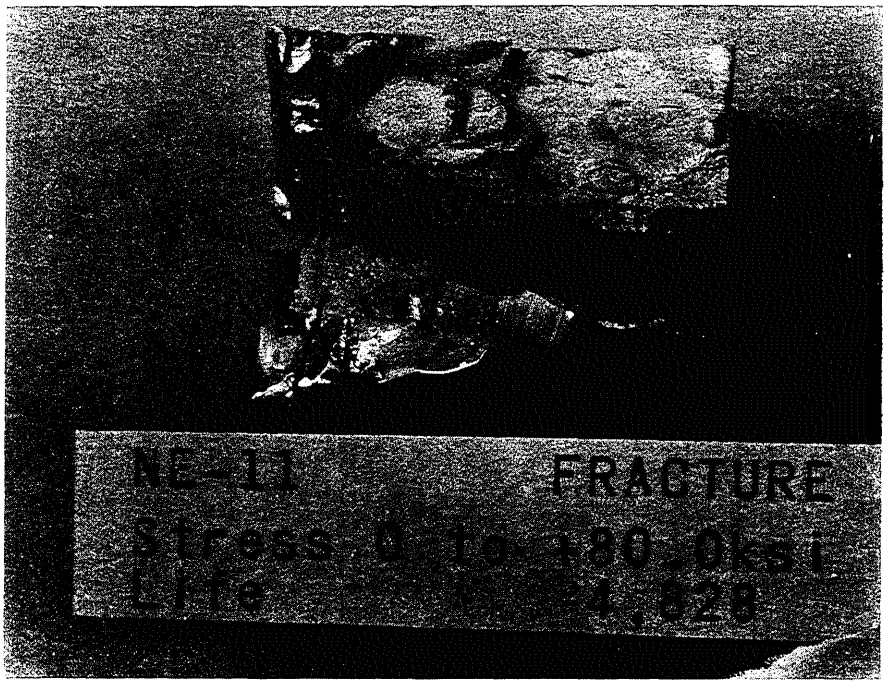

Photograph Of Fracture Surface

FIG.3.35 (cont.) FRACTURE SURFACE, AND ULTRASONIC INDICATIONS RECORDED FOR SPECIMEN NE-11

SPECIMEN NE-12
Stress Cycle: 0 to + 80.0 ksi

Key.

Fracture Surface

1) Internal weld flaws visible on fracture surface
2) Extent of fatigue crack propagation at intersection with surface

Ultrasonic Readings

1) Location and extent of responses as indicated on detector scope
2) a. Number designation corresponds to magnitude of peak response as indicated on detector scope
   b. Letter designation corresponds to vertical location on specimen surface

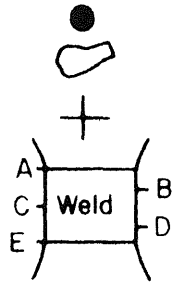

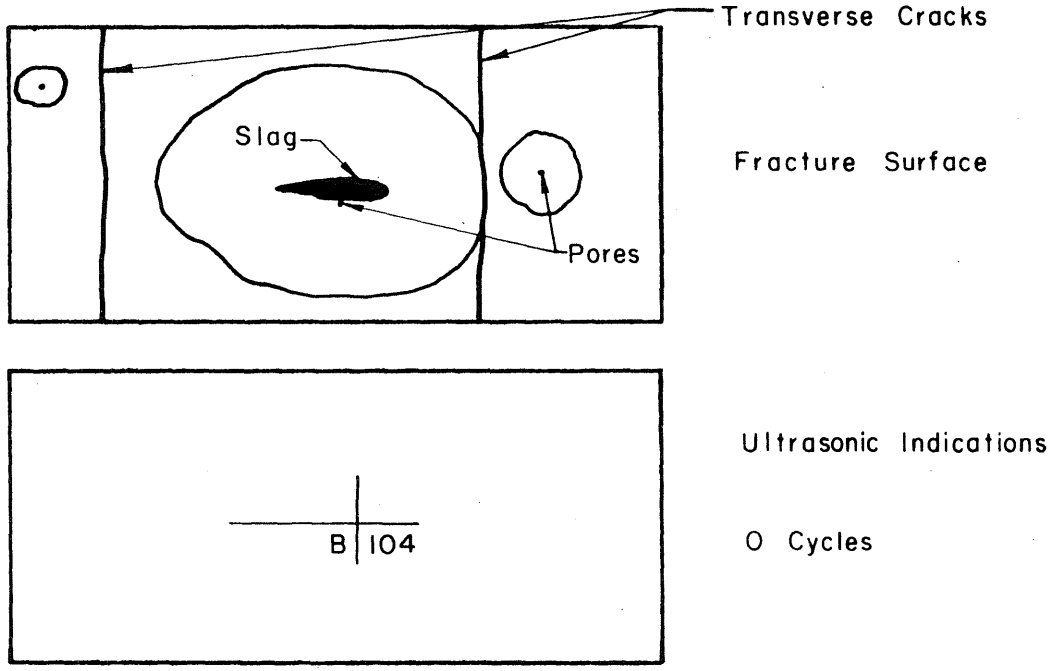

FIG. 3.36 FRACTURE SURFACE, AND ULTRASONIC INDICATIONS RECORDED FOR SPECIMEN NE-12

SPECIMEN NE-12 (Cont.)

(c)

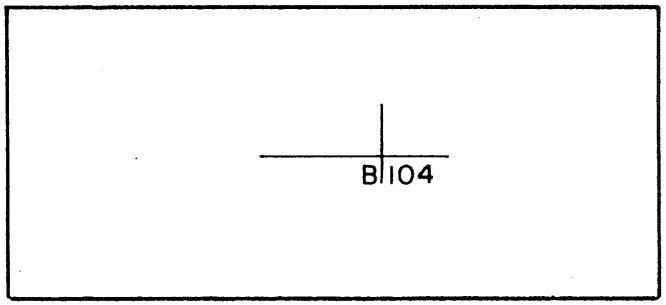

Ultrasonic Indications

2000 Cycles

FIG. 3.36 (cont.) FRACTURE SURFACE, AND ULTRASONIC INDICATIONS RECORDED FOR SPECIMEN NE-12

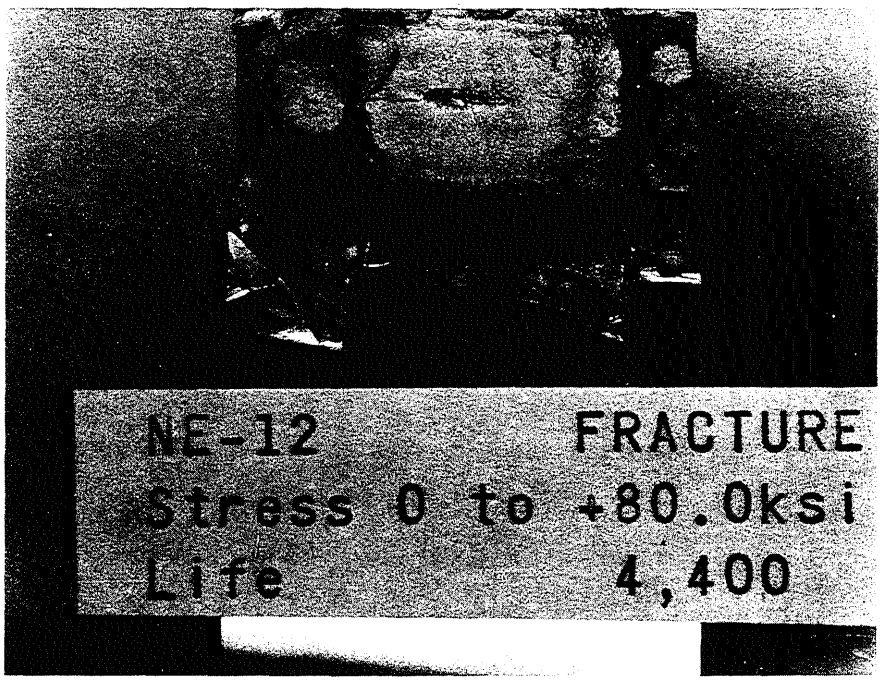

Photograph Of Fracture Surface

FIG. 3.36(cont.) FRACTURE SURFACE, AND ULTRASONIC INDICATIONS RECORDED FOR SPECIMEN NE-12

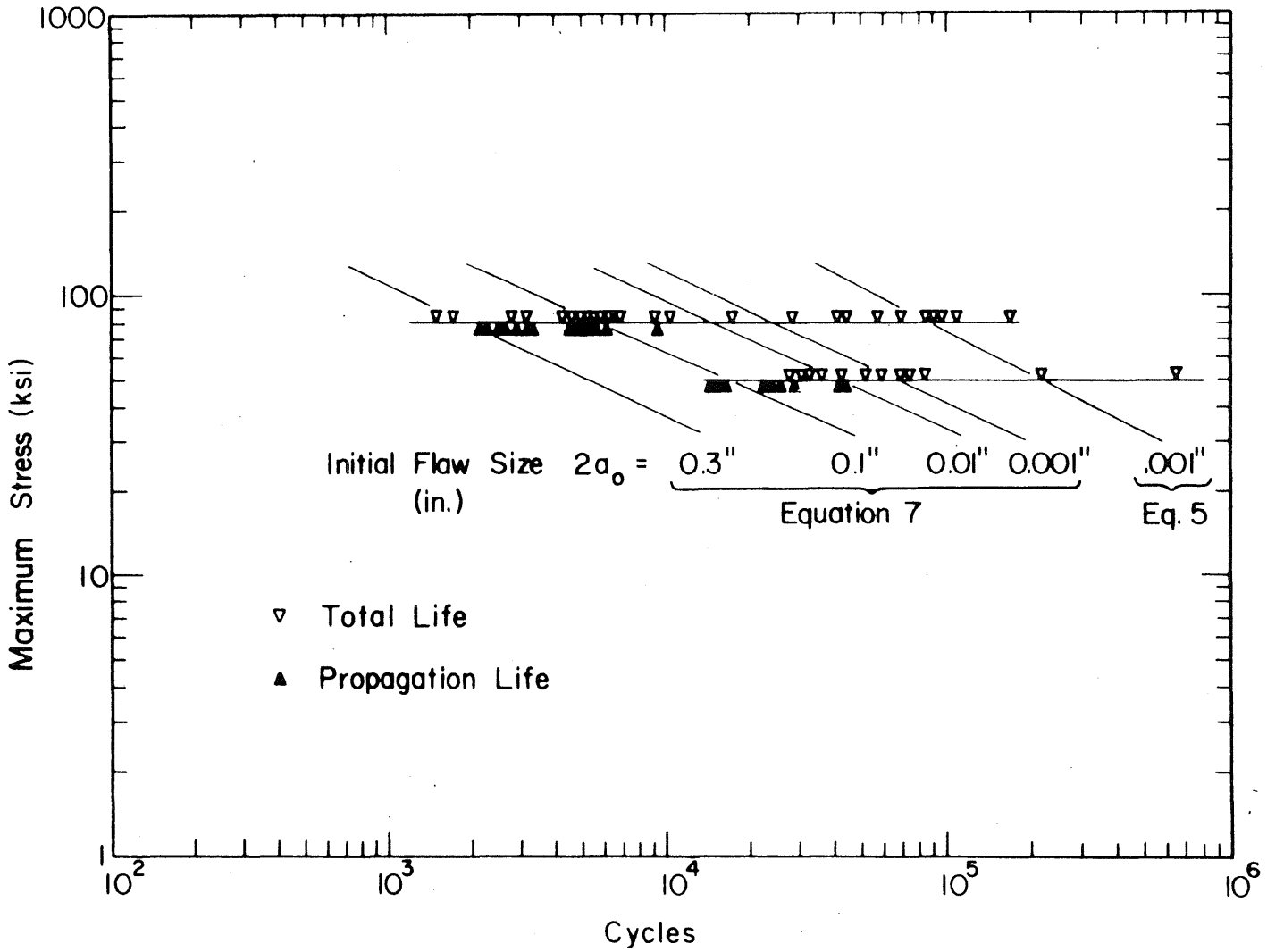

FIG. 3.37 TOTAL AND CRACK PROPAGATION PORTIONS OF FATIGUE LIFE OF HY-130 (T) BUTT WELDS INITIATING FAILURE AT INTERNAL WELD DISCONTINUITIES

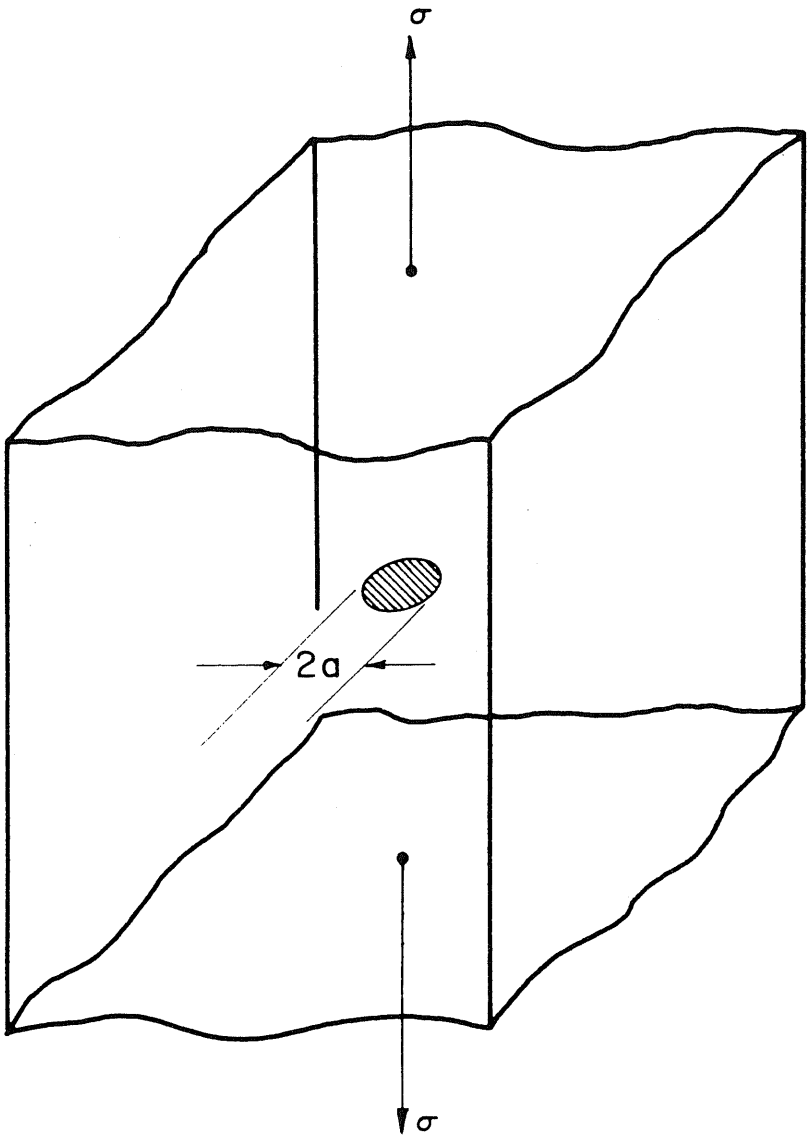

$$\Delta K = \frac{2}{\pi} \sigma \sqrt{\pi a}$$

FIG. 3.38 MODEL FOR FLAWED WELDMENT : DISC-SHAPED CRACK IN AN INFINITE BODY

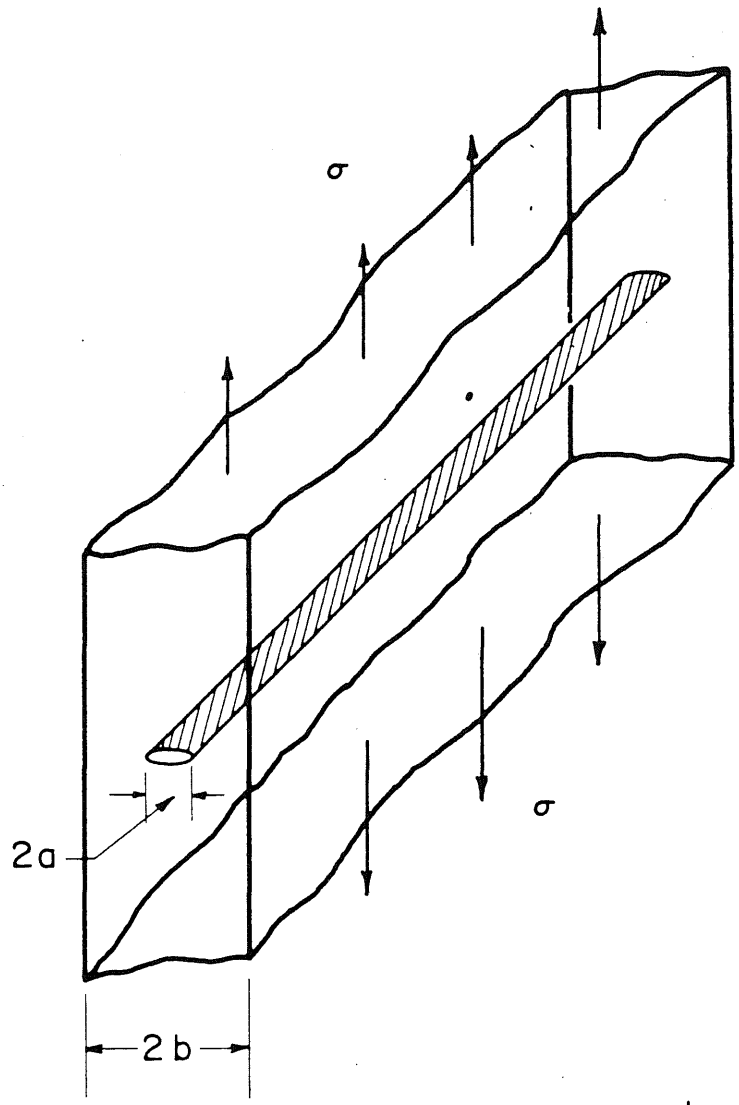

$$\Delta K = \sigma \sqrt{\pi a} \left(\sec \frac{\pi a}{2b}\right)^{1/2}$$

$$(0 \leq a \leq 0.8b)$$

FIG. 3.39 MODEL FOR FLAWED WELDMENT: THROUGH CRACK IN A FINITE PLATE

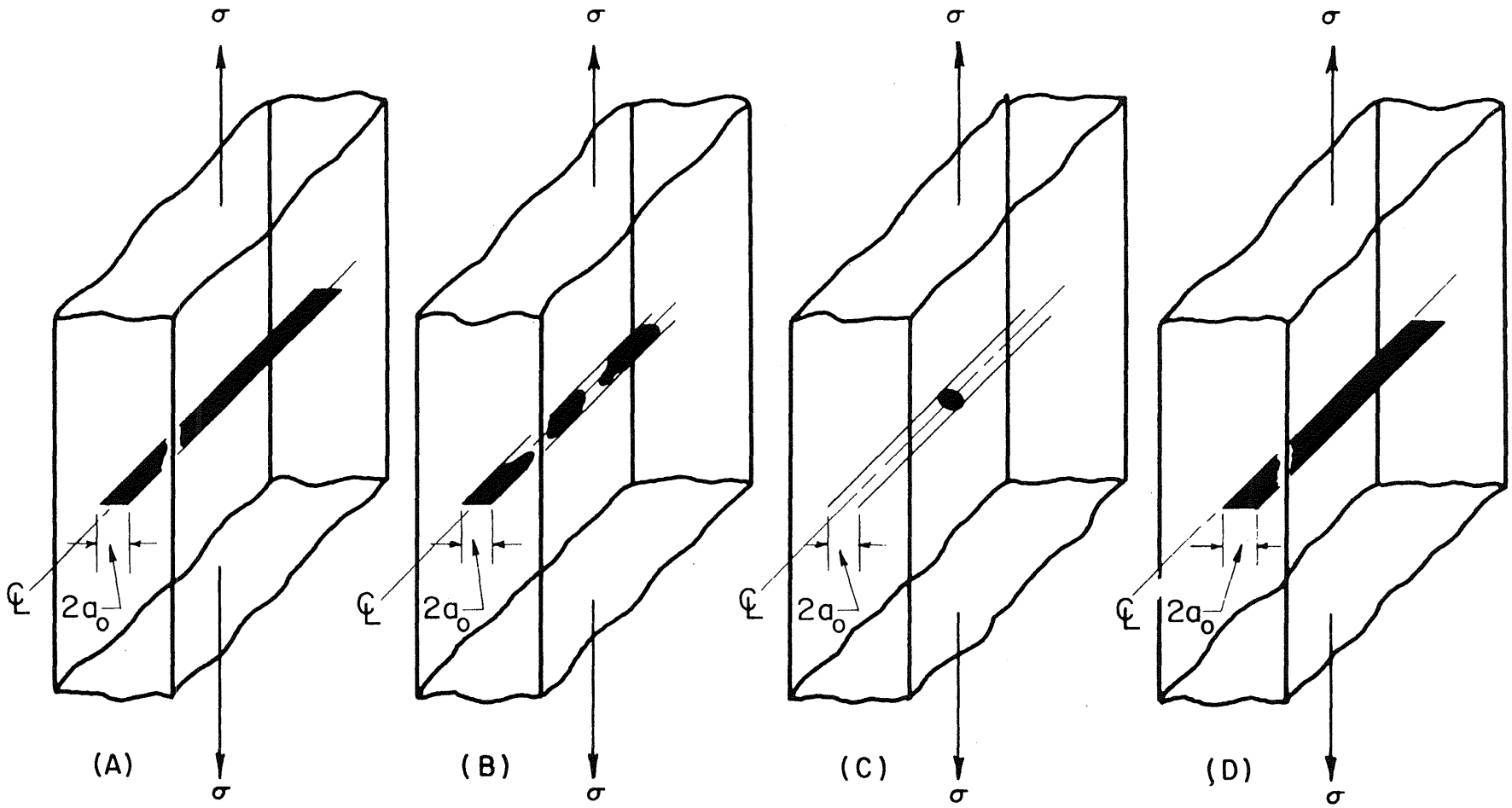

FIG. 3.40 TYPES OF FLAWS FOUND IN WELDMENTS

(A) CONTINUOUS LINEAR DEFECTS AT THE CENTER OF THE WELDMENT, *e.g.*, LACK OF FUSION, CONTINUOUS SLAG.

(B) INTERMITTENT LINEAR DEFECTS AT THE CENTER OF THE WELDMENT, *e.g.*, INTERMITTENT LACK OF FUSION, INTERMITTENT SLAG, LINEAR POROSITY.

(C) ISOLATED PORES AT THE CENTER OF THE WELDMENT, *e.g.*, SMALL VOIDS, PORES, VERY SMALL DEFECTS OF ALL KINDS.

(D) CONTINUOUS LINEAR DEFECTS LOCATED OFF CENTER IN THE WELDMENT.

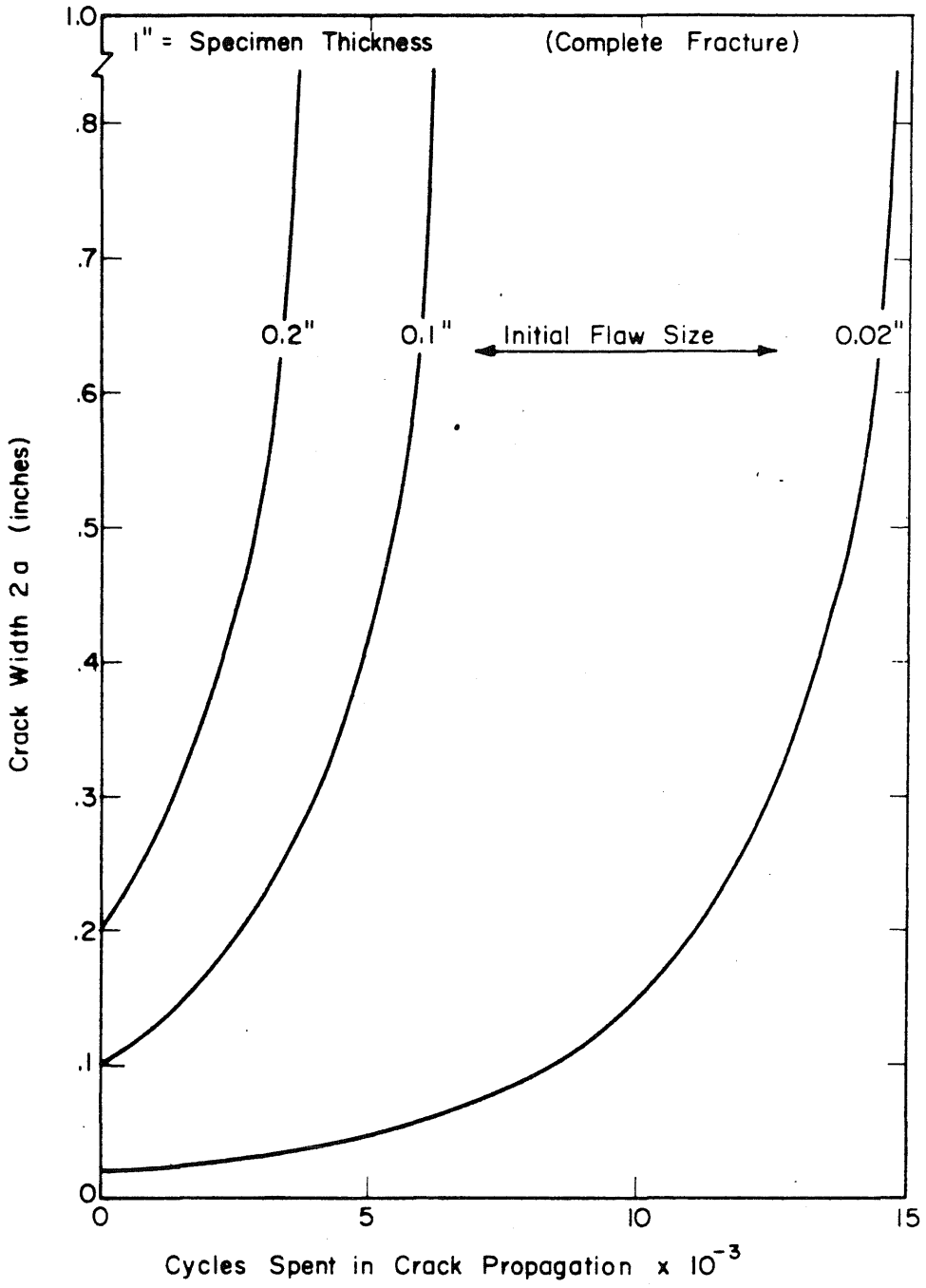

FIG. 3.41 EFFECT OF INITIAL FLAW SIZE ON CRACK PROPAGATION LIFE OF FLAWED, ONE-INCH THICK HY-130(T) WELDMENT

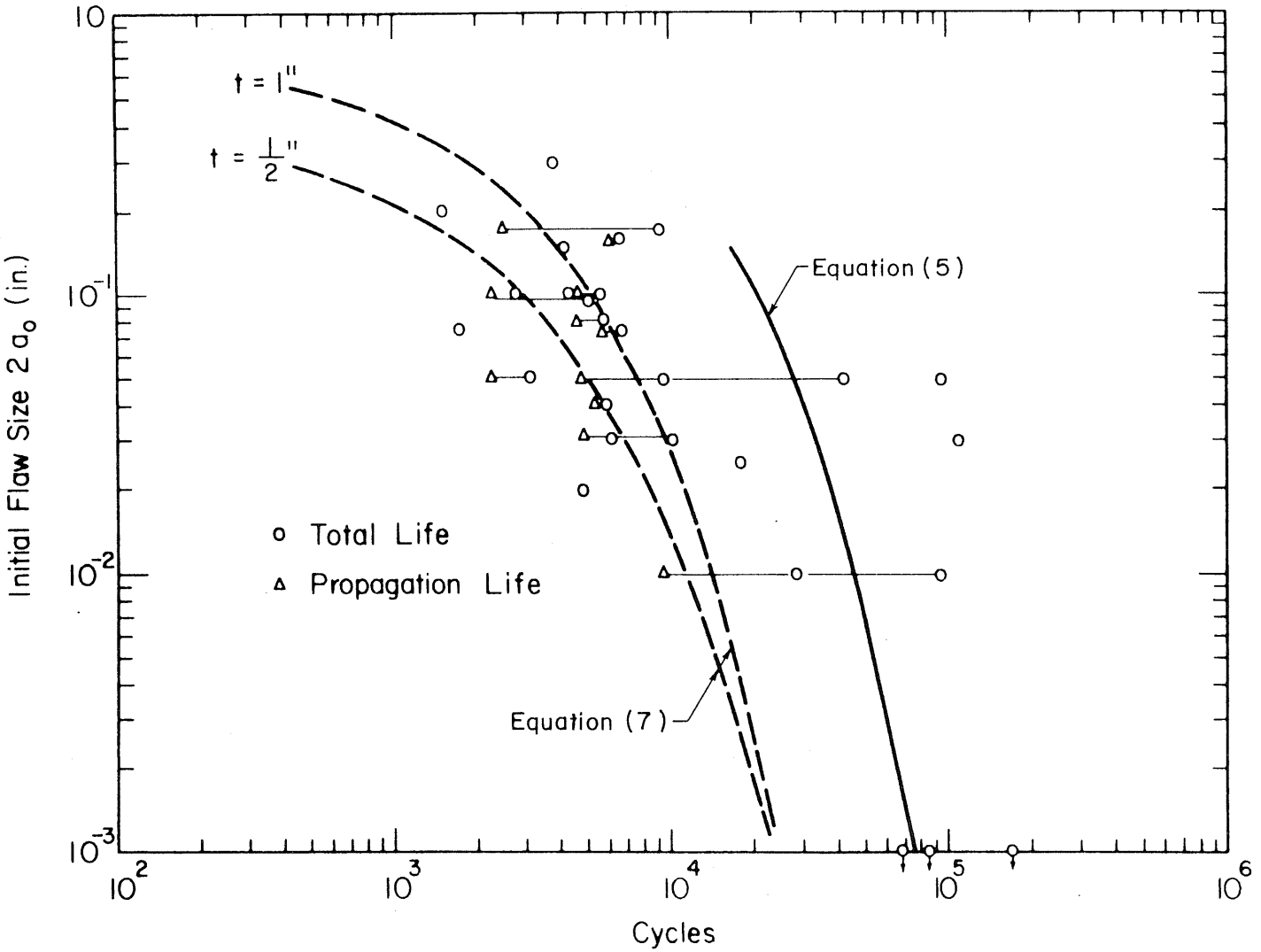

FIG. 3.42 CRACK PROPAGATION AND TOTAL FATIGUE LIVES AS A FUNCTION OF INITIAL FLAW SIZE (WIDTH) STRESS CYCLE: 0 TO +80 ksi

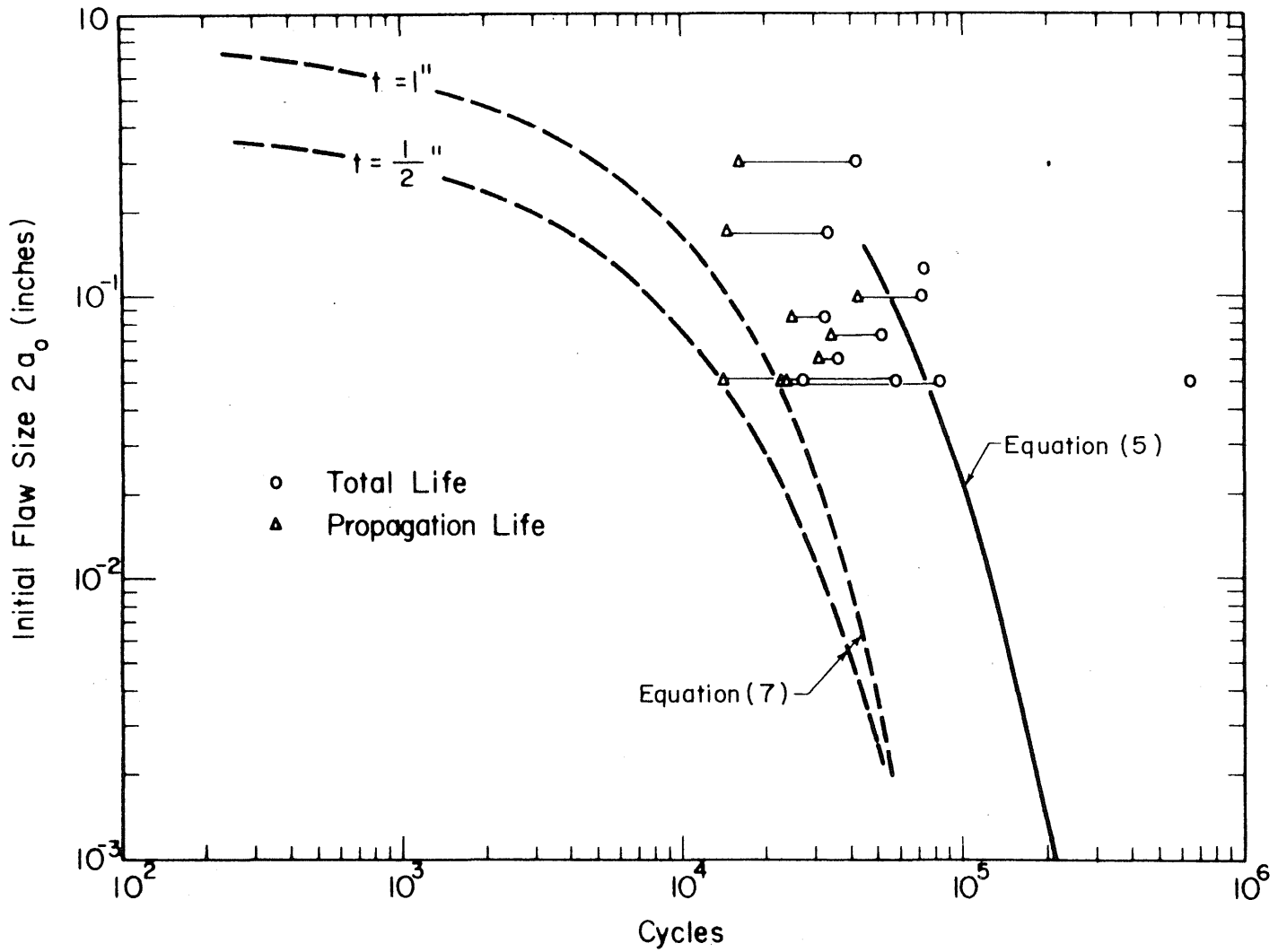

FIG. 3.43 CRACK PROPAGATION AND TOTAL FATIGUE LIVES AS A FUNCTION OF INITIAL FLAW SIZE (WIDTH) STRESS CYCLE: 0 TO +50 ksi

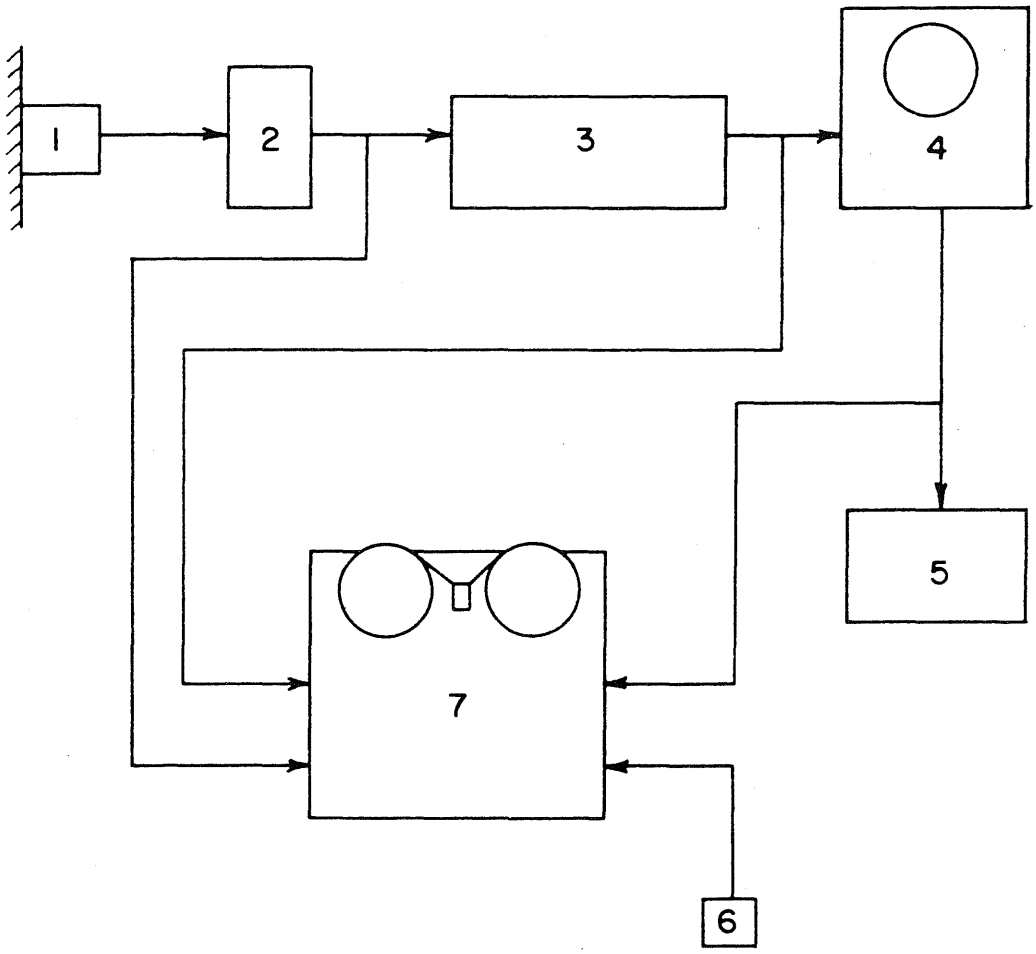

1. Transducer
2. Amplifier
3. Electronic Filter
4. Oscilloscope
5. Digital Counter
6. Microphone
7. Tape Recorder

FIG. 3.44 BLOCK DIAGRAM OF INSTRUMENTATION SETUP FOR ACOUSTIC EMISSION MEASUREMENTS

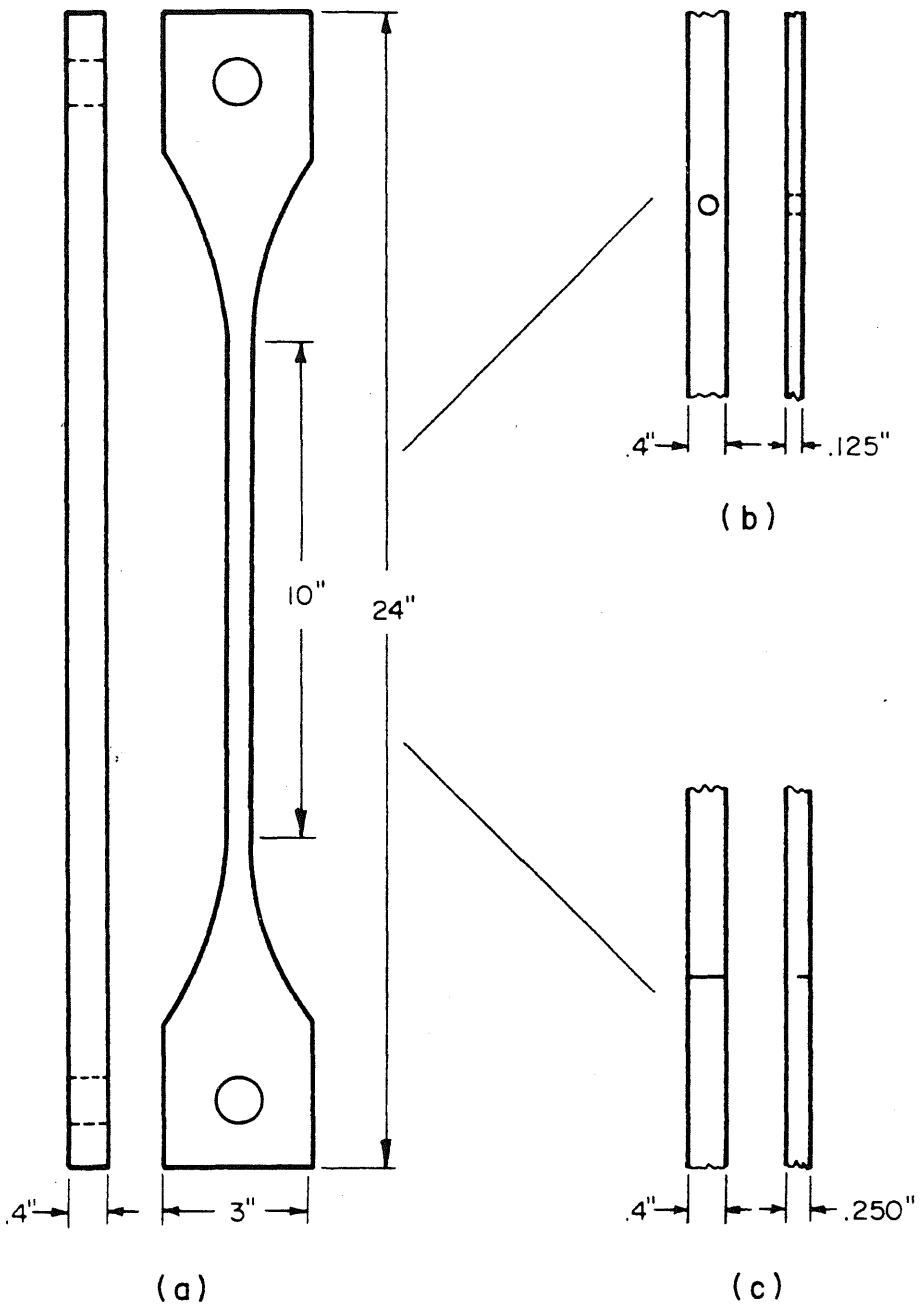

(a) Unnotched Tensile Specimen

(b) Center Notched Fatigue Specimen

(c) Single Edge Notched Tensile Specimen

FIG.3.45 TEST SPECIMENS USED IN EXPERIMENTS OF ACOUSTIC EMISSION

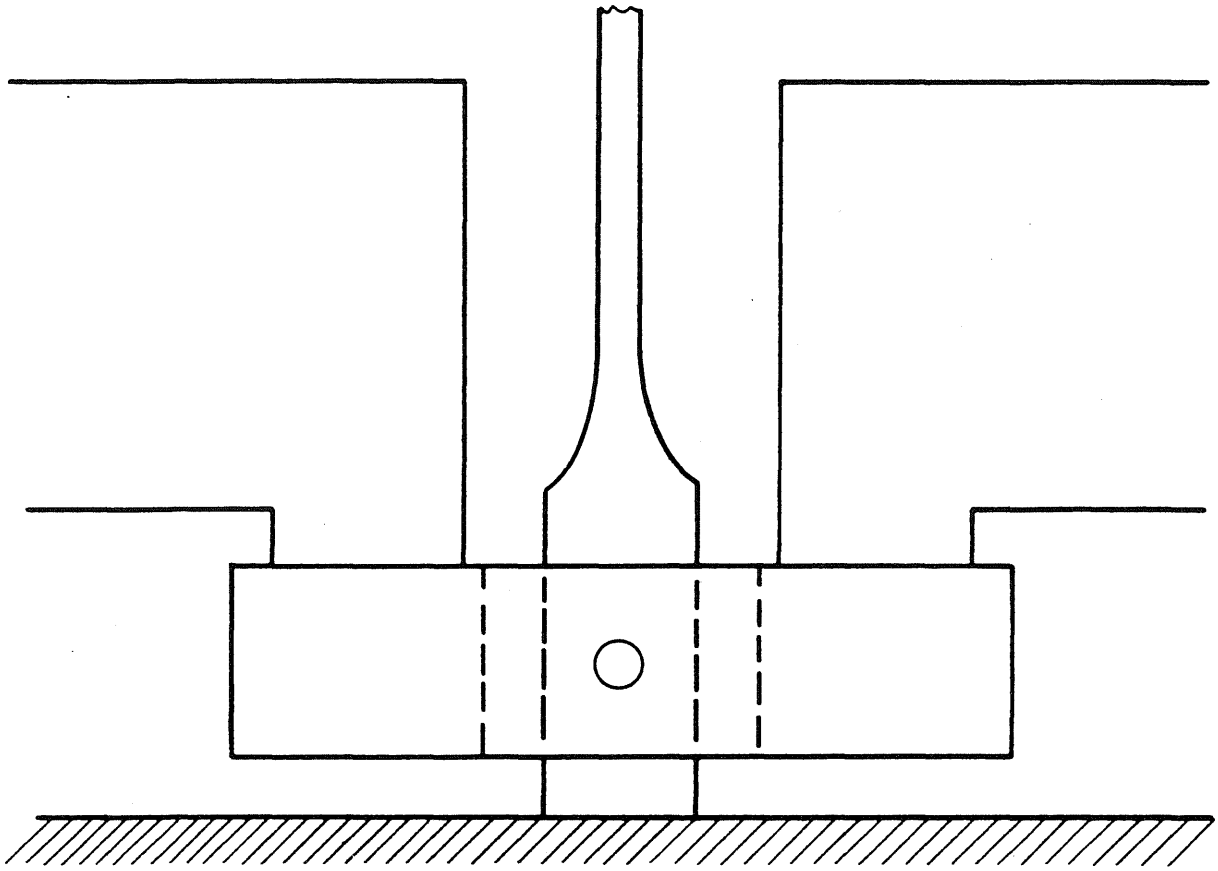

FIG. 3.46 PRELOADING MECHANISM FOR SPECIMENS

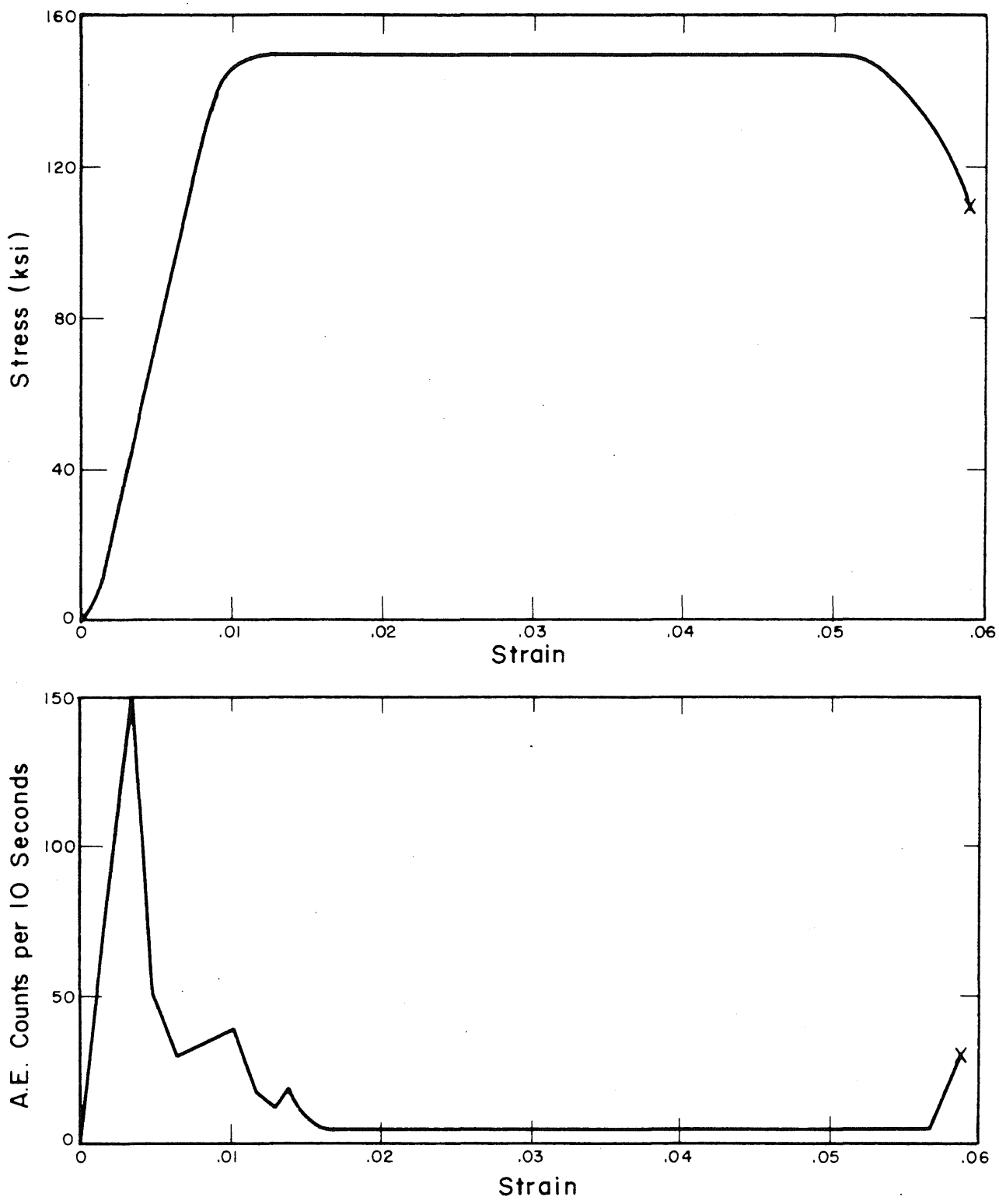

FIG. 3.47 ACOUSTIC EMISSION AND STRESS AS A FUNCTION OF STRAIN FOR UNNOTCHED HY-130(T) STEEL

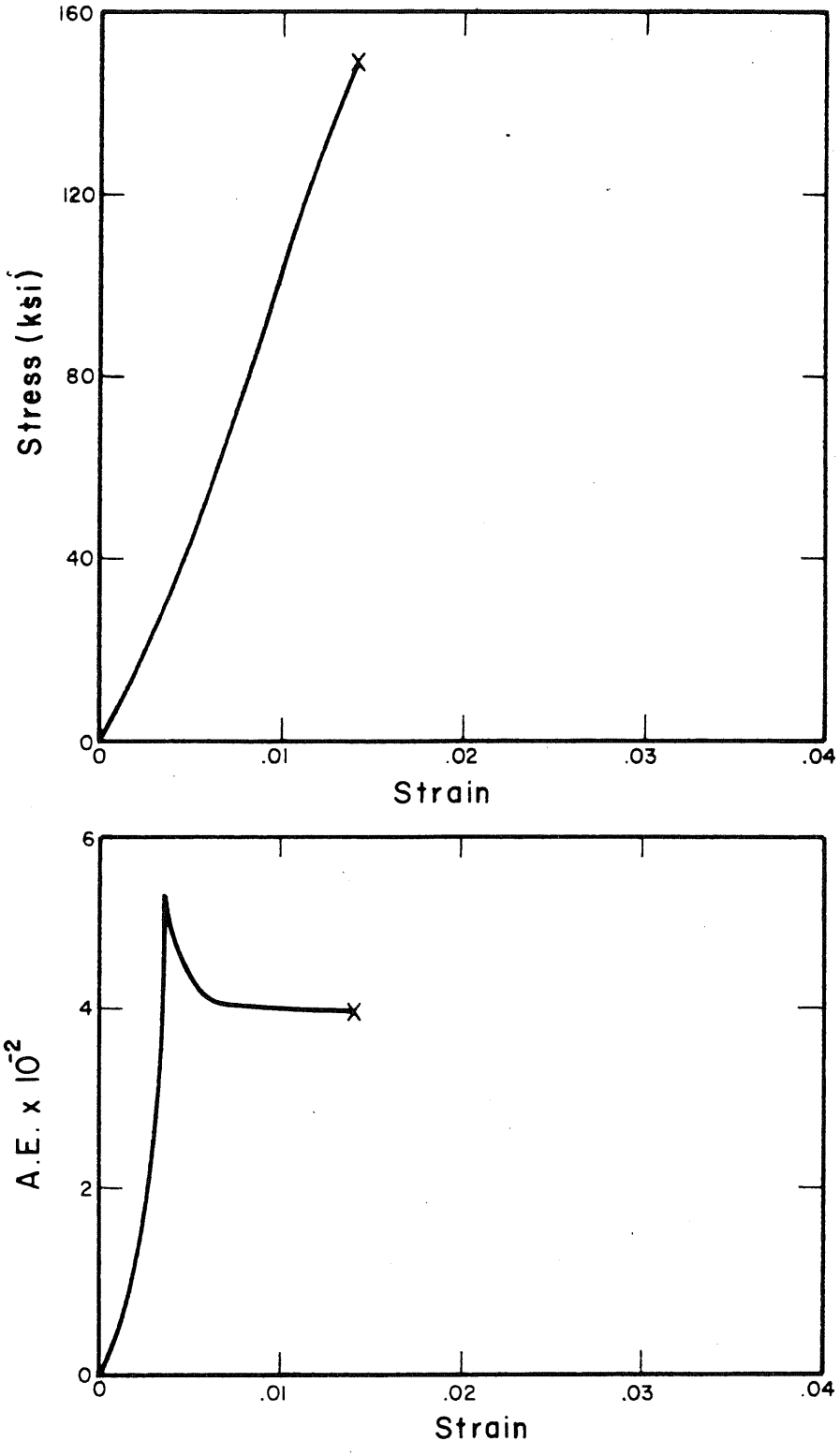

FIG.3.48 ACOUSTIC EMISSION AND STRESS AS A FUNCTION OF STRAIN FOR NOTCHED HY-130(T) STEEL

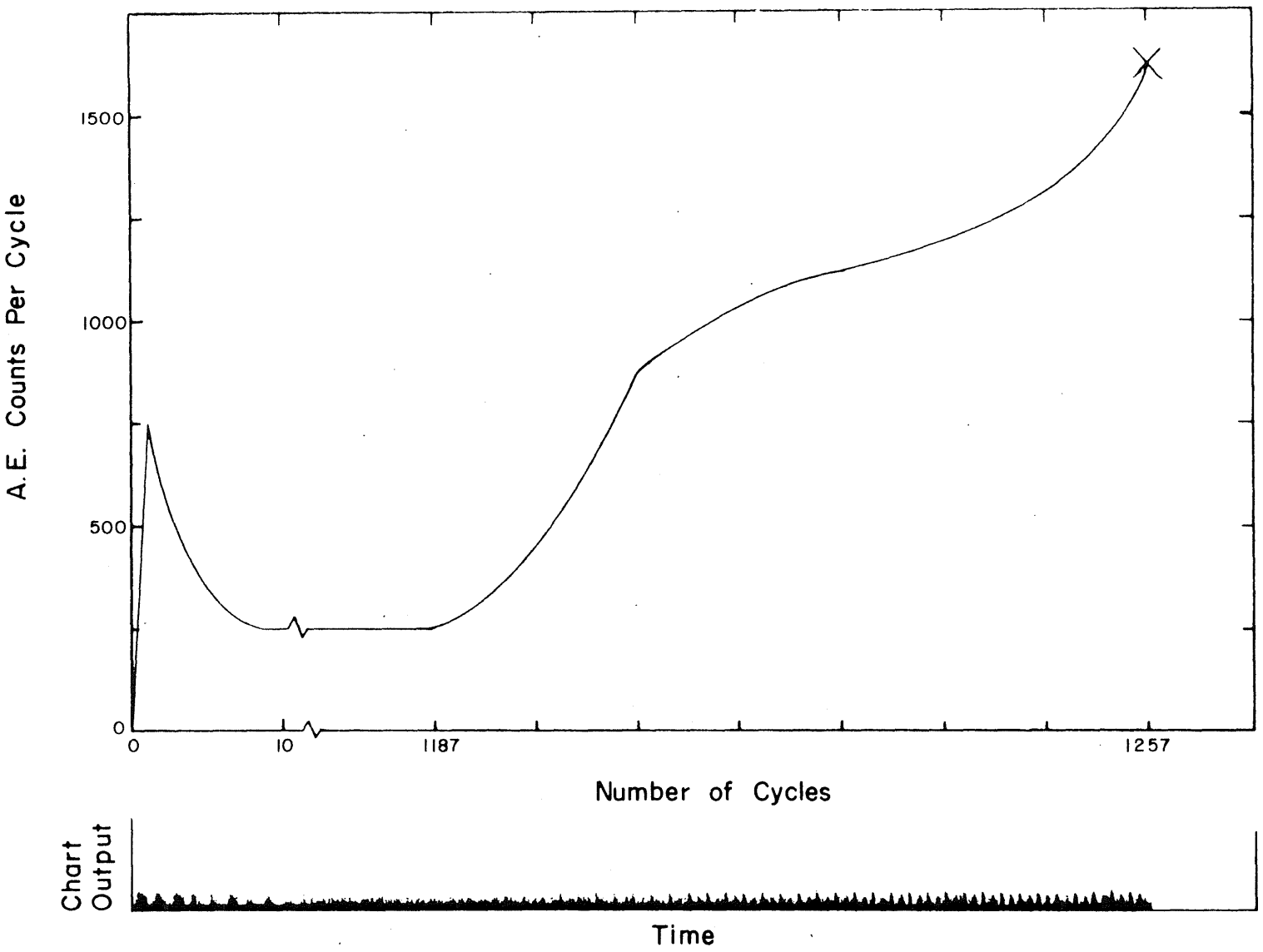

FIG.3.49 PLOT OF ACOUSTIC EMISSION FROM AN HY-130(T) SPECIMEN UNDERGOING FATIGUE

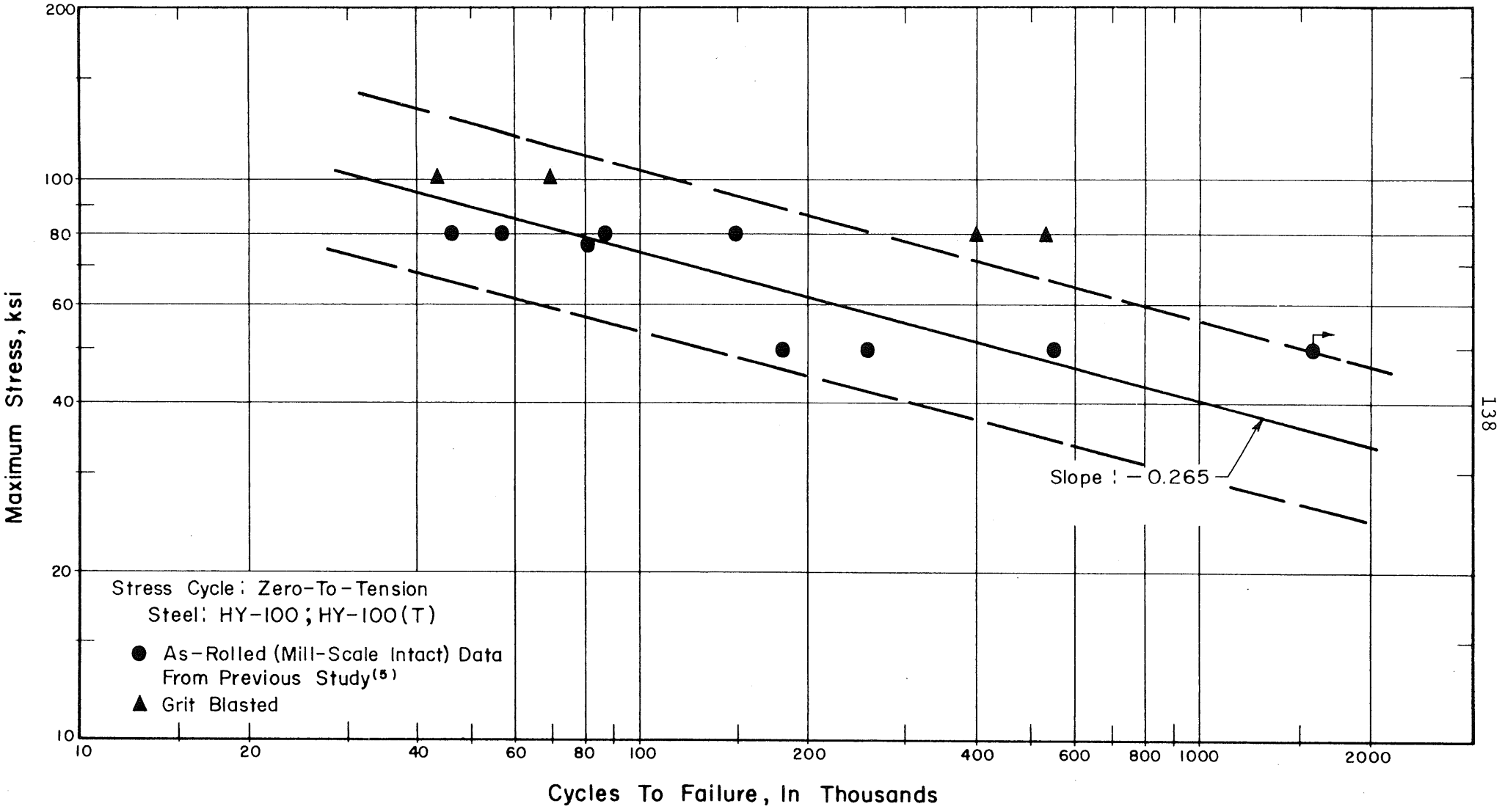

FIG. 4.1 RESULTS OF FATIGUE TESTS OF HY-100 (T) PLAIN PLATE SPECIMENS

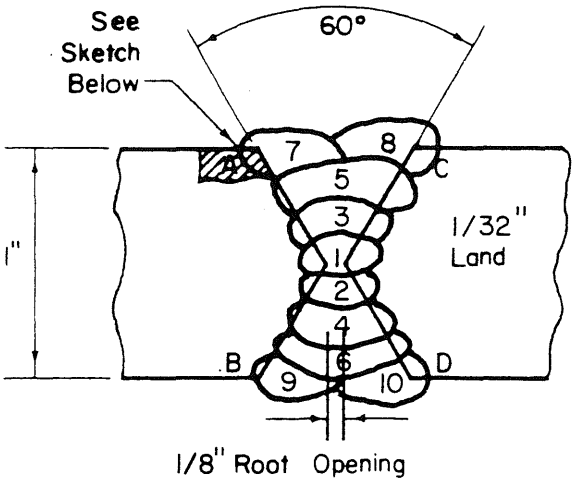

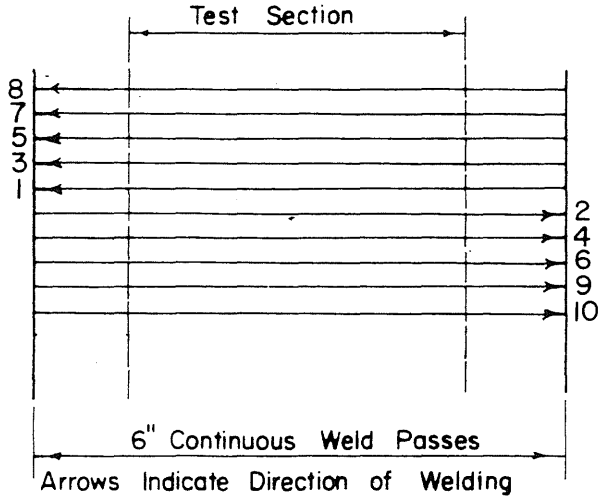

Pass	Electrode Size, in.	Current, amps	Rate of Travel, in./min.
1	5/32	140	5
2	5/32	140	5
3	3/16	220	7
4 - 10	3/16	220	7

Welding Electrode: McKay 12018 Coated Electrode

Voltage: 21 Volts
Polarity: DC Reversed
Preheat Temperature: 250°F
Interpass Temperature: 250°F
Heat Input: 40,000 Joules/In. (Maximum)
All Welding in Flat Position
Underside of Pass 1 Ground With Carbide Wheel Before Placing Pass 2

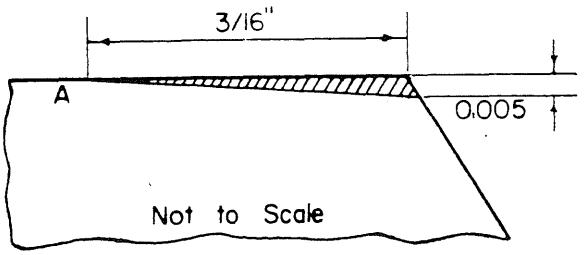

Preparation of Joint Before Welding:
Cross Hatched Area Removed by Milling on Corners A, B, C, D.
Beveled Joint Surfaces Filed and Cleaned With Acetone

FIG. 4.2 WELDING PROCEDURE P110-M12018-A

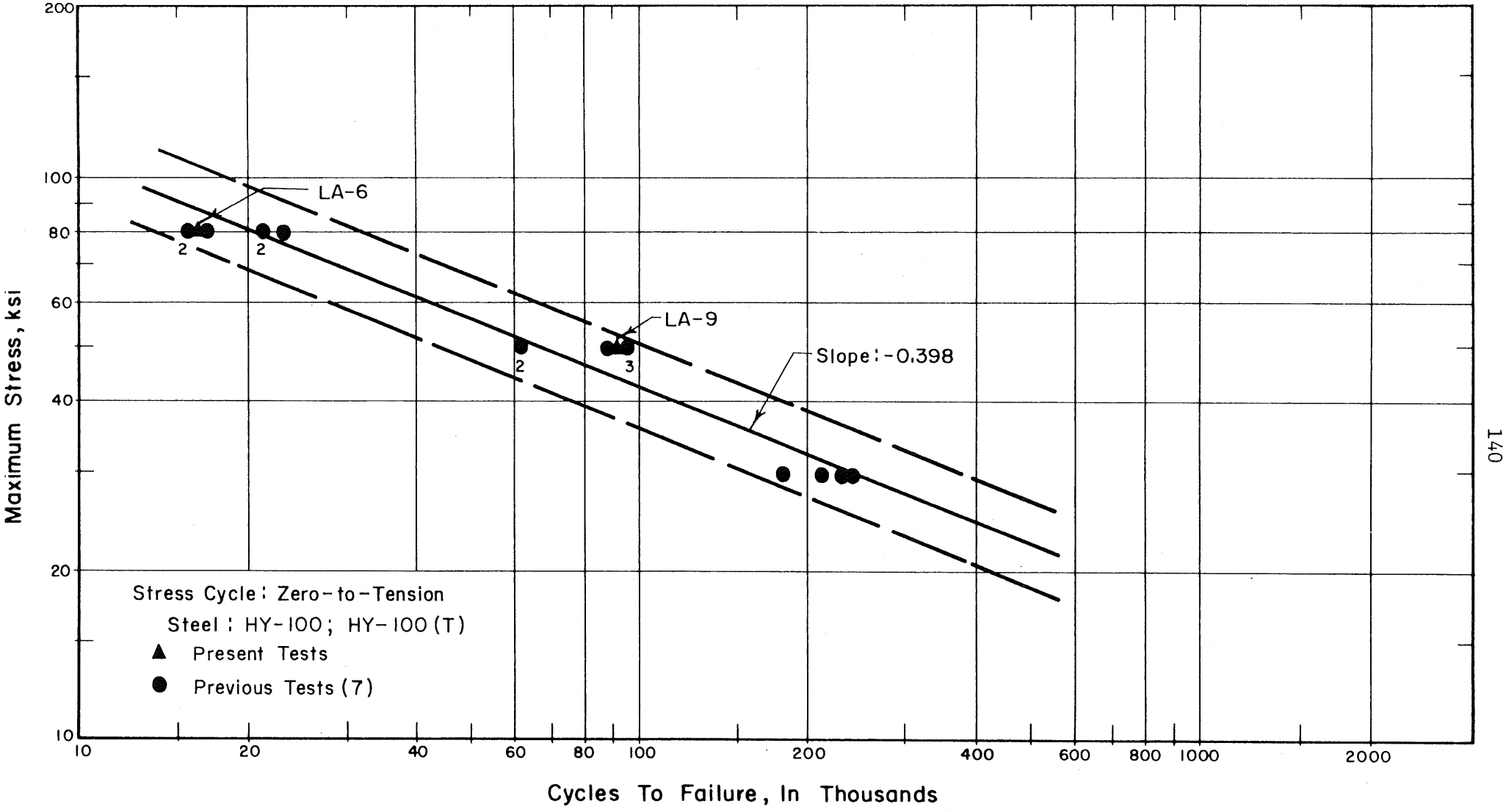

FIG. 4.3 FATIGUE TEST RESULTS AND S-N CURVE FOR HY-100 (T) TRANSVERSE BUTT WELDS (AS-WELDED) INITIATING FAILURE AT TOE OF WELD

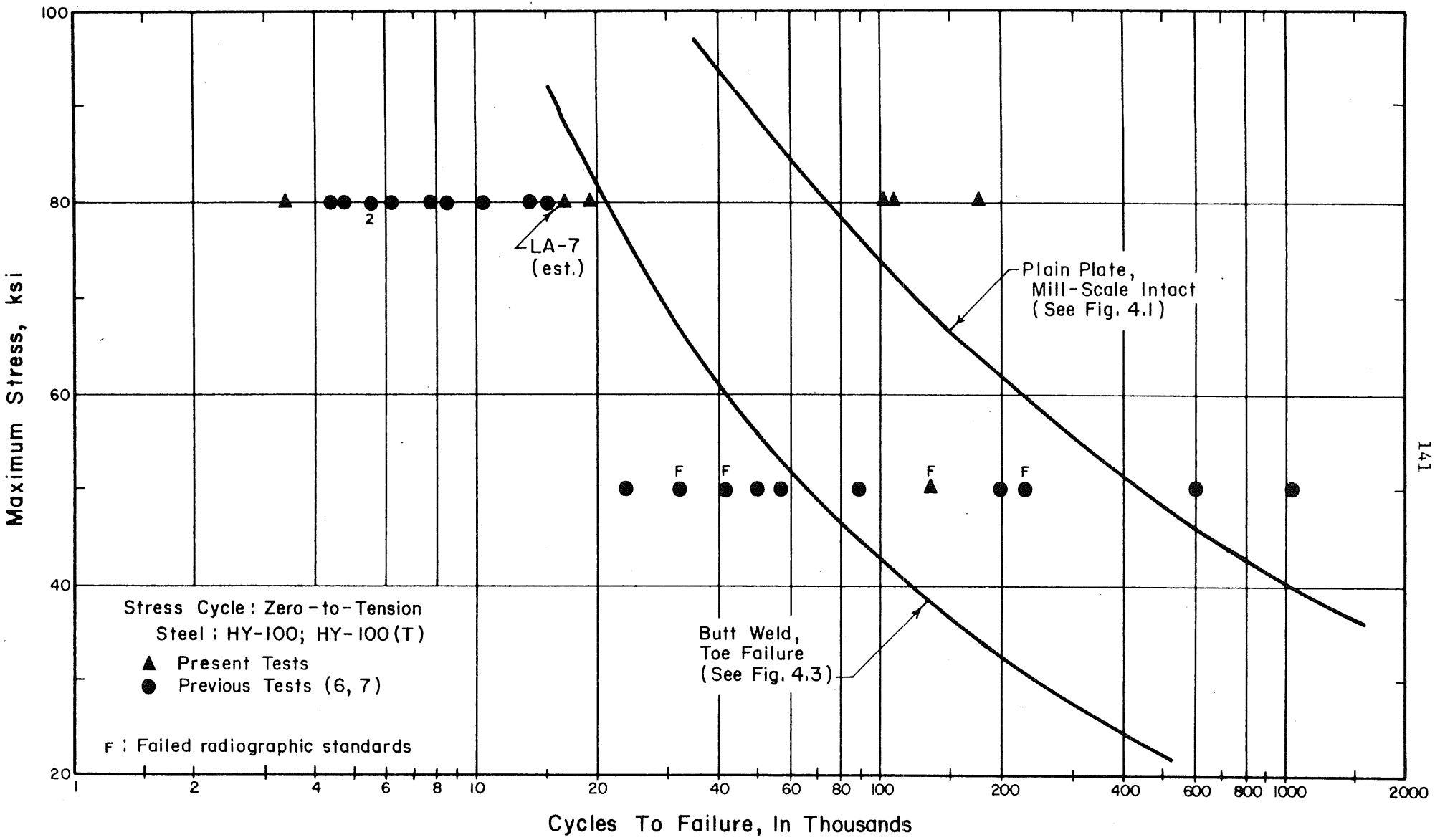

FIG. 4.4 FATIGUE TEST RESULTS FOR HY-100(T) BUTT-WELDED SPECIMENS EXHIBITING CRACK INITIATION AT INTERNAL WELD DISCONTINUITIES

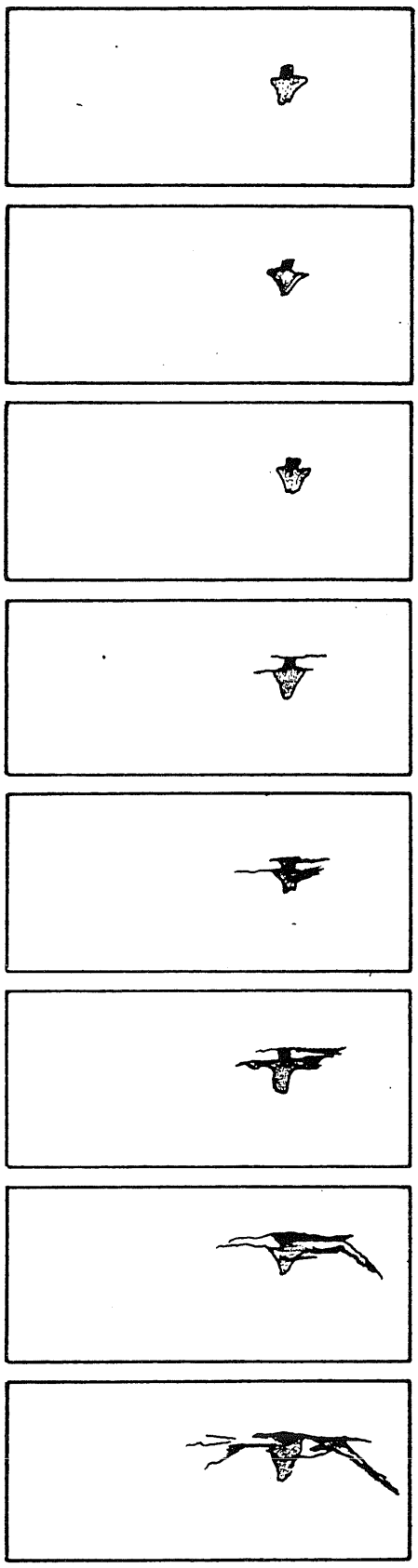

FIG. 4.5 TRACINGS OF RADIOGRAPHS TAKEN DURING FATIGUE TEST OF SPECIMEN LA-10

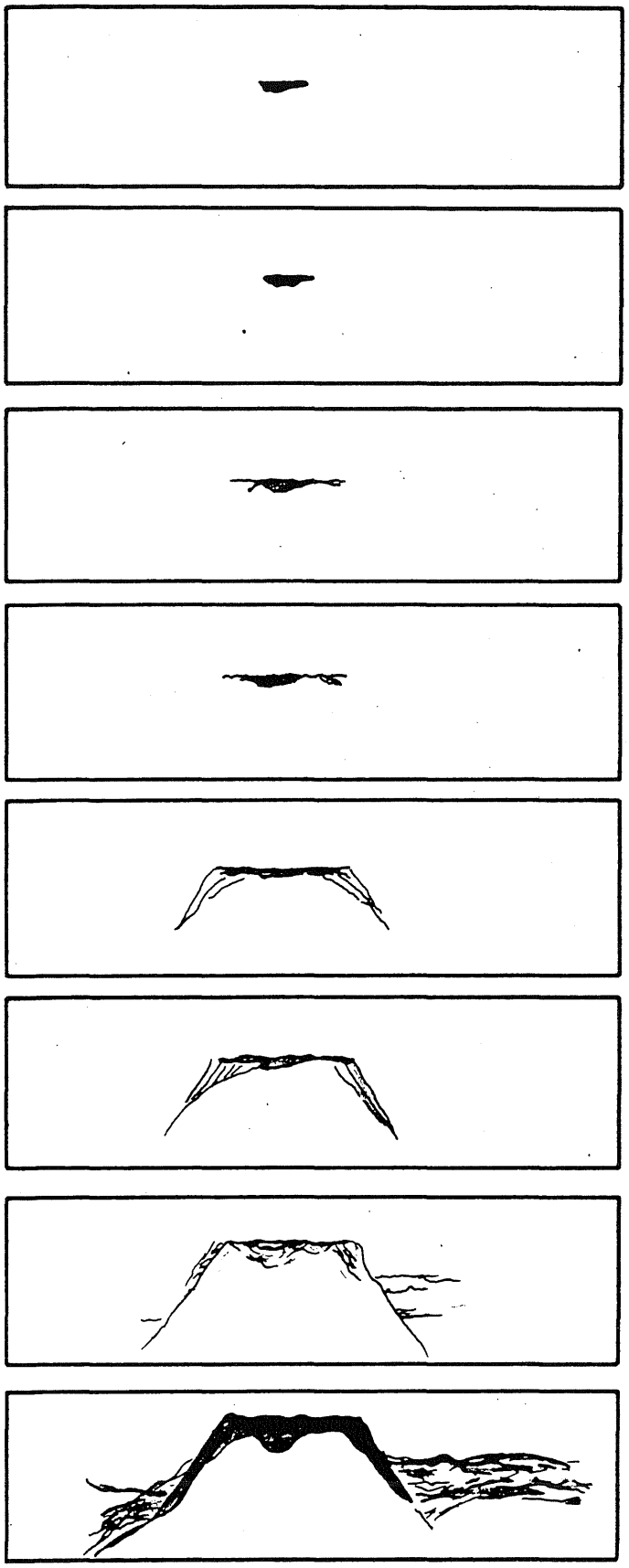

FIG. 4.6 TRACINGS OF RADIOGRAPHS TAKEN DURING FATIGUE TEST OF SPECIMEN LA-II

DISTRIBUTION LIST

Administrative Requirements

Commander
Naval Ship Engineering Center
Center SEC 6101D
Department of the Navy
Washington, D. C. 20360 (6)

Commander
Naval Ship Engineering Center
Center SEC 6120
Department of the Navy
Washington, D. C. 20360

Commander
Naval Ship Engineering Center
Center SEC 6132
Department of the Navy
Washington, D. C. 20360

Commander
Naval Ship Systems Command
Code 2052
Department of the Navy
Washington, D. C. 20360 (2)

Commander
Naval Ship Systems Command
Code 0342
Department of the Navy
Washington, D. C. 20360

U. S. Naval Research Laboratory
Washington, D. C.

U. S. Naval Applied Science Laboratory
Flushing and Washington Avenues
Brooklyn, New York

Commander
Naval Ship Research and
Development Center
Annapolis Division
Annapolis, Maryland (2)

Defense Documentation Center
Cameron Station
Alexandria, Virginia 22314 (20)

United States Steel Corporation
1025 "K" Street, N. W.
Washington, D. C. 20005
ATTN: Mr. S. L. Magee

Lukens Steel Company
Coatesville, Pennsylvania

Babcock and Wilcox Company
Barberton, Ohio

Defense Metals Information Center
Battelle Memorial Institute
505 King Avenue
Columbus, Ohio 43201

Pressure Vessel Research Committee
Welding Research Council
345 East 47th Street
New York, New York 10017

Weldability Committee
Welding Research Council
345 East 47th Street
New York, New York 10017

National Academy of Science
(Material Advisory Board)
2101 Constitution Avenue
Washington, D. C. 20018

Southwest Research Institute
8500 Calebra Road
San Antonia, Texas

Battelle Memorial Institute
505 King Avenue
Columbus, Ohio 43201

Columbia University
Columbia Heights
New York, New York 10027
ATTN: A. M. Freudenthal

Shefield Division
Armco Steel Corporation
P. O. Box 1367
Houston, Texas
ATTN: V. W. Butler

Electric Boat Division
General Dynamics Corporation
Groton, Connecticut
Via: SUPSHIPS Groton, Conn.
ATTN: Mr. E. Franks

Newport News Shipbuilding and
Drydock Company
Newport News, Virginia
Via: SUPSHIPS NPTNWS
ATTN: Mr. F. Daly

Ingalls Shipbuilding Corporation
Pascagoula, Mississippi
Via: SUPSHIP Pascagoula
ATTN: F. G. Ranson

Republic Steel Corporation
1625 "K" Street, N. W.
Washington, D. C.

UNCLASSIFIED

Security Classification

DOCUMENT CONTROL DATA - R & D

(Security classification of title, body of abstract and indexing annotation must be entered when the overall report is classified)

1. ORIGINATING ACTIVITY *(Corporate author)*

University of Illinois, Urbana, Illinois
Department of Civil Engineering

2a. REPORT SECURITY CLASSIFICATION

Unclassified

2b. GROUP

3. REPORT TITLE

LOW CYCLE FATIGUE OF BUTT WELDMENTS OF HY-100(T) AND HY-130(T) STEEL

4. DESCRIPTIVE NOTES *(Type of report and inclusive dates)*

Final Report; January 1969 - June 1970

5. AUTHOR(S) *(First name, middle initial, last name)*

James B. Radziminski
Frederick V. Lawrence
Thomas W. Wells
Richard Mah
William H. Munse

6. REPORT DATE	7a. TOTAL NO. OF PAGES	7b. NO. OF REFS
July 1970	143	31

8a. CONTRACT OR GRANT NO.	9a. ORIGINATOR'S REPORT NUMBER(S)
N00024-69-C-5297	Structural Research Series No. SRS 361
b. PROJECT NO. SF51-541-002; Task 729	
c.	9b. OTHER REPORT NO(S) *(Any other numbers that may be assigned this report)*
d.	

10. DISTRIBUTION STATEMENT

Qualified requesters may obtain copies of this report from DDC

11. SUPPLEMENTARY NOTES	12. SPONSORING MILITARY ACTIVITY
	Naval Ship Systems Command U. S. Navy

13. ABSTRACT An evaluation of the axial fatigue behavior of plain plates and full penetration butt-welded joints in HY-130(T) steel is presented. Fatigue tests were conducted with sound weldments and weldments containing internal defects including slag, porosity and lack of fusion. Radiographic and ultrasonic inspection techniques were used to study the initiation and propagation of fatigue cracks originating at internal weld flaws. Acoustic emission measurements were taken for smooth and notched HY-130(T) specimens tested in static tension and in fatigue. The results of preliminary tests of plain plates and butt weldments of HY-100(T) [HY-110] steel are presented.

Comparison of the fatigue results for the HY-130(T) specimens with equivalent data for HY-80 and HY-100 steel has indicated that, within the range of lives from approximately 10^4 to 10^6 cycles, the fatigue behavior of as-rolled (mill-scale intact) plain plates of the three materials may be described by a single S-N regression line. Surface treatments, including grit-blasting and polishing, were found to significantly increase the fatigue lives of the HY-130(T) plate specimens.

Wide variations in fatigue life were exhibited by the HY-130(T) and HY-100(T) butt-welded specimens in which cracking initiated at internal weld discontinuities. The scatter in lives could not be explained on the basis of the type of weld defect initiating failure, nor could it be attributed to differences in the weld metal composition or in the welding process. However, through application of the concepts of fracture mechanics, it was found that the fraction of the total fatigue life spent in macroscopic crack propagation could be estimated with reasonable reliability if the nominal cyclic stress, and the through-thickness dimension and position of the crack-initiating defect are known.

14. KEY WORDS	LINK A		LINK B		LINK C	
	ROLE	WT	ROLE	WT	ROLE	WT
HY-130(T) Steel						
HY-100(T) Steel						
Fatigue (Mechanics)						
Crack Initiation						
Crack Propagation						
Fracture Mechanics						
Welds						
Butt Welded Joints						
Welding						
Manual Shielded Metal Arc Welding						
Gas Metal Arc Welding						
Weld Defects						
Ultrasonic Inspection						
Radiographic Inspection						
Acoustic Emission						